This is to certify that the
dissertation entitled

INVESTIGATION OF THERMOMECHANICAL FATIGUE (TMF) BEHAVIOR IN TIN-SILVER BASED SOLDER JOINTS

presented by

JONG-GI LEE

has been accepted towards fulfillment
of the requirements for the

Ph.D. degree in Materials Science

K. N. Subramanian.

Major Professor's Signature

March 30, 2005

Date

INVEST
BE

INVESTIGATION OF THERMOMECHANICAL FATIGUE (TMF) BEHAVIOR IN TIN-SILVER BASED SOLDER JOINTS

By

JONG-GI LEE

A DISSERTATION

Submitted to
Michigan State University
in partial fulfillment of the requirements
for the degree of

DOCTOR OF PHILOSOPHY

Department of Chemical Engineering and Materials Science

2005

INVESTIC
BEH

Curren

to lead base

including the

the use of lea

challenge the

concern beca

electronic com

solders curren

Solder

creep, during

Incorporation

particularly th

capability. Se

times at these

temperature ch

Sn-Ag

temperature ex

ABSTRACT

INVESTIGATION OF THERMOMECHANICAL FATIGUE (TMF) BEHAVIOR IN TIN-SILVER BASED SOLDER JOINTS

By

JONG-GI LEE

Currently, there are two major driving forces for considering alternative materials to lead based products, specifically interconnections, in electronics applications, including the impending legislation or regulations which may tax, restrict, or eliminate the use of lead, and the trend toward advanced interconnection technology, which may challenge the limits of present soldering technology. The reliability of solder joints is a concern because fracture failures in solder joints accounts for 70% of failures in electronic components. Lead- free solders are being investigated as replacements for lead solders currently used in electronics.

Solder joints experience thermomechanical fatigue, i.e. interaction of fatigue and creep, during thermal cycling due to temperature fluctuation in service conditions. Incorporation of allying addition has been pursued to improve the mechanical and particularly thermomechanical behavior of solders, and their service temperature capability. Several service parameters, such as temperature extremes encountered, dwell times at these temperatures, and the ramp-rates representing the rate at which the temperature changes, were carried out to investigate the roles of these parameters.

Sn-Ag based solder joints that experienced a long dwell time at the high temperature extreme exhibited less surface damage accumulation and loss of residual

shear strength

temperature e

amounts of C

during TMF v

Faster

surface dama

significant de

surface dama

faster heating

A cra

sliding. Ther

during TMF,

better TMF

extreme due

retard Sn-Sn

shear strength than that of solder joints that experienced a long dwell time at the low temperature extreme. In particular, quaternary solder joints that containing small amounts of Cu and Ni in Sn-Ag solder were significantly improved the TMF behaviors during TMF with a long dwell time at the high temperature extreme.

Faster ramp rate during heating segment of TMF cycles caused highly localized surface damage in eutectic Sn-3.5Ag and Sn-4Ag-0.5Cu solder joints that resulted significant deterioration in residual shear strength in these solder joints. No significant surface damage and drop in residual strength were found in quaternary solder joints with faster heating rate during TMF.

A crack initiated and propagated along Sn-Sn grain boundaries by grain boundary sliding. There was significant residual stress within the solder joint causing more damage during TMF. Addition of small amounts of Cu and Ni into Sn-Ag solder resulted in better TMF performance under TMF with a long dwell time at the high temperature extreme due to presence in fine, hard, and sub-micron sized IMC precipitates that can retard Sn-Sn grain boundary sliding.

I would like to
members. Dr. J
like to thank th
my work. I wo
and my son for

ACKNOWLEDGEMENTS

I would like to thank my main advisor, Dr. K.N. Subramanian, and the other committee members, Dr. J. P. Lucas, Dr. T.R. Bieler, and Dr. P. Duxbury, for their support. I would like to thank the National Science Foundation (NSF) for funding to enable me to pursue my work. I would also like to give a special thanks to my family and especially my wife and my son for their love and support.

TABLE OF CONTENTS

LIST OF TABLES

LIST OF FIGURES

Figure 6.2

Figure 6.3.

Figure 6.4.

Figure 6.5.

Figure 6.6.

Figure 6.7.

Figure 6.8.

Figure 6.9.

Figure 6.10

Figure 6.11.

1.1. Motiv

Lea

interconnec

past severa

wettability

developmer

environmen

The

Electronic E

hazardous n

Japanese Er

disposed in

the United S

lead-free sta

the world. N

is to eliminat

[6].

Anoth

capability sin

for greater pa

CHAPTER 1

INTRODUCTION

1.1. Motivation

Lead-tin (Pb-Sn) alloys have been the most important solders for the interconnection and packaging of modern electronic components and devices over the past several decades due to their low cost, good manufacturability, as well as good wettability on common substrate such as Cu and Ni used in electronics [1-5]. However, developments of alternative lead-free solders are required due to increasing environmental and health concerns of the toxicity of lead.

The effort made in the European Union's Directive for Waste Electrical and Electronic Equipment (WEEE) will be in effect from January 2006. The disposal of hazardous materials from electrical and electronics products will be banned [6]. The Japanese Environmental Agency has proposed that lead-containing scrap must be disposed in sealed landfills to prevent lead leaching. Consequently electronics sold by the United States and other worldwide electronics producers to these countries must meet lead-free standards to maintain trade. The United States is the largest consumer of lead in the world. Nevertheless, the trend being set by some of the major countries in the world is to eliminate the use of lead in consumer products for health and environmental reasons [6].

Another concern is that Sn-Pb solders are reaching the limit of performance capability since the adoption of surface mount technology (SMT). Increasing demands for greater packaging density and high performance are being realized with the advent of surface

package

I

been exte

tin-silver

demandin

service co

lead-bearin

physical pr

and rare-ea

based lead-f

to improve p

Rene

in electronic

the printed c

reliability be

connector and

an entire mach

The ma

strain on the joi

solder joint fai

the combination

coefficient of th

surface mount technology, resulting in an increase in the numbers of solder joints per package and reduction of joint dimensions [3,10].

In order to satisfy the requirement of replacing lead-bearing solder, there have been extensive studies of lead-free solders. Among the various lead free solders, eutectic tin-silver (Sn-Ag) is an attractive candidate alloy to meet the requirement for the demanding high temperature service environment such as automotive under-the-hood service conditions. However, the melting temperature of this alloy is higher than that for lead-bearing solder. For depressing the melting temperature and also improving its physical properties, some additional elements such as copper, nickel, indium, antimony, and rare-earth elements are added to Sn-Ag solderas [11-16]. Thus, candidate Sn-Ag based lead-free solder will be a ternary or quaternary alloy containing additional elements to improve properties of eutectic Sn-Ag solder.

Renewed interest in solder has been driven by reliability concerns of solder joints in electronic packaging schemes. In SMT the solder joint alone joins the chip carrier to the printed circuit board (PCB). A major problem of SMT is that the solder joint reliability becomes increasingly critical, as the joint must act both as an electrical connector and mechanical bond. The failure of this single joint could render a device, or an entire machine, inoperable.

The major failure of solder joint arises from the imposition of the mechanical strain on the joints in service. It was shown that low-cycle fatigue is the primary cause of solder joint failure in electronic assemblies [17]. This low cycle fatigue is produced by the combination of fluctuations in temperature acting on the materials of differing coefficient of thermal expansion (CTE) mismatched between substrate, component, and solder us

in solder

fluctuatio

Th

is the maj

Sn-Ag bas

creep resis

microjoints

solder joint

solder in se

the processi

dissolution

the high ho

microstructu

mechanical p

made joint.

reliability an

contribute to

dwell times at

dwell times at

temperatures w

precipitates), a

Among these fa

solder used in the electronic package. This CTE mismatch that causes low-fatigue cycle in solder joints is produced from environmental temperature changes and/or temperature fluctuations from the joule heating of the device during service [17].

Thermomechanical fatigue (TMF) due to temperature fluctuations during service is the major low-cycle fatigue mode that the solder joint can result in failure. Therefore, Sn-Ag based lead-free solder should have mechanical properties such as fatigue strength, creep resistance, rigidity, and so on, which are sufficient to ensure the reliability of microjoints in a modern electronic device. However, the deformation behavior of the solder joint becomes more complicated due to the complexity of microstructure of the solder in service. The solder is used in an as-solidified microstructure that depends upon the processing history [18]. The microstructure of the solder is also altered due to the dissolution of substrate materials into the solder during soldering [19, 20]. Because of the high homologous temperature in service for Sn based solders, the as-solidified microstructure of the solder changes continuously during service [21]. As a result, the mechanical properties of the solder joint during service are different from those of the as-made joint. The microstructural evolution of the solder makes the deformation and reliability analysis of the solder joint very difficult. There are several factors that can contribute to TMF during service, such as ramp rates (related to strain rate imposed), dwell times at each temperature extreme (creep/stress relaxation), static aging (especially dwell times at the high temperature extreme), reversed repeated shear (due to change in temperatures with thermal cycle), microstructural features (effect of second phase IMC precipitates), anisotropy of tin (due to high population of tin in tin-based solders), etc. Among these factors, it is not clear which is the most dominant factor that can affect fatigue of

understand

1.2. Objec

The

behaviors a

based solder

with small a

parameters, s

and the ramp

out to invest

Finally, a sin

TMF will be

fatigue of solder joints due to TMF. Thus, it is important to establish fundamental understanding of behavior of solder joints that underwent actual TMF.

1.2. Objective

The objective of this study is to investigate the thermomechanical fatigue (TMF) behaviors and the mechanisms that are responsible for the deformation of the Sn-Ag based solder joints. Using the eutectic Sn-Ag solder as a model system, the Sn-Ag solder with small amounts of Cu and, (Cu + Ni) alloy solders will be used. Several service parameters, such as temperature extremes encountered, dwell times at these temperatures, and the ramp-rates representing the rate at which the temperature changes, will be carried out to investigate the role of individual service parameter in Sn-Ag based solder joints. Finally, a simple model to predict the service capability of Sn-Ag based solders under TMF will be investigated.

OVERVI

2.1. ROLE STRU

The p

in the electro

or drop of w

chips should

package, but

consisting of

be sent to se

This is the m

electrical co

components.

assemblies, i

electronic co

used in electr

board (PCB)

Figure 2.1(a),

auto-insertion

applied. Wave

of molten solde

CHAPTER 2

OVERVIEW OF THERMOMECHANICAL FATIGUE (TMF) BEHAVIOR IN EUTECTIC TIN-SILVER BASED SOLDER JOINTS

2.1. ROLES OF SOLDER JOINT IN ELECTRONIC PACKAGING AND ITS STRUCTURES

The purposes of electronic packaging are mainly to protect semiconductor devices in the electronic devices. Since silicon chips are very delicate, even a tiny speck of dust or drop of water can hinder their functions. Thus, ensuring the functionality of silicon chips should be established. Silicon chips are not only needed to be protected by the package, but also, they need to exchange signals with the outside. Attaching metal "legs" consisting of lead frame (soldered balls in the case of BGA), therefore allows signals to be sent to semiconductor devices from outside, and the results of processing accessed. This is the major function of solder in electronic packaging. Solder joints not only are electrical connections, but also, are mechanical connection between substrate and components. In order to have a good understanding of their functions in electronic assemblies, it is important to overview the different types of mounting techniques of electronic components. Figure 2.1 illustrates the types of mounting techniques currently used in electronic industries. The basic element may be considered as the printed circuit board (PCB) that is mainly made by a reinforced polymer material. As can be seen in Figure 2.1(a), the PCB contains holes and components have stiff lead-frame. Using an auto-insertion machine, the holes in a PCB are filled with lead-frames while flux is applied. Wave soldering is performed to attach PCB and lead-frames by exposing a wave of molten solder.

Throug

types have bee

lighter weight.

Through hole mount types have been used for many years, but surface mount types have been developed due to demands of high packaging density, smaller height, lighter weight, and better performance.

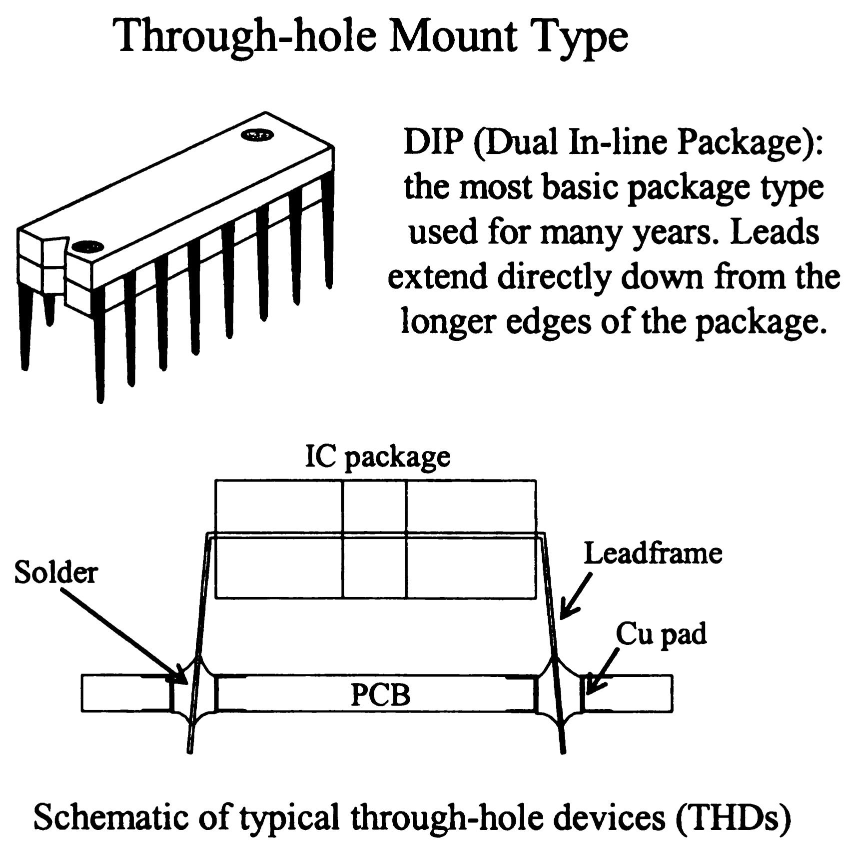

Figure 2.1(a). Schematic of typical through hole devices (THDs)
(cont'd)

Surface Mount Type

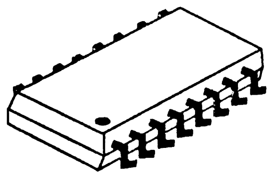

SOP (Small Outline Package): This is the main type of surface mounting and is very widely used.

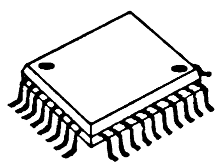

QFP (Quad Flat Package): This is the evolved version of the SOP package. This is most commonly used in surface mount type packaging recently.

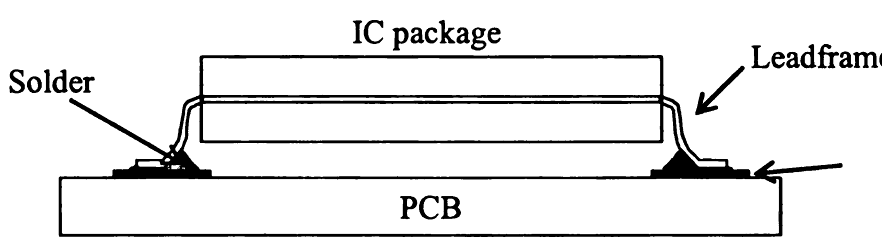

Schematic of a Leaded Chip Carrier Package (LDCC)

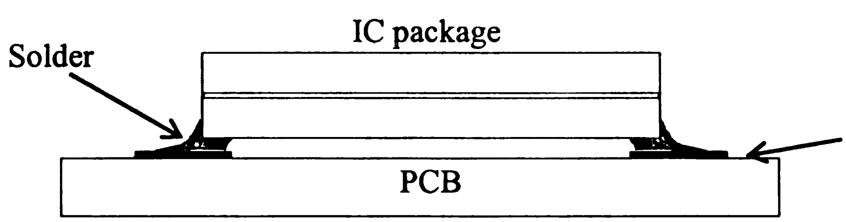

Schematic of a Leadless Chip Carrier package (LLCC)

Figure 2.1(b). Schematic of surface mount devices (SMDs). (cont'd)

So

Fi

Unlike the thro

Figure 2.1(b) i

using solder pas

screen printer.

joint.

The rapi

significant increa

are needed to sati

Figure 2.1(c)) hav

performance and ar

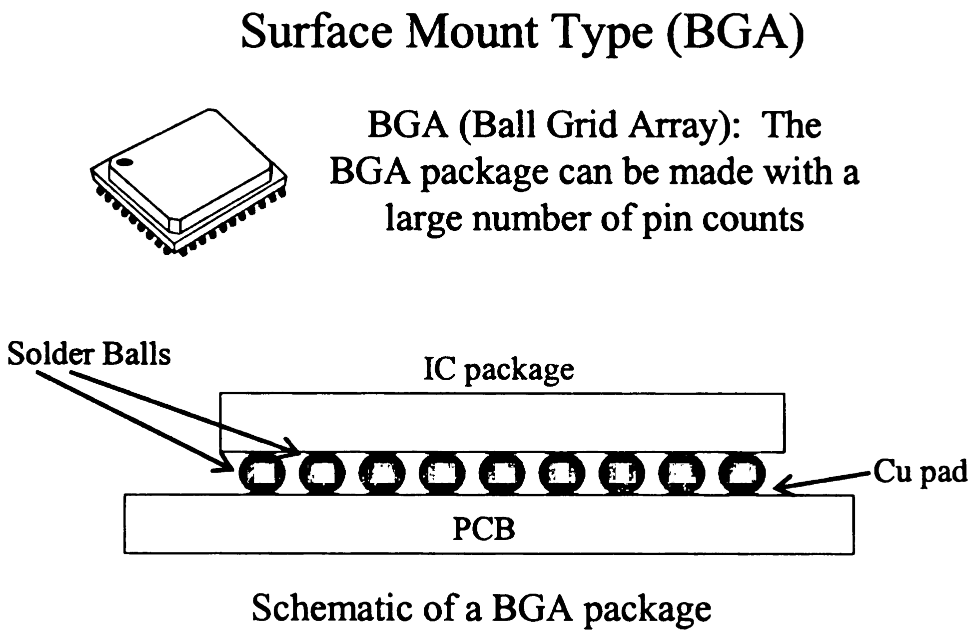

Figure 2.1(c). Schematic of surface mount (BGA) devices [22].

Unlike the through-hole mounting, the components are directly mounted on PCB surface. Figure 2.1(b) illustrates typical surface mount types. Soldering is usually performed using solder paste (a mixture of solder powder, flux and binder agent) that is applied via a screen printer. Reflow soldering is used to melt and re-solidify for forming the solder joint.

The rapid development of silicon device technology in recent years demands significant increases in service performance. Thus, a larger numbers of interconnections are needed to satisfy such requirements. Ball grid array (BGA) packages (illustrated in Figure 2.1(c)) have been developed to suit this purpose. They have excellent electrical performance and are suitable for high frequency and high pin count.

2.2 PRO

Sc

(Sn) and s

tin (Sn).

2.2-1. An

Tin

tetragonal (

material b

directions (

exhibits an

directions, a

between larg

ratcheting",

between adja

that is locate

vertical direc

direction. Th

tries to expan

adjacent grain

nature of tin,

ratcheting [25].

2.2 PROBLEMS INVOLVED IN HIGH TIN SOLDERS

Solders, especially, lead-free solders mainly consist of more than 90 wt% of tin (Sn) and some other elements. Thus, it is important to understand physical properties of tin (Sn).

2.2-1. Anisotropy of β–Tin

Tin exists as the white tin (β-tin) at room temperature and it has the body-centered tetragonal (BCT) crystal structure as is shown in Figure 2.2. Tin is a highly anisotropic material because it possesses different physical properties along different lattice directions (see Table 2.1). Barry et al. [23] suggested that "It will be noted that tin exhibits anisotropy of thermal expansion properties in different crystallographic directions, and this may lead to steps appearing in a free surface at the boundaries between large grains in samples subjected to severe thermal cycling". The term "thermal ratcheting", is defined as the accumulation of plastic strain due to different orientations between adjacent grains during thermal cycling. As can be seen in Figure 2.3, grain 1, that is located in the center of grain 2, is oriented so that plastic flow occurs easily in the vertical direction while grain 2 is oriented so that plastic flow is easy in the horizontal direction. Thus, grain 1 tries to expand in vertical direction during heating and grain 2 tries to expand in horizontal direction. Such different tendency to expansion in two adjacent grains will result in up-hill of grain 1 during thermal cycling. Due to anisotropic nature of tin, the surface becomes textured and holes appear resulting from thermal ratcheting [25].

Figure

Grai

C

Figure 2.3. S

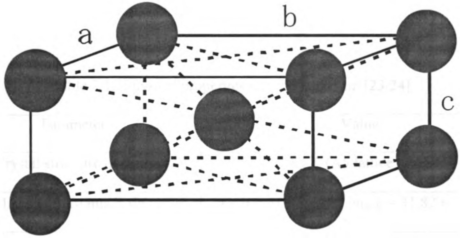

Figure 2.2. Schematic illustration of the body-centered tetragonal structure [23]

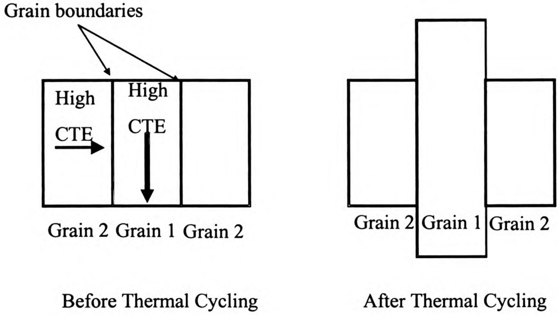

Figure 2.3. Schematic illustration of the elongation of grain 1 due to thermal ratcheting [25].

Cry
La
Youn
Re
Tensi
α to β tran
Crysta
Lattic
De
Volume
Resi

Table 2.1. Physical properties of β-tin and α-tin [23,24].

Parameter	Value
Crystal structure of β-tin	BCT (A5 lattice type)
Lattice constants β-tin	$a = b = 58.32 \times 10^{-2}$ nm, $c = 31.82 \times 10^{-2}$ nm
Density of β-tin	7.3 gm/cm^3
Young's Modulus of β-tin	a axis = 85 GPa , c axis = 54 GPa
CTE of β-tin	a axis = 15.4×10^{-6}/°C , c axis = 30.5×10^{-6}/°C
Resistivity of β-tin	12.6 μΩ•cm (direction unknown)
Tensile Strength of β-tin	2600 psi, ~ 18MPa
α to β transformation temperature	13.2°
Crystal structure of α-tin	Diamond cubic (A4 lattice)
Lattice constants α-tin	$a = 64.9 \times 10^{-2}$nm
Density of α-tin	5.75 gm/cm^3
Volume change (%), β to α	21 %
Resistivity of α-tin	300 μΩ•cm

2.2-2. A

Th

can be n

structure

substantial

experience

complete lo

Only a fe

[27,28]. Ti

the Sn-0.5C

Sn-Ag base

that there is

physical pro

environment

2.3 FATIGU

2.3-1. Isothe

Stresse

to the materia

develop into cr

well below a g

fracture the mat

resistance is the

2.2-2. Allotropic Phase Transformation of Tin

The allotropic transformation in tin is not a well understood phenomenon yet. As can be noted from Table 2.1, tin can change its crystal structure from BCT crystal structure to diamond cubic crystal structure below 13.2°C. This will result in a substantial volume change (21 %) as the transformation occurs and causes the metal to experience internal stresses which are sufficient to cause fracturing and ultimately the complete loss of integrity [26]. This allotropic transformation in tin is termed "tin-pest". Only a few studies have attempted to understand tin-pest in high tin-based solders [27,28]. Tin-pest has never been observed in Sn-37Pb alloys, but has been reported for the Sn-0.5Cu solder alloy aged at -18°C for 46 months [26]. Formation of tin pest in the Sn-Ag based solders has not been established but long term aging tests at -18 °C indicate that there is such a possibility [27]. Tin-pest may cause significant deterioration of physical properties in high tin-based solder joint. Storage at very low temperature environment may cause serious problems in the electronic devices due to tin-pest.

2.3 FATIGUE

2.3-1. Isothermal Mechanical Fatigue on Sn-Ag Based Solders

Stresses resulting from cyclic loading can lead to microscopic physical damages to the materials. These damages can accumulate with continued cycling until they develop into cracks or other damage that lead to failure of the materials even at stresses well below a given material's ultimate strength. Cyclic loading will often ultimately fracture the material. Fracture due to this cyclic loading is called fatigue. Thus, fatigue resistance is the ability to endure the cyclic loading in the materials [28].

The r

between co

amplitude.

reaches ε_{min}

time the stra

fixed-freque

continued ur

constant and

loading is nc

and these ca

state, a meta

Figure 2.5. sh

be seen in th

constant and

from linearity

From th

From re

equation can b

elastic modulus

The most common fatigue test involves completely reversed (R = -1) cycling between constant strain limits as given in Figure 2.4 (where R is $\sigma_{min}/\sigma_{max}$). A strain amplitude, $\varepsilon_a = \Delta\varepsilon/2$, is selected, and an axial test specimen is loaded until the strain reaches $\varepsilon_{min} = -\varepsilon_a$, and the test is continued, with direction of loading being reversed each time the strain reaches $+\varepsilon_a$ or $-\varepsilon_a$. Fixed strain rate between these limits, or sometimes a fixed-frequency sinusoidal variation of strain is used. Such cyclic strain tests are continued until fatigue failure starts. In the strain-controlled cycling, the strain range is constant and the stress changes. Since the plastic deformation produced during cyclic loading is not completely reversible, structural modifications occur during cyclic loading and these can result in changes in the stress-strain responses. Depending on the initial state, a metal may undergo cyclic hardening, cyclic softening, or remain cyclically stable. Figure 2.5. shows the complete stable stress-strain hysteresis loop with one cycle. As can be seen in this figure, from point 1 to 2, the slope of the stress-strain path is at first constant and close to the elastic modulus ($E = \Delta\sigma \bullet \varepsilon$). Then the path gradually deviates from linearity as plastic strain occurs, for example, path from 2 to 3.

From this figure, the total strain range can be ($\Delta\varepsilon$) written as,

$$\Delta\varepsilon = \frac{\Delta\sigma}{E} + \Delta\varepsilon_p, \text{ where } \varepsilon_p \text{ is plastic strain}$$

From relation between $\Delta\varepsilon$ and ε_a ($\varepsilon_a = \Delta\varepsilon/2$), $\Delta\sigma$ and σ_a, and $\varepsilon_{pa} = \Delta\varepsilon_p$, above equation can be re-written as, $\varepsilon_a = \frac{\sigma_a}{E} + \varepsilon_{pa}$, where, ε_a is a strain amplitude, E is the elastic modulus σ_a is a stress amplitude, and ε_{pa} is a plastic strain amplitude.

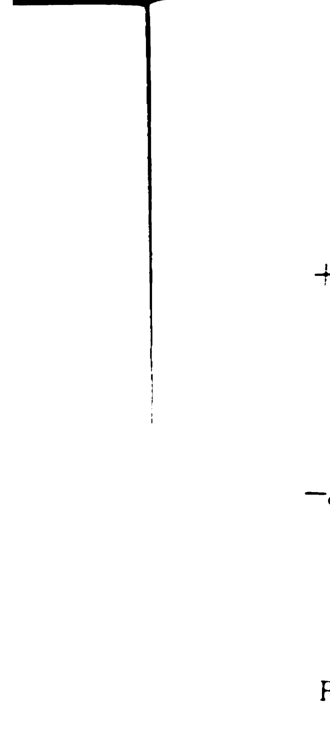

Figure 2.5. Sc

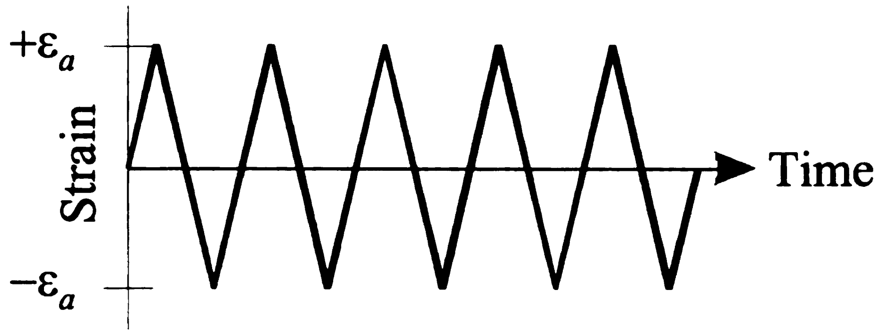

Figure 2.4. Schematic illustration of strain-controlled cycling [29].

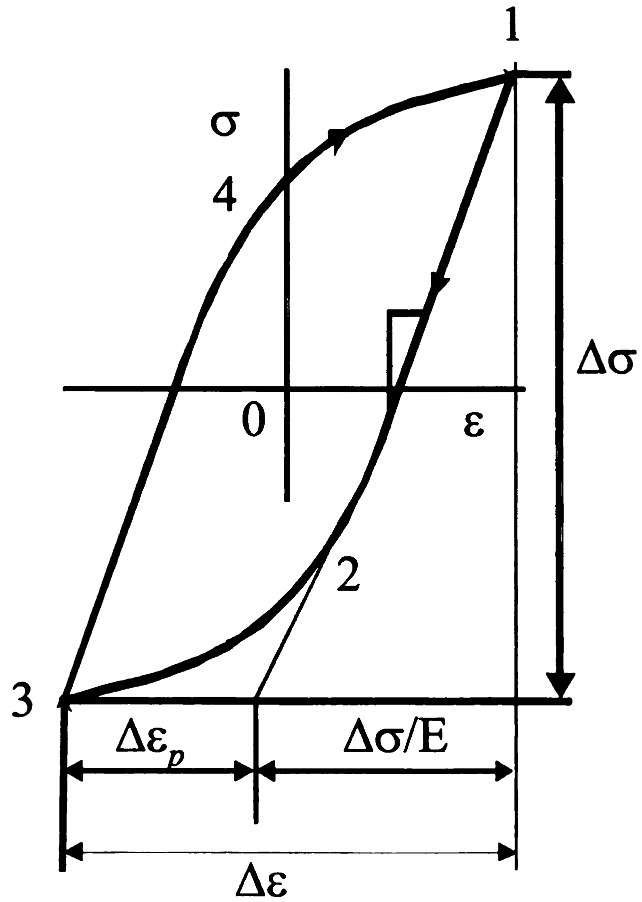

Figure 2.5. Schematic illustration of stable stress-strain hysteresis loop under strain-controlled cycling [29].

Stra

stresses. A

versus life

estimates in

The

so, equation

It is also use

as can be s

between 1 a

between poi

lines.

Since, $\frac{\sigma_f'}{E}$ a

$(2N_f)$ in abov

Note: σ_f', b,

called Coffin

The equation

solders or sold

Strain-based approach to fatigue is more appropriate for case of cyclic thermal stresses. A plot of strain amplitude versus cycles to failure is called S-N curve (strain versus life curve). This curve is used in the strain-based approach for making life estimates in a manner analogous to the use of the S-N curve in the stress-based approach.

The strain amplitude can be divided into elastic and plastic parts.

$$\varepsilon_a = \varepsilon_{ea} + \varepsilon_{pa}$$

so, equation will be $\varepsilon_a = \frac{\sigma_a}{E} + \varepsilon_{pa}$, as explained in previous equations.

It is also useful to plot ε_{ea} and ε_{pa} separately as functions of number of cycles to failure N_f as can be seen in Figure 2.6. The slope of the elastic part can be plotted from point between 1 and 2 with each cycle and the plot for plastic can be obtained from slop between point 2 and 3 as can be seen in Figure 2.5. Equations can then be fitted to these lines.

$$\varepsilon_{ea} = \frac{\sigma_a}{E} = \frac{\sigma_f'}{E}(2N_f)^b, \qquad \varepsilon_{pa} = \varepsilon_f'(2N_f)^c$$

Since, $\frac{\sigma_f'}{E}$ and ε_f' are the intercept constants at $N_f = 0.5$, requiring use of the quantity $(2N_f)$ in above equation. So strain amplitude can be rewritten as,

$$\varepsilon_a = \frac{\sigma_f'}{E}(2N_f)^b + \varepsilon_f'(2N_f)^c$$

Note: σ_f', b, ε_f', and c are considered to be material properties. This equation the so called Coffin-Manson relationship represents the total strain amplitude (ε_a) in Figure 2.6. The equation or modified version of this equation has been used to evaluate life of solders or solder joints under isothermal strain-controlled cycling.

Figure 2.6. S

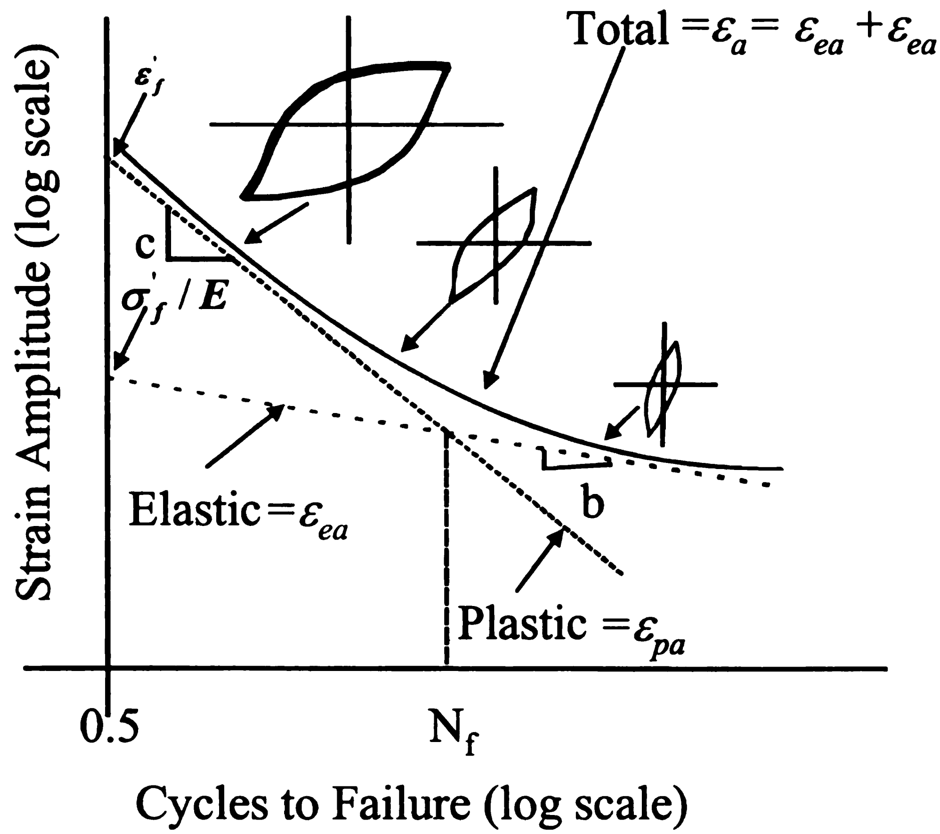

Figure 2.6. Schematic illustration of elastic, plastic, and total strain vs, life curve [30]

Th

where N_f i

are materia

with the dev

failure [31].

where ΔP is

as illustrated

Isoth

Sn-Ag and S

isothermal fa

frequency of

a fatigue failu

and Sn-40Pb

increasing pla

The number o

Sn-40Pb solde

Coffin-

failure and th

However, solde

The most frequently used Coffin-Mason equation is given as

$$N_f^{\alpha} \Delta \varepsilon = C$$

where N_f is number of cycles to failure, $\Delta\varepsilon$ is total or plastic strain range, and α and C are materials constants. The load drop in the hysteresis loop is believed to be correlated with the development and growth of fatigue cracks and is used as a measure of the fatigue failure [31]. The load drop is characterized by the load drop parameter Φ,

$$\Phi = 1 - \left(\frac{\Delta P}{\Delta P_m}\right)$$

where ΔP is the load range at any number of cycle and ΔP_m is the maximum load range as illustrated in Figure 2.7.

Isothermal fatigue tests were conducted by Solomon et. al. [31], using eutectic Sn-Ag and Sn-40 Pb single shear lap solder joints under plastic stain control. The two isothermal fatigue tests conducted in this study were at 35°C and 150°C with cycling frequency of 0.3 Hz without hold time at each strain extreme. 50% load drop was used as a fatigue failure criterion. Figure 2.8 shows the comparison of fatigue lives of Sn-3.5Ag and Sn-40Pb solder joints. The numbers of cycles to failure were decreased with increasing plastic strain range, following a Coffin-Mason low cycle fatigue relationship. The number of cycles to failure of Sn-3.5Ag solder joints exhibited longer than that of Sn-40Pb solder joints at both temperatures over most plastic strain ranges.

Coffin-Manson equation assumes that the product of the number of cycles to failure and the plastic strain is a constant. This model addresses only plastic stain. However, solder joints do not deform homogenously due to complex geometry.

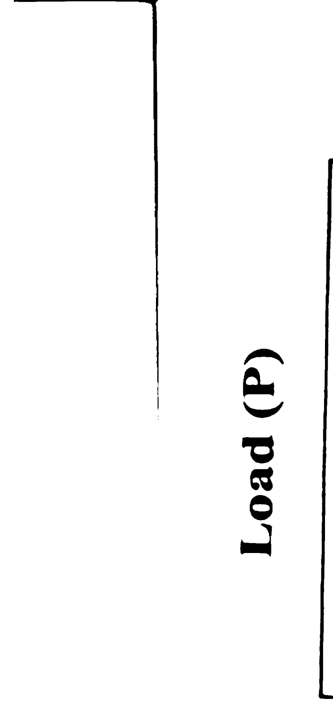

Figure 2

Figure 2.8.
jo

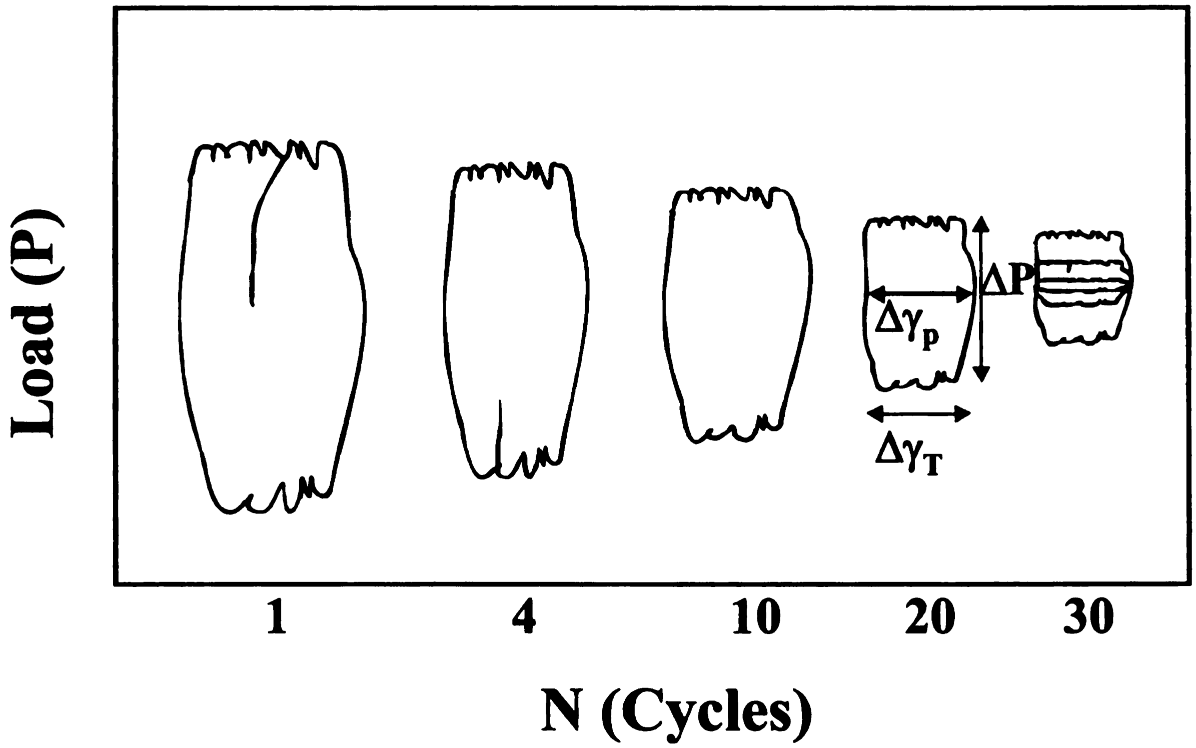

Figure 2.7. Schematic drawing of hysteresis loop showing load drop with increasing number of cycles [32].

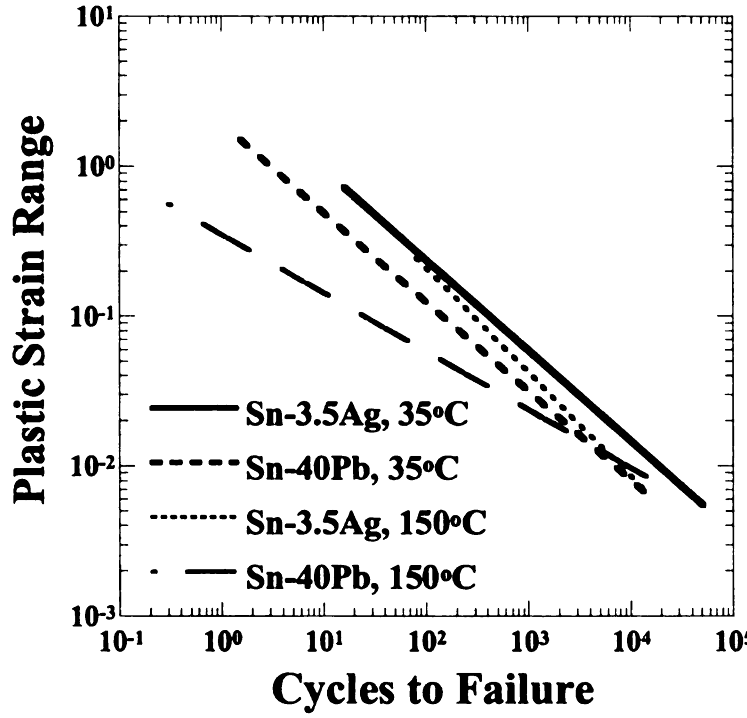

Figure 2.8. Example of isothermal fatigue test conducting Pb-free and Pb-bearing solder joints at 35°C and 150°C using a 50 % load drop failure criterion [31]

This issue w

in the actua

out that inh

joint geome

assumption

application c

model as Co

the actual so

predictions.

the effects of

for materials

2.4. THERM

Therm

due to chang

expansion (C

common fatig

relatively low

conditions. F

dominated ev

high-cycle fati

On the

component of

This issue was criticized by Winterbottom [3]. He reported that the deformation process in the actual solder joint was highly inhomogeneous after thermal cycling. He pointed out that inhomogeneous and highly localized deformation was found depending on the joint geometry under actual thermal cycling. This indicated that the uniform strain assumption throughout the simplified solder joints or bulk solders employed in application of the Coffin-Manson type relation was not appropriate. Thus, such a simple model as Coffin-Manson relation is an over-simplification in assessment of fatigue life of the actual solder joints and a more accurate model will be needed for more accurate life predictions. In addition to the above issues, Coffin-Manson model does not account for the effects of hold time and temperature extreme which are very important considerations for materials stressed above 0.5 of their melting point (T_m).

2.4. THERMOMECHANICAL FATIGUE

Thermomechanical fatigue usually refers to the cyclic displacement that occurs due to change in temperature when two materials with dissimilar coefficient of thermal expansion (CTE) are joined. High-cycle fatigue and low-cycle fatigue are the two common fatigue modes. High-cycle fatigue occurs when the specimen is subjected to relatively low loads and the elastic strains are much greater than the plastic strains in such conditions. Fatigue failure typically occurs after about 10^4 cycles and it is a stress-dominated event. Vibrational loads in the microelectronic packages generally cause high-cycle fatigue failures and this is a stress-based fatigue.

On the other hand, low-cycle fatigue occurs at higher loads where the plastic component of the strain is comparable to or even greater than the elastic strain.

Temperat

failures in

dominatec

joints is te

changes in

mismatch.

fatigue ph

and propa

melting po

can range

mechanism

thermally a

which resu

solder joint

2.4-1. Ty

In th

proper testi

condition.

are characte

been propos

test or servic

the failure of

time, and ste

Temperature cycling and power cycling are the primary causes of the low-cycle fatigue failures in microelectronic packages. Low-cycle fatigue is characterized as a strain-dominated event rather than a stress-dominated event [33]. Low-cycle fatigue in solder joints is termed themomechanical fatigue (TMF) as the solder joint is experiencing both changes in temperature as well as a change in the mechanical strain imposed by the CTE mismatch. Fatigue in solder joints can be considered as a high temperature low cycle fatigue phenomenon [34]. At low temperatures, fatigue causes damage by the initiation and propagation of microcracks. But even room temperature is high compared to the melting point of solder, and in general electronic components see thermal cycling which can range from 0.5 T_m to 0.8 T_m. As a consequence, creep is an operative deformation mechanism whenever the temperature is above $0.5T_m$. Creep strain is a result of thermally activated dislocation motion and/or the movement of vacancies and atoms, which results in the elongation of the material. Thus, the thermal fatigue damage on the solder joints is stored by a combination of creep and fatigue mechanism [35].

2.4-1. Types of Thermal Cycles

In the automotive and computer industries, there has been a challenge to design proper testing methods of thermal cycling test, which would correspond to service condition. Failures due to either thermal cycle tests or environmental service conditions are characterized by thermomechanical fatigue behaviors. Several fatigue models have been proposed, but none of these models take into account all of the parameters of the test or service environment. In thermal cycling, there are many factors that can influence the failure of solder joints due to TMF, such as the temperature range, ramp rate, dwell time, and stepped heating and cooling [36].

Th

shock, (ii

componen

relatively

be carried

effects of

each of th

dwell time

more life ti

experience

shock is th

joint can ex

2.9(a) and (

Actu

on service c

where the a

reach as hig

be varied by

For c

damage since

environment a

There are three means by which thermal cycles may be imposed: (i) thermal shock, (ii) temperature cycling, and (iii) power cycling. Thermal shock involves cycling components between two thermal baths at high and low temperature extremes. This is relatively easier than actual thermechanical fatigue cycling since the accelerated test can be carried out in a short period of time. However, thermal shock considers neither the effects of ramp rates for heating and cooling segment nor the effects of dwell times at each of the temperature extreme. Actual solder joints experience these ramp rates and dwell times during thermal cycling. Kubik et al. [37] reported that the solder exhibited more life time when it experienced thermal shock than that of the life time of a solder that experienced thermal cycling with slower ramp rates. The other disadvantage of thermal shock is that the result of this test might not represent the actual situation that the solder joint can experience. Schematics of two types of thermal shock are illustrated in Figure 2.9(a) and (b).

Actual TMF cycle must consider appropriate dwell time and ramp rate depending on service conditions. Figure 2.9(c) represents an automotive under-the-hood situation where the automotives experience very low temperature (maximum –40°C) and also can reach as high as 160°C due to heating from the engine after ignition. The ramp rates can be varied by situations, such as surrounding temperatures or times of service, or both.

For computer industries, power cycling is the major factor that can cause TMF damage since the power on and off causes thermal cycling rather than the surrounding environment as can be seen Figure 2.9(d).

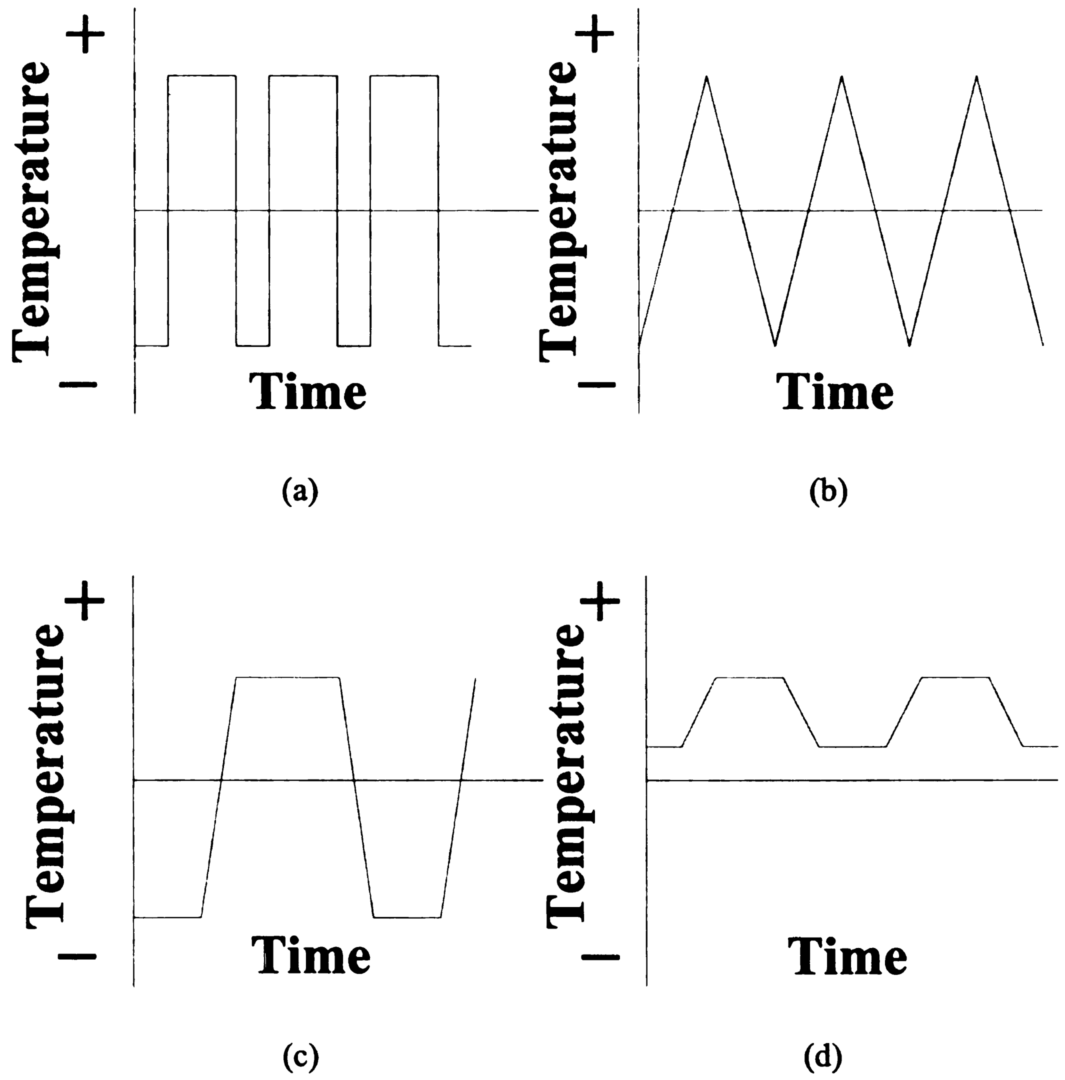

Figure 2.9. Schematic illustrations of types of thermal cycling. (a) thermal shock with no ramp rates consideration, (b) thermal shock with no dwell times at each temperature extremes, (c) actual thermal cycling that solder joints can experienced during TMF, especially automotive under-the hood situation (ramp rates and dwell times will vary with service), and (d) power cycling which can be effected by turning on and off of components in ambient environment [36].

2.4.-2. De

The

of thermal

Thermal fl

strains whi

softest ma

cyclic dam

example o

difference

significant

more comp

developed i

adjacent Sn

and substra

separation b

during temp

geometry, i.

solder joints

Table 2.1 an

Therm

temperature-t

the cycle and

2.4.-2. Deformation Characteristics of Solder Joints During TMF

The source of TMF of solder joints is the significant difference in the coefficient of thermal expansion (CTE), α, that exists between the material components of a joint. Thermal fluctuations due to change in temperature during a service environment generate strains which lead to crack initiation, crack propagation, and final failure. Solder is the softest material in the electronic components, and solder accommodates most of the cyclic damage (strain absorbing material) during thermal fluctuations. The classic example of TMF of an interconnection on a PCB is given in Figure 2.10. Due to difference in the CTE between the material components, solder joints experience significant straining. However, this example is a global situation. The actual case is more complex than the global situation. During thermal fluctuations, thermal strains developed in the material components may be categorized into (i) anisotropy effects in adjacent Sn grains in the solder area, (ii) solder material and IMC layer, (iii) IMC layer and substrate, and (iv) a geometrical mismatch determined by the component size and the separation between individual solder joints. Various forms of these thermal strains during temperature changes are illustrated in Figure 2.11 [38]. In case of a simpler joint geometry, i.e. solder joints made with Cu substrates, the possible CTE mismatches in solder joints are given in Figure 2.12. CTE values of Sn, Cu and Cu_6Sn_5 are given in Table 2.1 and 2.2.

Thermal strains caused by TMF can lead to significant surface damages. The temperature-time profiles in service introduce dwell times at each temperature extreme in the cycle and establish low-cycle creep-fatigue conditions. There are three distinct

T_{min}:

During

cooling

T_0:

T_{max}:

During

heating

Figu

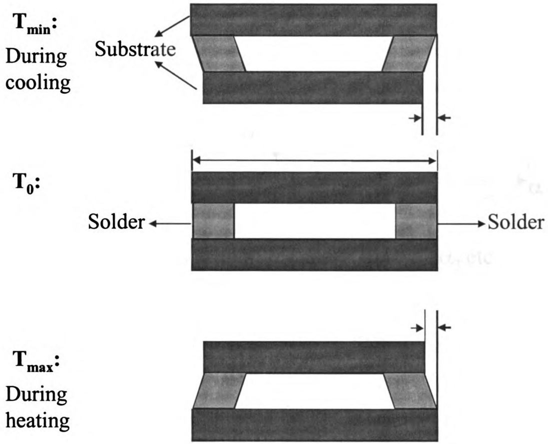

Figure 2.10. Schematic illustration of classic model for TMF of a soldered interconnection on a PCB [38].

Cont

Single

Figure

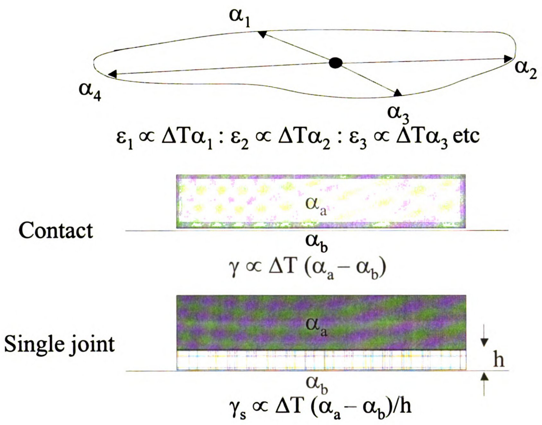

Figure 2.11. Various forms of thermal strains due to thermal fluctuations [38].

Figure 2.12.
Cu subs
IMC(Cu_6Sn
c

regimes of the

fatigue dominat

Table 2.2. CTE values of Cu, Cu_3Sn, and Cu_6Sn_5 [39].

Material	CTE value ($\times 10^{-6}$/°C)
Cu	17.1
Cu_3Sn	19.0±0.3
Cu_6Sn_5	16.3±0.03

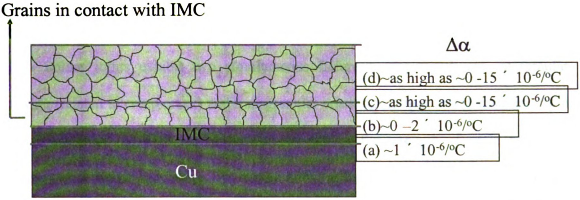

Figure 2.12. Schematic illustration of CTE mismatches involved in solder joints made on Cu substrate. Note: values are CTE mismatches between (a) Cu substrate and IMC(Cu_6Sn_5) layer, (b) IMC layer and Sn grains in contact with IMC, (c) Sn grains in contact with Sn grains adjacent to IMC, and (d) Sn grains in bulk

regimes of the failure modes in materials under cyclic loading. Such failure modes are fatigue dominated, fatigue-creep dominated, and creep dominated. Fatigue dominated failure ari

material, w

dominated

Intergraula

2.13(b)). D

cavitations

observed in

interact wit

endurance a

Sold

cracking (re

thermal cyc

becomes we

temperature

polycrystalli

the absolute

temperature

sliding, and b

As m

develop both

cracking may

failure arises due to the growth of surface cracks, i.e. fatigue striations, through the material, with no evidence of any creep damage as illustrated in Figure 2.13(a). Creep dominated failure is mainly due to dwells at various locations in the thermal cycle. Intergraular crack resulting from creep cavitations is major failure mode (see Figure 2.13(b)). During creep-fatigue interactions, surface fatigue damage developed with creep cavitations damage within the material. The fatigue crack growth rate is the same as that observed in a fatigue dominated fracture initially. However, the fatigue crack may interact with the creep damage, resulting in accelerated crack growth, a reduction in endurance and a fatigue crack interaction failure [40].

Solder joints exhibit two simultaneous failure modes which are intergraular cracking (related to creep crack) and transgranular cracking (fatigue crack) resulting from thermal cycling. At high temperature above $0.5T_m$, the strength of grain boundary becomes weaker than the lattice. As can be noted in Figure 2.14, there may be a certain temperature (equicohesive temperature) to change the deformation mode in polycrystalline materials. The equicohesive temperature may be approximately 50% of the absolute melting temperature of the materials. Thus, above the equicohesive temperature (depicted as T_c in Figure 2.14), the deformation is due to grain boundary sliding, and below T_c, the deformation is due to dislocation glide on lattice plane [41].

As mentioned earlier, solders will experience creep-fatigue interaction and develop both intergraular cracking and transgranular cracking. The transgranular cracking may be due to deformation in a grain resulting from dislocation glide on lattice

Tra
cra

Inte
crac

Inte
crac
tran
crak

2.1

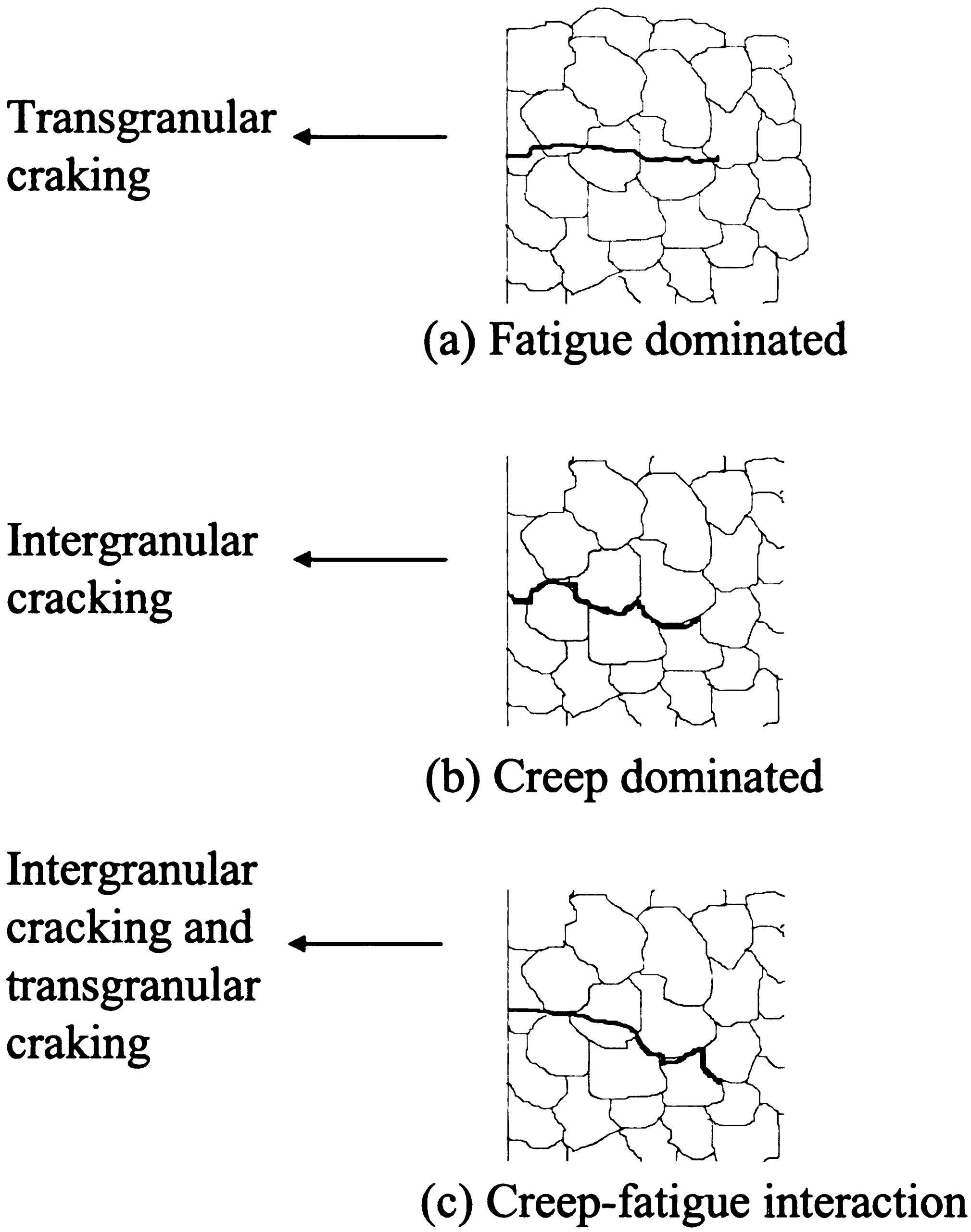

2.13. Schematic drawing of possible failure modes under TMF[40]

Figure 2.14

Figure 2.15. S

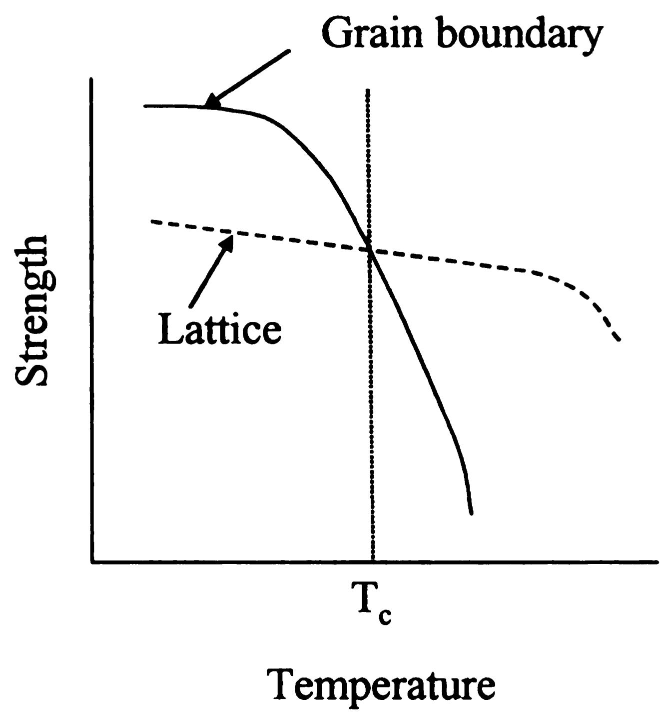

Figure 2.14. Graphical illustration of the effect of temperature on the strength of grain boundary and grain lattice materials [41].

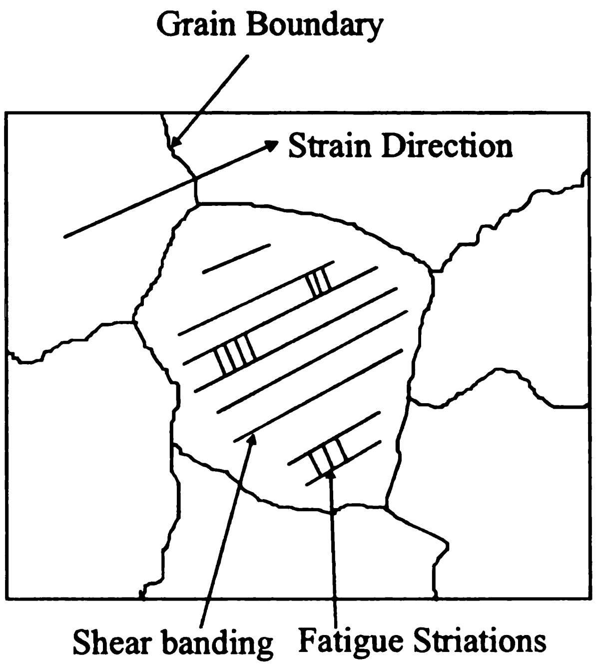

Figure 2.15. Schematic illustration of a possible surface damage in a grain due to TMF.

plane. Thi

[41].

Gra

when a sol

[42]. The s

is increased

grain bounc

grain bound

2.4-2. Com
bear

Stud

from TMF i

such as inte

decohesion,

expected. T

TMF is esse

been few st

experienced a

Kariy

showed bette

temperature e

Poon e

and reported th

plane. This can cause shear bandings and fatigue striations as illustrated in Figure 2.15 [41].

Grain boundary sliding can cause intergraular cracking during thermal cycling when a solder joint is being strained during temperature excursions in product application [42]. The solder undergoes plastic deformation due to stresses introduced as temperature is increased. Grain boundary sliding occurs with initiated cracks propagating along the grain boundaries resulting increase in surface (crack) area and energy [41]. Keying this grain boundary motion may be a best way to prevent crack propagation during TMF.

2.4-2. Comparison of Residual Mechanical Behavior after TMF between Lead-bearing and Lead-free Solder

Studies have clearly documented a significant amount of surface damage resulting from TMF in Sn-Ag based solder joints [43,44]. Based upon the evolution of damage such as intense shear bending, solder joint surface upheaval, grain boundary sliding and decohesion, degradation of residual strength of the solder joints due to TMF should be expected. Thus, an investigation of residual-mechanical properties of solder joints in TMF is essential to evaluate their reliability in microelectronic applications. There have been few studies dealing with residual-strength of lead-free solder joints that have experienced actual TMF [45,46].

Kariya et al. [45] reported that eutectic Sn-3.5Ag and Sn-Ag-0.5Cu solders showed better mechanical properties than eutectic Sn-37Pb after 1600 TMF cycles with temperature extremes between –30°C and 130°C in quad flat pack leads.

Poon et. al. [46] investigated residual shear strength of Sn-Ag and Sn-Pb solders and reported that Sn-Ag solder showed better thermal shock resistance than that of Sn-Pb solder wh

minutes o

reports are

solders are

2.5. ALLO

Mar

replacement

alloys are li

design to re

categorized

alloys are S

alloys, eutect

lead-free sol

shown in Fig

2.5.-1. Eutec

Studies have

equivalent to,

wettability, th

comparable to

solder is about

use eutectic Sn

limited solubilit

solder when solder joints were cycled 1000 times between –25°C and 125°C with 15 minutes of dwell at each temperature extreme. However, only a limited number of reports are available, and low-cycle fatigue characteristics and mechanisms of lead-free solders are not yet fully understood.

2.5. ALLOYING ADDITION IN TIN-SILVER BASED SOLDERS

Many investigators have attempted in the past decades to choose the best possible replacement candidates for lead-bearing solder. The requirements for suitable lead-free alloys are listed in Table 2.3 [47]. Various numbers of lead free solder alloys have been design to replace lead-bearing solders. They are all high tin solders. They can be categorized into binary, ternary and complex multi component systems. Binary solder alloys are Sn-Cu, Sn-Ag, Sn-Bi, Sn-Zn, and Sn-Sb, etc. Among these binary solder alloys, eutectic Sn-Ag solder has shown better mechanical properties than other Sn-based lead-free solder alloys under creep rupture test in the temperature range of 25-100°C as shown in Figure 2. 16 [48].

2.5.-1. Eutectic Sn-Ag system

Studies have shown that eutectic Sn-Ag solder exhibited thermal fatigue reliability equivalent to, or even better than, eutectic Sn-Pb solder [45-46]. Electrical conductivity, wettability, thermal conductivity, and CTE in eutectic Sn-Ag solder are noted to be comparable to conventional Sn-Pb solders. The melting temperature of eutectic Sn-Ag solder is about 40°C higher than conventional Sn-Pb solders. This can be an advantage to use eutectic Sn-Ag solder in high temperature applications. Also, Sn-Ag system has a limited solubility of Ag in Sn, making it more resistant to microstuctural coarsening, and

Relatively
Relatively
No Potenti > In > Sn <
Capable of
Alloys must
Capable of solder voids.
Compatible
Corrosion-res
Compatible lead substrate
Alloys must b
Metals used in
Low melting ter
Good electrical
Easy to repair
Adequate stren
Alloys must be a

Table 2.3. Requirements for suitable alternative lead-free alloys [22].

Requirements
Relatively Low-cost
Relatively non-hazardous
No Potential Environmental Problems; Ranking in decreasing order of safety is: Bi > Zn > In > Sn < Cu > Sb > Ag > Pb.
Capable of wetting common lead-free component and board finishes
Alloys must function with existing flux technologies and designations
Capable of forming a reliable solder joint, free of oxide inclusions and with minimal solder voids.
Compatible with relatively low temperature processing.
Corrosion-resistant and not prone to electrolytic corrosion potential
Compatible with copper substrates, immersion gold-over-nickel, and a variety of non-lead substrates, as well as leaded substrates
Alloys must be available in bar, wire, performs, spheres and paste forms
Metals used in alloying must be available in sufficient quantities
Low melting temperatures (< 240°C)
Good electrical conductivity and Good thermal conductivity.
Easy to repair
Adequate strength properties.
Alloys must be able to be easily recycled.

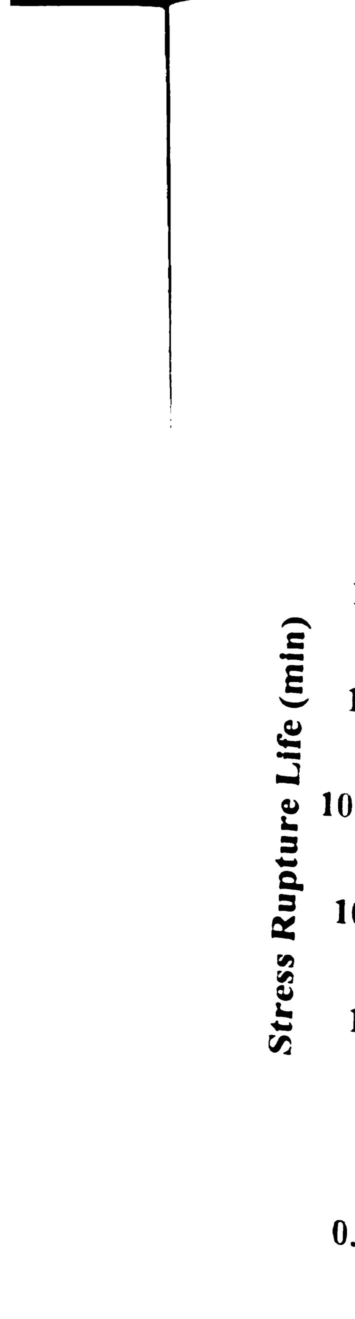

Figure 2.16. C

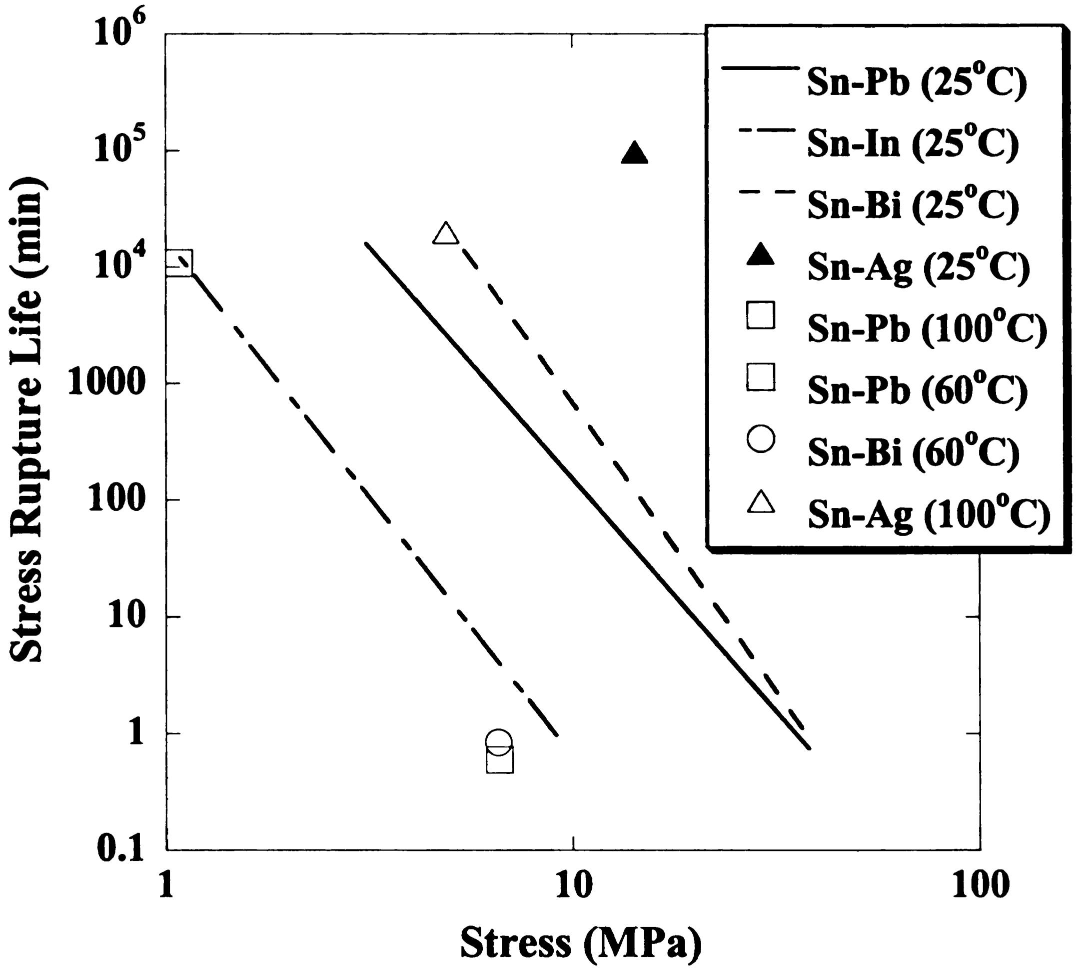

Figure 2.16. Comparison of creep rupture times of eutectic Sn-Ag, Sn-Bi, Sn-In, and Sn-Pb solders [50].

the Ag_3Sn

mechanical

Ag solder,

elements to

to replace le

2.5.-2. Sn-A

Near

The near-eut

Ag_3Sn and C

wt%: 0.5 to

during reflow

in solder joint.

by adding sma

Ag solder, Sn

properties than

Sn-Ag-Cu, and

temperature, Sn

Ag. However,

better creep-rup

found by Guo

joints. He repor

solder joints un

temperature to 85

the Ag_3Sn IMC precipitates are uniformly distributed to cause improvement in mechanical properties [50]. In order to improve the mechanical properties of eutectic Sn-Ag solder, significant number of studies have been conducted by adding alloying elements to Sn-Ag system. Currently, Sn-Ag-Cu alloys are believed to be the best choice to replace lead-bearing solders.

2.5.-2. Sn-Ag-Cu system

Near eutectic Sn-Ag-0.5Cu alloying is the leading candidate for lead-free solders. The near-eutectic ternary, alloys yield three phases upon solidification which are Sn, Ag_3Sn and Cu_6Sn_5 [51]. The melting point of Sn-Ag-Cu alloys (Ag wt%: 3.0 to 4.0, Cu wt%: 0.5 to 1.0) is typically observed as 217°C. Thickness of IMC layer that formed during reflow can be reduced with adding Cu. Because of the brittle nature of IMC layer in solder joints, it is believed to be an advantage to reduce the layer thickness of this layer by adding small amounts of Cu to eutectic Sn-Ag solder [52-53]. Similar to eutectic Sn-Ag solder, Sn-Ag-Cu solder alloys have shown equivalent to, or better mechanical properties than Sn-Pb. Grusd [54] have investigated creep rupture resistance of Sn-Ag, Sn-Ag-Cu, and Sn-Pb solders at both room temperature and at 100°C. Under ambient temperature, Sn-Ag-Cu solder exhibited better creep rupture resistance than eutectic Sn-Ag. However, at high temperature (100°C) creep-rupture test, Sn-Ag solder showed better creep-rupture than eutectic Sn-Ag-Cu (see Figure 2. 17). Similar behavior was found by Guo et. al [55] in eutectic Sn-Ag and Sn-4Ag-0.5Cu single shear lap solder joints. He reported that Sn-4Ag-0.5Cu solder joints performed better than eutectic Sn-Ag solder joints under creep at room temperature. However, upon increasing the test temperature to 85°C, eutectic Sn-Ag and Sn-4Ag-0.5Cu solder joints switched positions.

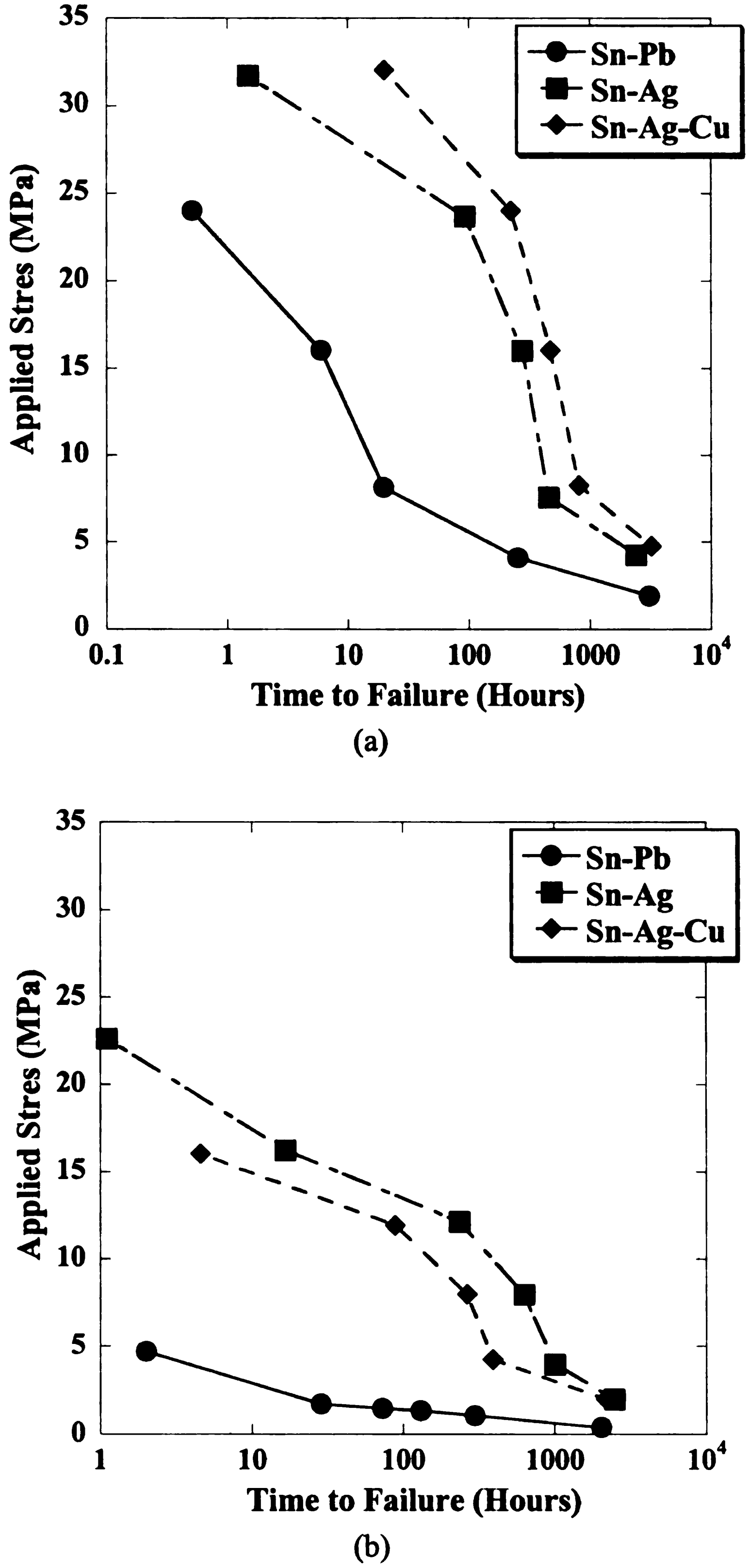

Figure 2.17. Creep rupture-resistance test of Sn-Ag, Sn-Ag-0.5Cu, and Sn-Pb. (a) room temperature, (b) 100°C [54].

Suhl

compared t

conducted u

with 50 min

0.7Cu) exhib

+125°C. Ho

joints for the

such results

substitutions

adding bism

properties un

indicates tha

properties of

2.5-3. Sn-Ag

The m

reduced melti

the Bi solubil

in better mec

adding Bi cau

isothermal fati

brittle for a me

2.5-4. Sn-Ag-

Similar

Suhling et. al. [56] reported TMF reliability of Sn-Ag-Cu-X solder joints compared to 67Sn-37Pb solder joint using leadless chip carriers. TMF tests were conducted using two different temperature ranges (-40°C to 125°C, and -40°C to 150°C) with 50 minutes hold times at each temperature extreme. The SAC alloy (95.5Sn-3.8Ag-0.7Cu) exhibited similar reliability to standard 63Sn-37Pb after TMF test from -40°C to +125°C. However, 63Sn-37Pb joints dramatically outperformed the lead-free SAC alloy joints for the more extreme TMF test between -40°C and +150°C. He pointed out that such results further emphasize the need to be cautious when proposing lead-free solder substitutions for SMT configurations in harsh environments. He also pointed out that adding bismuth (Bi) or indium (In) into SAC alloy improved the residual mechanical properties under TMF test with imposing temperature range from -40°C to +150°C. It indicates that a certain alloy addition can play significant roles to improve mechanical properties of SAC alloy.

2.5-3. Sn-Ag-Cu-Bi system

The most important advantage to adding bismuth (Bi) in Sn-Ag-Cu system is a reduced melting temperature that is desired for manufacturing purposes [57]. However, the Bi solubility is limited to about 1% in Sn-Ag-Cu alloys. Initially, adding Bi resulted in better mechanical properties than other Sn-Ag based lead-free solders. However, adding Bi causes drastic degradation on fatigue life after larger number of cycles under isothermal fatigue cycling or TMF cycling. This is likely due to the fact that Bi is rather brittle for a metal [45, 57-58].

2.5-4. Sn-Ag-Cu-In system

Similarly with adding Bi into the Sn-Ag-Cu (SAC) alloy, the addition of indium

(In) to the S.

indium into S

effects of In

exhibited gre

the melting te

However, Ind

using indium

2.5-5. Sn-Ag

Study c

of Sn-1.2Ag-0

Ag-0.5Cu all

microstructure

together with

strain hardeni

quaternary sol

fourth alloy ele

2.6. ALLOYI OF TIN-S

Hardeni

through the ma

the dislocation.

from the interac

homogeneity wh

(In) to the SAC alloy assists in a reducing melting temperature. The ranges of adding indium into SAC alloy are from 4 wt % to 8 wt %. Hwang [57] et. al. have reported effects of In addition on fatigue life of SAC alloy. Sn-4.1Ag-0.5Cu-8.0In solder joints exhibited greater strength and fatigue life than eutectic Sn-Pb solder joints (SMT), and the melting temperature was about 200°C which was about 20°C lower than Sn-Ag solder. However, Indium is an expensive material. Thus, processing cost may be a problem for using indium containing solder alloys.

2.5-5. Sn-Ag-Cu-Ni system

Study carried out by Kariya et. al. [59] indicated that low cycle fatigue resistance of Sn-1.2Ag-0.5Cu-0.05Ni for flip chip interconnections was equivalent to that of Sn-3 Ag-0.5Cu alloy. He also pointed out that this quaternary solder alloy had fine microstructure and Ag_3Sn intermetallic compound which made a network structure together with fine $(Cu,Ni)_6Sn_5$ compound. This microstructure resulted in high cyclic strain hardening exponents, which lead to good low cycle fatigue endurance of the quaternary solder alloy. However, only a few studies have investigated the effects of fourth alloy elements to SAC alloy.

2.6. ALLOYING APPROACHES TO ENHANCE MECHANICAL PROPERTIES OF TIN-SILVER BASED SOLDERS

Hardening of a material can be achieved by pinning the motion of dislocation through the material. In the structure, an obstacle is immobile, which exerts a force on the dislocation. Forces on dislocations arise from externally applied stresses and also from the interaction of the stress field which surrounds every dislocation with any in homogeneity which produces a distortion in the crystal structure [60]. In order to achieve high stren

barriers sh

in most st

strengthene

introduced

solution or

and system-

can prevent

Sn-Ag based

motion betw

hard second-

adjacent Sn-

been significa

Sn-Ag based

generation ar

based solder j

high strength in a metal, all dislocations should be eliminated or as many as powerful barriers should be created for dislocation motion. The latter approach is the one chosen in most strengthening mechanisms. It is well known that metals and alloys can be strengthened by the presence of fine second-phase particles [61]. Such particles may be introduced to the solder either by precipitation from supersaturated solid or liquid solution or by external addition of foreign dispersoids [62]. The presence of fine, stable, and system-compatible second-phase precipitates located at the Sn-Sn grain boundaries can prevent grain boundary sliding, which is one of major deformation mechanisms in the Sn-Ag based solder alloys under TMF [63]. As illustrated in Figure 2.18, grain boundary motion between adjacent Sn-Sn grains can be retarded by introducing fine, stable, and hard second-phase precipitates as barriers to prevent grain boundary motion between adjacent Sn-Sn grains [63]. As mentioned in earlier sections (section 2.5), there have been significant attempts to improve the mechanical and, particularly, TMF behavior of Sn-Ag based solder alloys by adding alloying elements. However, more studies and data generation are needed to understand the roles of alloying elements in improving the Sn-based solder joint reliability.

Grain
betwe
grains

Figure 2.18. S
at high temp
obstacles, and
par

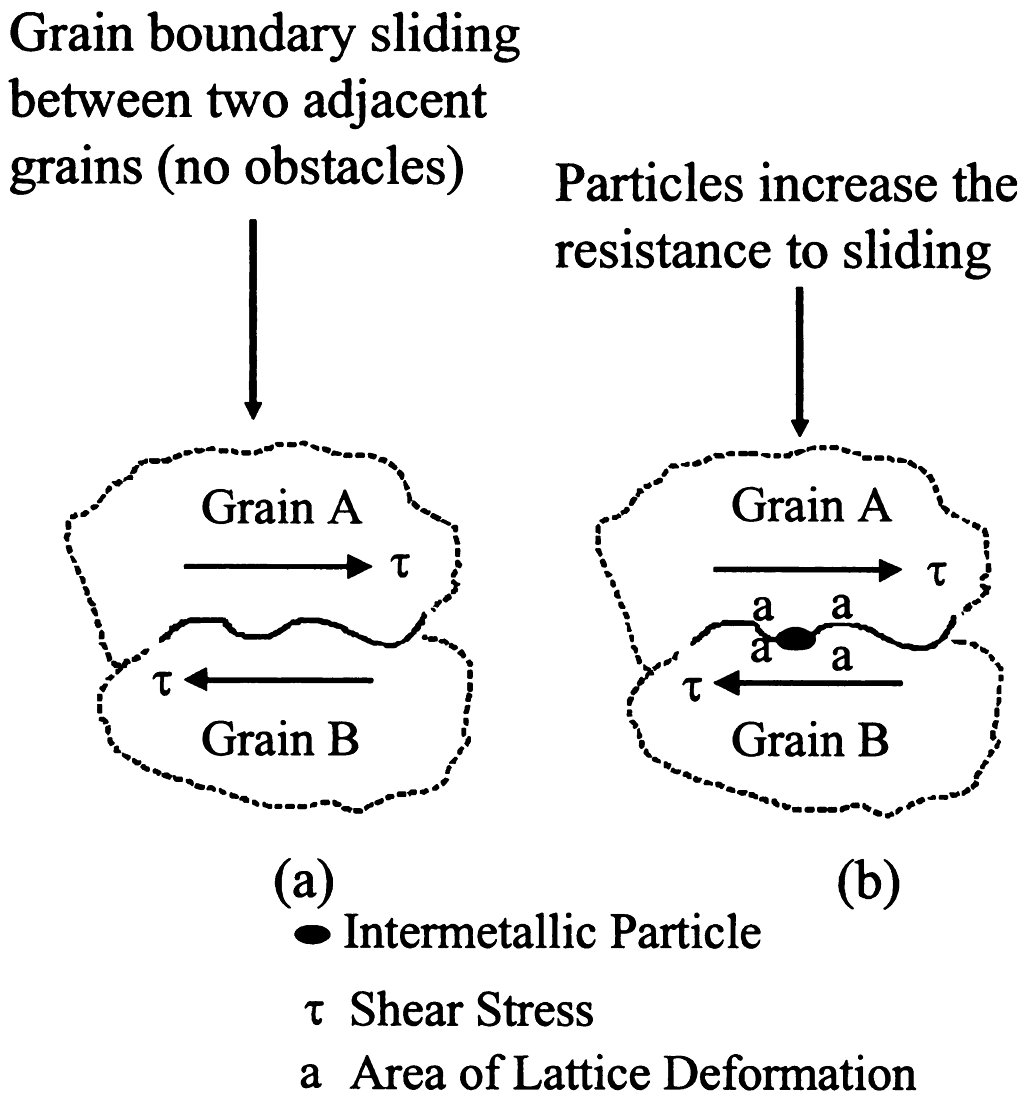

Figure 2.18. Schematic illustration of grain boundary sliding due to shear forces applies at high temperature. (a) grain boundary sliding between two adjacent grains with no obstacles, and (b) grains undergo lattice deformation due to presence of an intermetallic particle on the grain boundary during grain boundary sliding [63].

3.1. MATE

The s

(iii) Sn-2.5A

pastes are as-

alloys was pu

3.1 were mac

to simulate th

3.2. THE PR

Copper

to soldering to

aluminum fixt

each copper d

spread of sold

about 100 μm

sandwiched bet

The entire alun

allowed to reac

aluminum plate

only the eutectic

joints can be

heating cooling h

CHAPTER 3

EXPERIMENTAL PROCEDURE

3.1. MATERIALS USED

The solder materials used in this study are (i) eutectic Sn/Ag (ii) Sn-4Ag-0.5Cu, (iii) Sn-2.5Ag-0.5Cu-0.5Ni, and (iv) Sn-2Ag-1Cu-1Ni in paste forms. These solder pastes are as-received. The substrate material used to make solder joints using solder alloys was pure copper. Cu dogbone halves which had the dimensions shown in Figure 3.1 were machined using EDM, to obtain a reduced width of 1 mm from a copper sheet, to simulate the actual solder joint geometry in the electronic applications.

3.2. THE PREPARATION OF SOLDER JOINTS

Copper dog-bone halves were pre-cleaned with a 50 % aqueous HNO_3 just prior to soldering to remove the thin tarnish layers. Copper dog-bone halves were placed in an aluminum fixture designed to hold the Cu dog-bones in their proper alignment. Between each copper dog-bone, about 600 μm thickness of glass plates are placed to prevent the spread of solder beyond the 1 mm^2 soldered area at the end of each half and produce about 100 μm thickness of solder joints. Proper amounts of solder paste were sandwiched between the two Cu dog-bone halves. The assembly is shown in Figure 3.2. The entire aluminum fixture was placed on a preheated (about 500°C) hot plate and allowed to reach a temperature of 250°C for the solder before being removed to the an aluminum plate to cool. The Cu_6Sn_5 intermetallic η-phase remained in the solid state and only the eutectic Sn-Ag was reflowed and solidified during soldering process. Ten solder joints can be manufactured in the aluminum fixture at a time following the heating/cooling history shown in Figure 3.3.

0.5

Fi

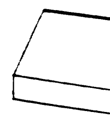

Figure 3.2

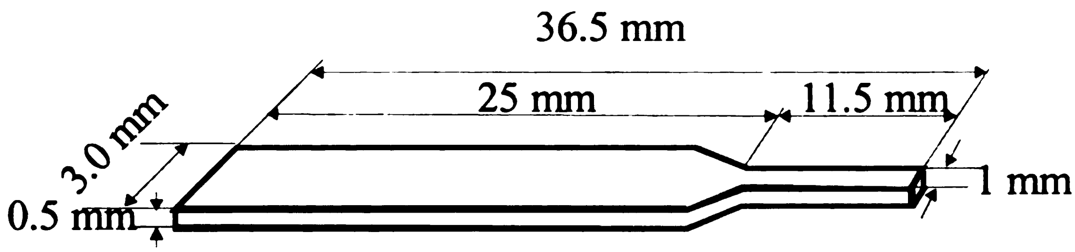

Figure 3.1. Schematic drawing of the dimensions of the Cu Substrate

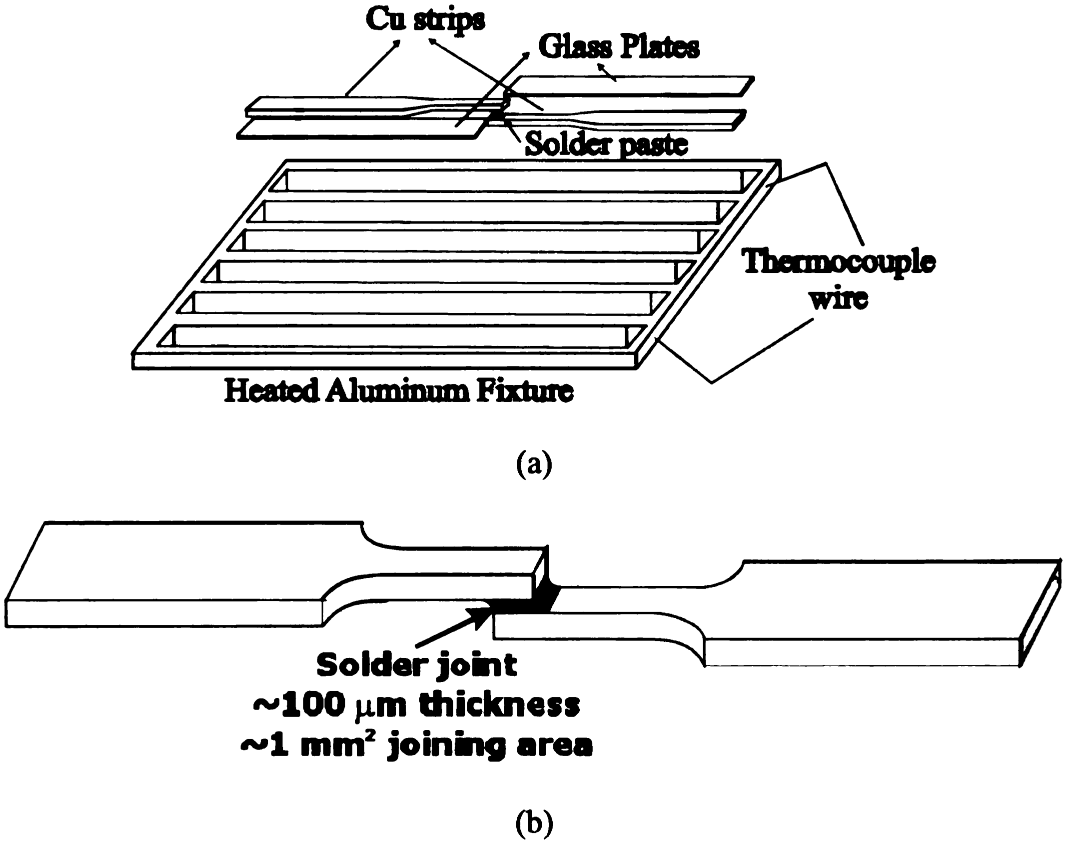

Figure 3.2. Schematic drawings of (a) the solder joint fixture assembly and (b) a fabricated single shear-lap joint

Figure 3.3.

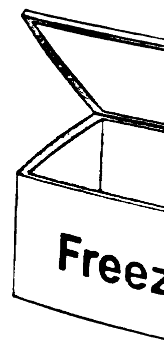

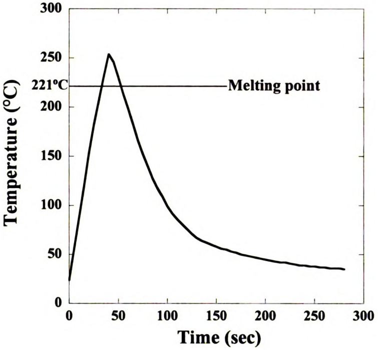

Figure 3.3. Temperature versus time profile for manufacturing of Sn-Ag based solder joints.

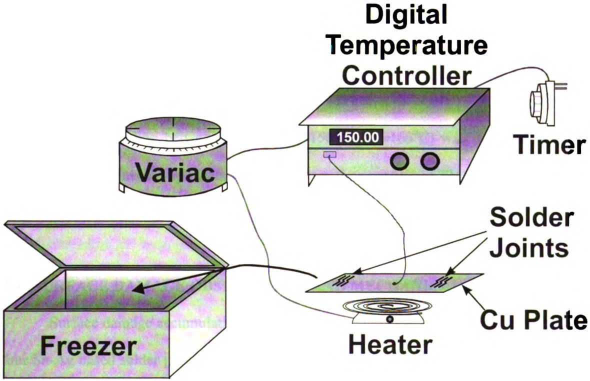

Figure 3.4. Schematic drawing of TMF set-up.

One s

from 400 to 2

suspensions.

microstructur

3.3. THERM

Figure

controllable ra

as a heating sc

as the cooling

solder joint sp

control the ten

Power to the

heating rate ca

was controlled

Therma

solder joints w

each chapter th

3.4. SURFAC

Surface

four Sn-Ag base

Microscopy (SE

One side of the single shear lap joint was polished using series of grinding papers from 400 to 2000 grit and then final polishing was done by using 0.05 μm SiO_2 colloidal suspensions. The specimen was washed with methanol prior to observing the microstructure in scanning electron microscope.

3.3. THERMOMECHANICAL FATIGUE (TMF) SET-UP

Figure 3.4 shows TMF set-up. A thermomechanical fatigue set-up with controllable ramp-up and dwell times was designed. This set-up consisted of a hot-plate as a heating source inside a common household freezer where temperature is -15°C, used as the cooling source. A copper plate placed on the hot plate was used as a stage for the solder joint specimens. Thermocouples were placed on the metal stage to measure and control the temperature. The heating element was turned on and off by an external timer. Power to the heating element was provided through a variable transformer so that the heating rate can be adjusted and controlled. The dwell times at the temperature extremes was controlled by the external timer, which turned the heater on or off.

Thermal cycling between –15°C and +150°C (ΔT=165°C) was imposed on the solder joints with this set-up. Detailed temperature-time profiles of TMF will be given in each chapter that investigates each service parameter during TMF.

3.4. SURFACE DAMAGE OBSERVATION AND MECHANICAL TESTS

Surface damage accumulation at the exact same-targeted area was observed in the four Sn-Ag based solder joints after 0, 250, 500, and 1000 cycles by Scanning Electronic Microscopy (SEM). Some of the solder joints were removed after 250 and 500 cycle intervals to a

screw-driven

room temper

microscope t

measured loa

stress values

fracture toug

obtained for s

3.5. ECHINO

To inv

these four Sn

1.5cm) with th

Due to difficu

was used to c

location of pre

the cut surface

solder joint pro

vol % methano

etched side of

and TMF studie

cross-sectioned

interface as illus

intervals to assess the residual mechanical behavior. The shear test was carried out on a screw-driven tensile testing machine using a fixed crosshead speed at 0.5 mm/min at room temperature. The failed solder joints were examined either in the SEM or optical microscope to determine the true soldered area after excluding the pore area. The measured load values from the screw-driven tensile testing machine were converted to stress values by using the true solder joint area. The residual shear strength and residual-fracture toughness (measured by the area underneath the stress-strain curve) were obtained for solder joint specimens that have experience selected TMF cycles.

3.5. ECHING PROCEURE

To investigate the role of microstructural features, specimens were made with these four Sn-Ag based solder pastes by reflow on copper substrates (2cm x 2cm x 1.5cm) with the same heating profile used to fabricate the single shear-lap solder joints. Due to difficulty to etch the small area of solder joint, the following alternative method was used to observe larger etched solder area to reveal Sn-Sn grain boundaries and location of precipitates. The solder buttons formed on Cu substrate were sectioned and the cut surfaces of these specimens were metallurgically polished as same procedure as solder joint preparations. These specimens were then etched with 5 vol % HNO_3 and 95 vol % methanol for 1 second and washed with water. Cross sections of polished and etched side of specimens were examined using SEM. The solder joints used for creep and TMF studies had a joint thickness about 100 μm. As a consequence, the specimens cross-sectioned and etched were observed in regions within 50 μm from Cu/solder interface as illustrated in Figure 3.5.

SECTION

300 µm
500 µm

Figure 3

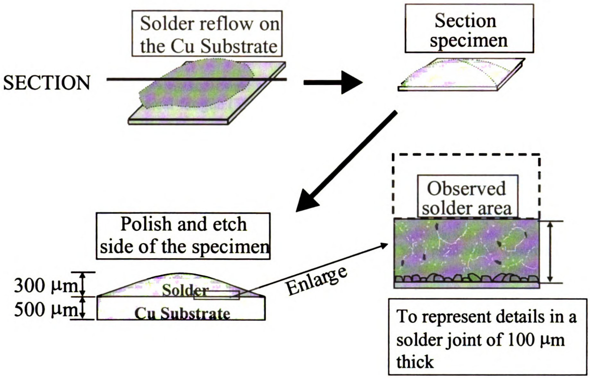

Figure 3.4. Schematic drawing of solder specimen preparation for etching.

RESIDU
FATIG
LO

ABSTRAC

Ther

expansion (

properties o

TMF on th

solder and

between –15

for the cooli

low extreme

TMF cycles

Alloying ele

TMF.

4.1. INTRO

Lead-

interconnecti

past several

environmenta

candidates is

comparable t

CHAPTER 4

RESIDUAL-MECHANICAL BEHAVIOR OF THERMOMECHANICALLY FATIGUED TIN-SILVER BASED SOLDER JOINTS UNDER TMF WITH LONGER DWELL TIMES AT LOW TEMPERATURE EXTREME

ABSTRACT

Thermomechanical fatigue (TMF) due to the mismatch in coefficients of thermal expansion (CTE) between solder and substrate gradually degrades the mechanical properties of electronic solder joints during service. This study investigated the role of TMF on the residual-mechanical behavior of solder joints made with eutectic Sn-Ag solder and Sn-Ag solder with Cu and/or Ni additions. TMF tests were carried out between –15°C and +150°C with a ramp rate of 25°C/min for heating segment and 7°C for the cooling segment. The hold times were 20 min at high extreme and 300 min at the low extreme. Residual shear strength was found to drop significantly during the first 250 TMF cycles, although it did remain relatively constant between 250 and 1000 cycles. Alloying elements were found to affect the residual creep strength of solder joints after TMF.

4.1. INTRODUCTION

Lead-tin solders have been used extensively as joining materials for the interconnection and packaging in modern electronic components and devices over the past several decades. However, alternatives for these solders are being sought due to environmental and economic issues [64-67]. One of the attractive lead-free solder candidates is tin-silver based solder because the reliability and mechanical properties are comparable to lead-tin solders. In high temperature applications such as in automotive under-the-h

due to it's

industrial a

elements to

physical m

of adding a

[68-70].

Sold

mismatches

to such the

service. As

been studies

data is neede

Studi

from TMF i

such as inten

decohesion a

to TMF shou

solder joints

applications.

solder joints

eutectic Sn-3.5

eutectic Sn-37

under-the-hood, aerospace, military applications, eutectic tin-silver solder is appropriate due to it's higher melting point. However, this solder may not be appropriate in some industrial applications due to cost concerns. It was found that adding third or fourth alloy elements to tin-silver solder can depress the melting temperature and/or improve some physical/mechanical properties. There have been several studies to investigate the effects of adding alloying elements in enhancing the performance of eutectic tin-silver solder [68-70].

Solder joints in service conditions experience internal thermal stresses due to CTE mismatches between the component leads, solder, and the substrate. TMF will occur due to such thermal stresses that develop during temperature excursions encountered during service. As a result, mechanical deformation will occur in the solder joints. There have been studies of TMF on lead-tin solder during last decade [71-74]. However, additional data is needed on the TMF on lead-free solders.

Studies have clearly documented a significant amount of surface damage resulting from TMF in Sn-Ag based solder joints [44,65]. Based upon the evolution of damages such as intense shear bending, solder joint surface upheaval, grain boundary sliding and decohesion and surface cracking, degradation of residual strength of the solder joints due to TMF should be expected. Thus, an investigation of residual-mechanical properties of solder joints in TMF is essential to evaluate their reliability in microelectronic applications. There have been few studies dealing with residual-strength of lead-free solder joints that have experienced TMF [4,45,46]. Kariya et. al. [45] reported that eutectic Sn-3.5Ag and Sn-Ag-0.5Cu solders showed better mechanical properties than eutectic Sn-37Pb after 1600 TMF cycles with temperature extremes between $-30^{o}C$ and

130°C in q

Ag and Sn

resistance t

with 15 min

understandi

lead-free so

In th

between −15

shear and cr

mechanical b

4.2. EXPER

Solder

0.5Cu-0.5Ni,

These

solder joints

configurations

procedure used

was metallurgic

15°C and +150

cooling segmen

extreme. The d

Specimens expe

130°C in quad flat pack leads. Poon et. al. [46] investigated residual shear strength of Sn-Ag and Sn-Pb solders and reported that Sn-Ag solder showed better thermal shock resistance than that of Sn-Pb solder when cycled 1000 times between –25°C and 125°C with 15 minutes of dwell at each temperature extreme. However, there is no guidance for understanding the role of alloying element addition to improve the TMF resistance of the lead-free solder joints in the published literature [44-46,75].

In this study, four different tin-silver based solder alloys were subjected to TMF between –15°C and 150°C. The residual-mechanical behaviors were examined by simple shear and creep tests to evaluate the effects of alloying element addition on the residual mechanical behavior of TMF'ed tin-silver based solder joints.

4.2. EXPERIMENTAL PROCEDURE

Solder joints made with (*i*) eutectic Sn-3.5Ag, (*ii*) Sn-4Ag-0.5Cu, (*iii*) Sn-2.5Ag-0.5Cu-0.5Ni, and (*iv*) Sn-2Ag-1Cu-1Ni solder pastes were used in this study.

These studies were designed to represent service environments experienced by the solder joints used in automotive/microelectronic industrial applications. The detailed configurations of the dog-bone shaped single shear-lap solder joint and the soldering procedure used have been reported in other publications [76,77]. The side of solder joints was metallurgically polished prior to TMF test. The TMF test was carried out between –15°C and +150°C with a ramp rate of 25°C/min for heating segment and 7°C/min for the cooling segment. The hold times were 20 min at high extreme and 300 min at the low extreme. The details of the TMF set up used in this study can be found elsewhere [44]. Specimens experienced 250, 500, and 1000 TMF cycles and the microstructure and mechanical

this study w

Mec

room tempe

(1) Simple s

The

using a fixed

shear strengt

stress-strain

selected TMF

(2) Creep test

Creep

loading on a

Figure 4.1. A

shown in Figu

elevated tempe

and the temper

joint as shown

duration of the

After si

observed using a

mechanical properties were evaluated. The maximum number TMF cycles employed in this study was 1000.

Mechanical evaluation consisted of (1) simple shear test, and (2) creep tests at room temperature and at 85°C.

(1) Simple shear test

The simple shear test was carried out on a screw-driven tensile testing machine using a fixed crosshead speed at 0.5 mm/min at room temperature. The residual-simple shear strength and residual-fracture toughness (measured by the area underneath the stress-strain curve) were obtained for solder joint specimens that have experience selected TMF cycles.

(2) Creep test

Creep tests were conducted at room temperature and at 85°C using dead weight loading on a miniature creep testing frame fixed on an optical microscope, as shown in Figure 4.1. An excimer laser ablation mapping technique was used to determine strain as shown in Figure 4.2. The detail of this technique can be found elsewhere [78,79]. For elevated temperature tests, a heating pad was affixed to the Cu strip as a heating source and the temperature was monitored using a thermocouple kept in contact with the solder joint as shown in Figure 4.3. The temperature was maintained to within ± 2°C for the duration of the creep test.

After simple shear and creep tests, the fracture surfaces of each joint were observed using a scanning electron microscope.

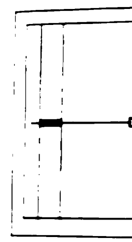

Figure

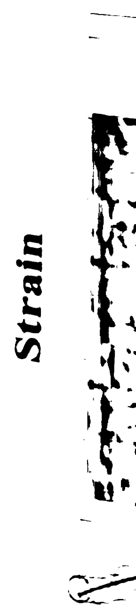

Figure 4.2.

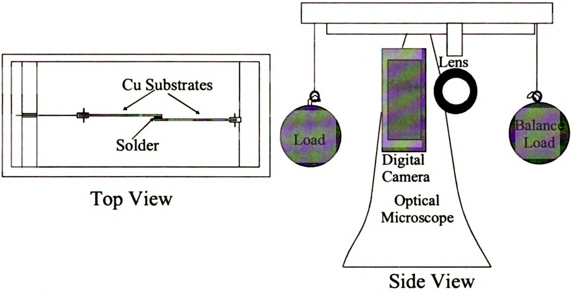

Figure 4.1. Schematic of setup of dead weight loading miniature creep flame.

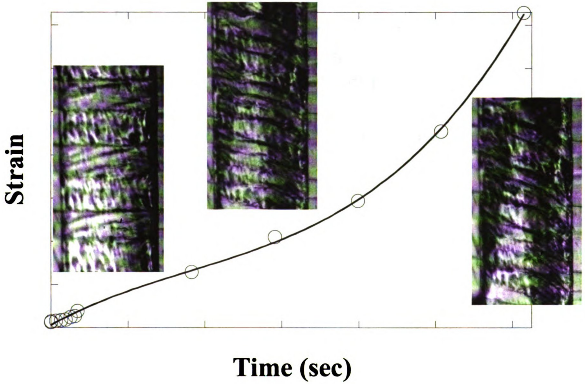

Figure 4.2. Illustration of analyzing creep strain using excimer laser-ablation mapping technique.

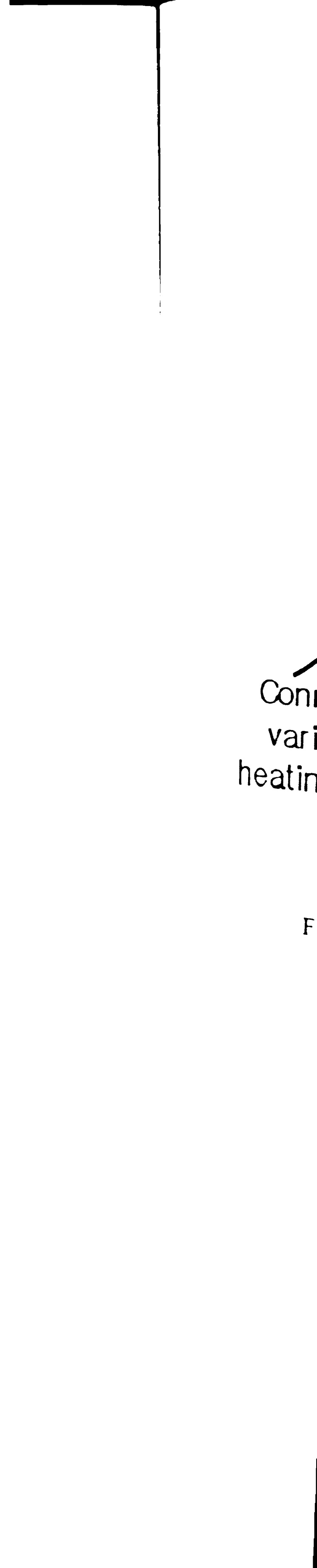

F

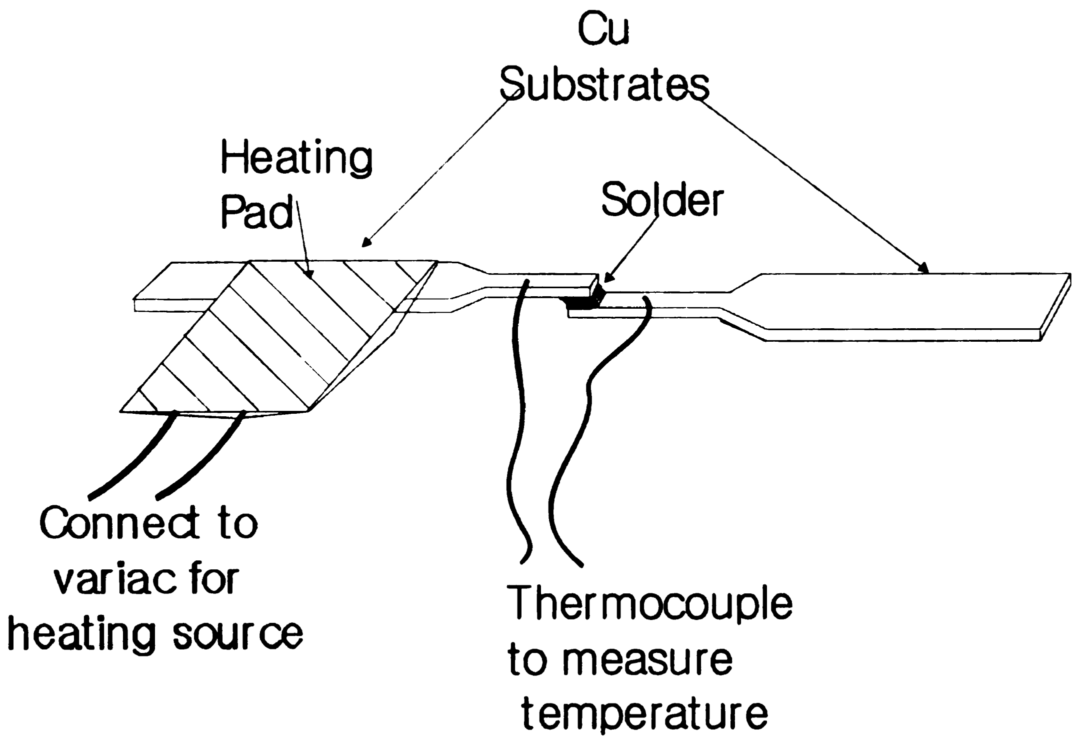

Figure 4.3. Schematic drawing of high temperature creep setup.

4.3. RES

4.3-1. Eff

Inte

decohesion

strength of

evaluate the

absolute and

are presente

strength as a

However, no

250 and 100

simple shear

elements coul

drop in the re

cycles [45-46]

Sn-Ag-0.5Cu s

after about 100

4.1. A similar

The are

joints studied.

condition. For

4.3. RESULTS AND DISCUSSION

4.3-1. Effect of TMF Cycles on Simple Shear Behavior of Solder Joints

Intense shear banding, solder joint surface upheaval, grain boundary sliding and decohesion and surface cracking, of solder joints resulting from TMF can reduce the strength of solder joints. The residual simple shear strength can be used to quantitatively evaluate the effect of TMF damage on solder joints. The effect of thermal cycles on the absolute and normalized residual simple shear strength of four Sn-Ag based solder joints are presented in Figures 4.4 and 4.5. There is an initial drop in residual-simple shear strength as a consequence of 250 TMF cycles in all four Sn-Ag based solder joints. However, no significant decrease of the residual-simple shear strength was noted between 250 and 1000 TMF cycles. Although Sn-4Ag-0.5Cu solder joint exhibited the highest simple shear strength in the as-joined condition, no apparent influence of alloying elements could be realized in the residual strength after 250 and 1000 TMF cycles. The drop in the residual-simple shear strength was approximately 30~60 % after 250 TMF cycles [45-46]. According to these studies the residual strength of eutectic Sn-Ag and Sn-Ag-0.5Cu solder joints were not significantly affected by thermally induced stress after about 1000 TMF cycles [45,46]. Findings of these studies are summarized in Table 4.1. A similar trend was reported in other studies that used different joint configurations.

The area under the stress-strain curve before fracture was measured for all solder joints studied, and normalized by corresponding value for the joint in the as-joined condition. For example, the fracture toughness of as-joined solder joint was set as 1 and

Table 4.1

Investigator
Kariya et. al
Poon et. al.
Ahat et. al.

Figure 4.4. Ef

Table 4.1. Comparison of residual strength of eutectic Sn-Ag solder joints in various specimen configurations [45-46,75]

Investigators	Specimen configuration	Range ΔT	Max. No. of cycles	Initial about after 200 cycles	Compared between 200 and Max cycles
Kariya et. al.	Quad Flat Pack Lead	160°C	1200 cycles	~97 %	~78 %
Poon et. al.	PCB	150°C	1000 cycles	~87 %	~67 %
Ahat et. al.	PCB	190°C	2000 cycles	~73 %	~ 41 %

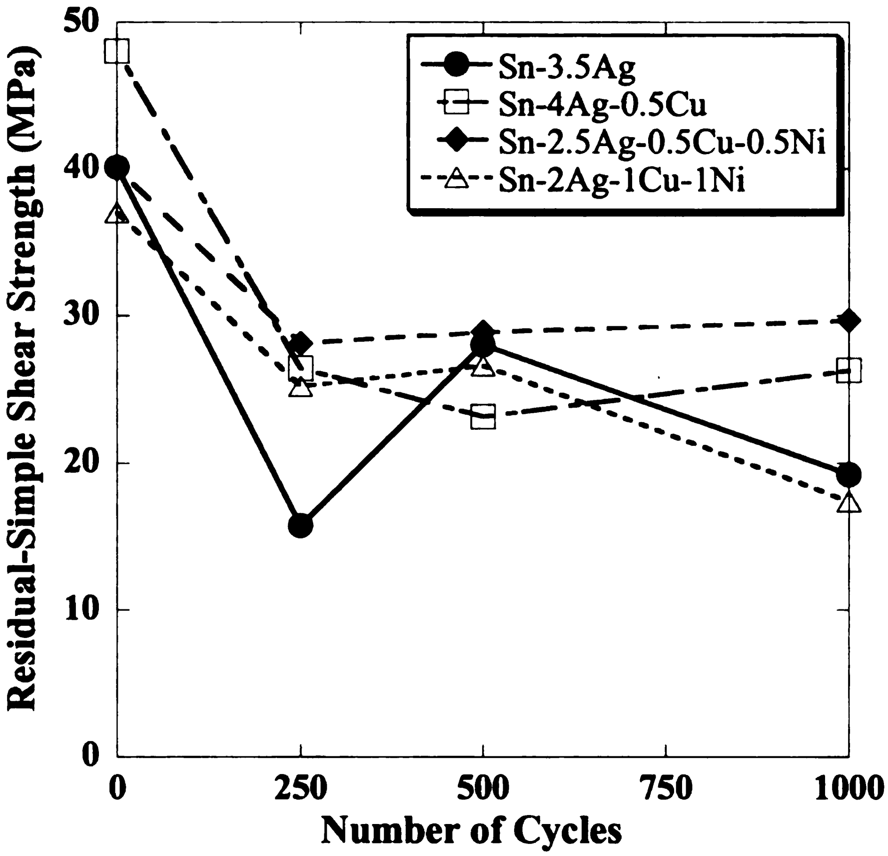

Figure 4.4. Effect of thermal cycles on the residual-simple shear strength of four Sn-Ag based solder joints

Figure 4.5. N

Figure 4.6. Nor

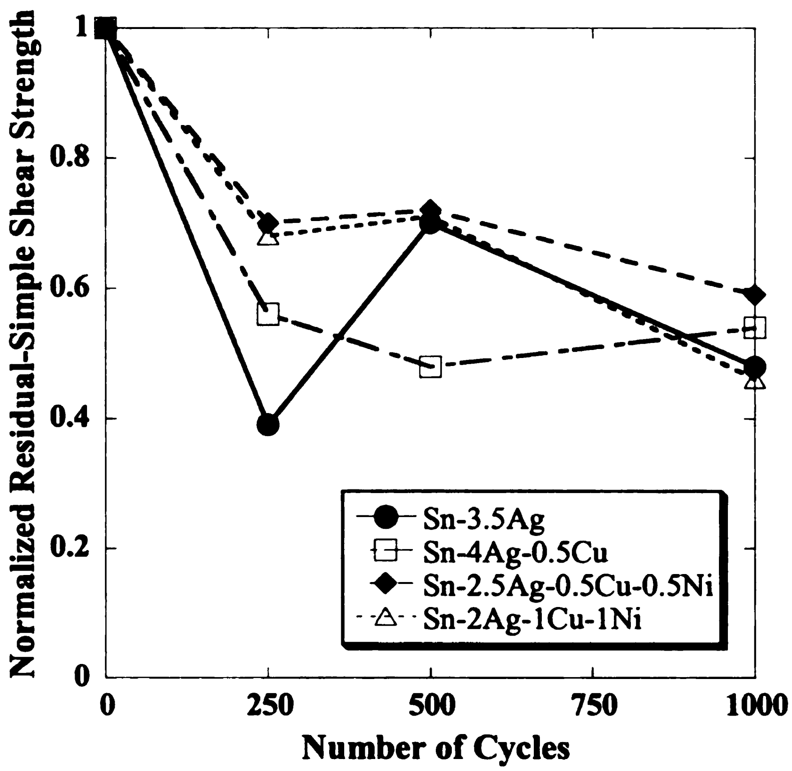

Figure 4.5. Normalized residual-simple shear strength as function of thermal cycles for four Sn-Ag based solder joints.

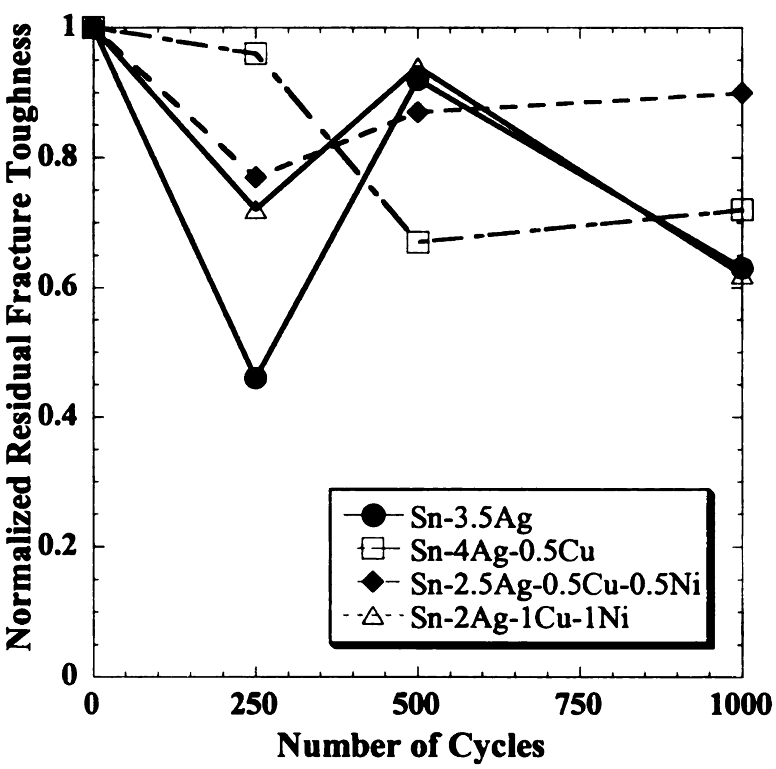

Figure 4.6. Normalized residual fracture toughness as function of thermal cycles for four Sn-Ag based solder joints.

fracture tou

fracture tou

in Figure 4.6

found to be

toughness is

significant d

a finding ind

of TMF cycl

4.3-2. Effect

Alloy

Ag based sol

joints subject

symbols repr

specimens cre

correspondin

also given in F

As can

deteriorates its

behavior was a

joints after 100

no significant d

fracture toughness of solder joints after TMF was indexed. Such normalized residual fracture toughness was plotted as a function of the number of TMF cycles and presented in Figure 4.6. The trend of a decrease in the residual fracture toughness due to TMF was found to be similar to that for residual-simple shear strength. The initial drop in fracture toughness is found to occur between 0 and 250 cycles. Similarly, there is no additional significant drop in residual fracture toughness between 250 and 1000 TMF cycles. Such a finding indicates that the ductility of the solder joints deteriorates during the early parts of TMF cycles.

4.3-2. Effect of TMF cycles on the Creep Resistance of Solder Joints

Alloy additions have been found to alter of the creep behavior of as-fabricated Sn-Ag based solder joints [55]. Secondary creep strain rates of the chosen three solder alloy joints subjected to TMF cycles are presented in Figure 4.7(a)-(c). In these figures, closed symbols represent specimens crept at room temperature while open symbols represent specimens crept at 85°C. Dotted lines were used to identify trends. For comparison the corresponding values for the as-fabricated joints adapted from our previous studies are also given in Figure 4.7(a)-(c) [55].

As can be observed from Figure 4.7(a), TMF of eutectic Sn-3.5Ag solder joint deteriorates its room temperature creep resistance by one order of magnitude. Similar behavior was also noted during creep at 85°C. The residual-creep resistance of solder joints after 1000 cycles was not significantly different from that of 250 cycles. There was no significant difference in the creep resistance of eutectic Sn-Ag solder joints as a

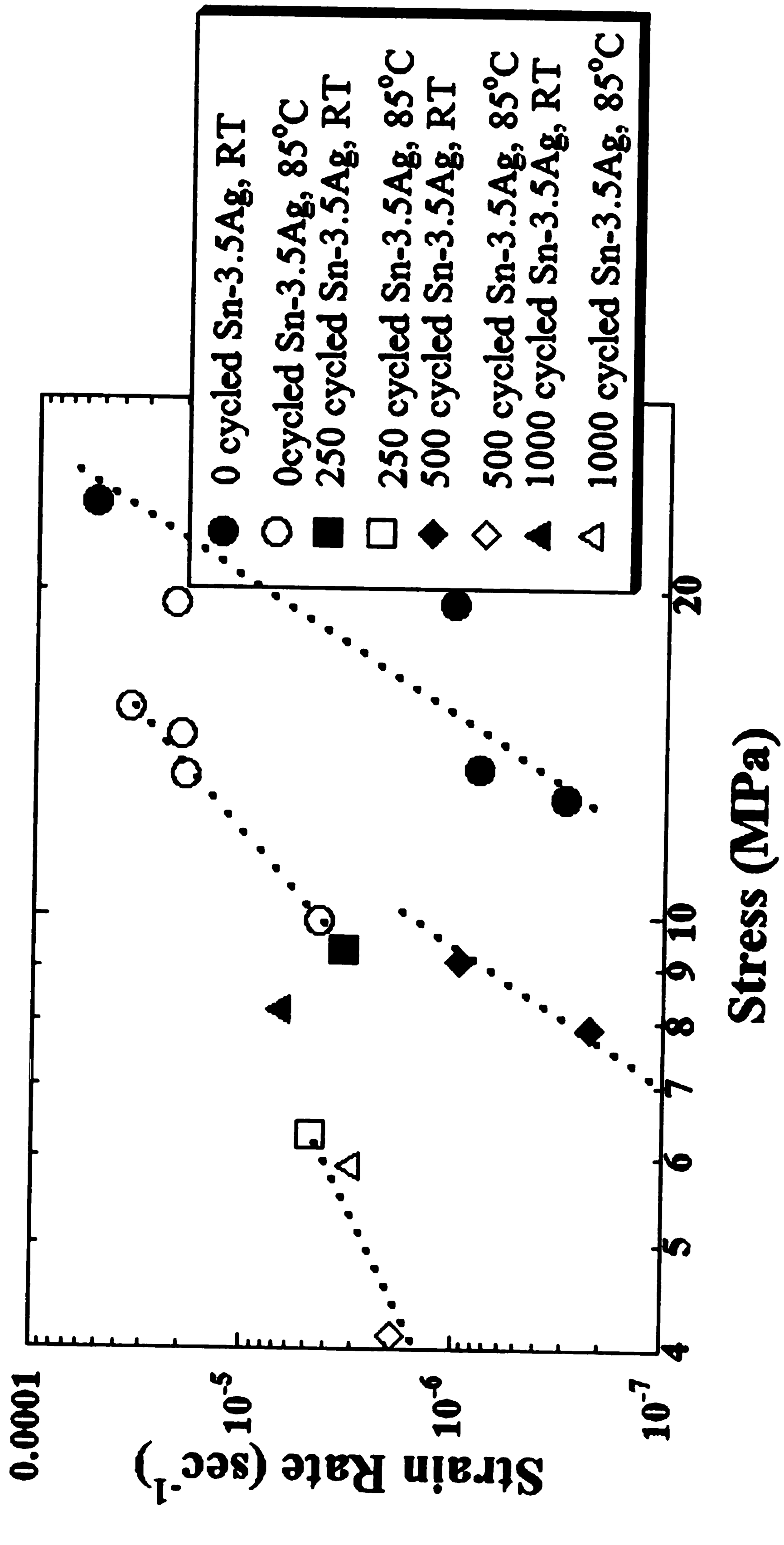

(a) Sn-3.5Ag (cont'd)

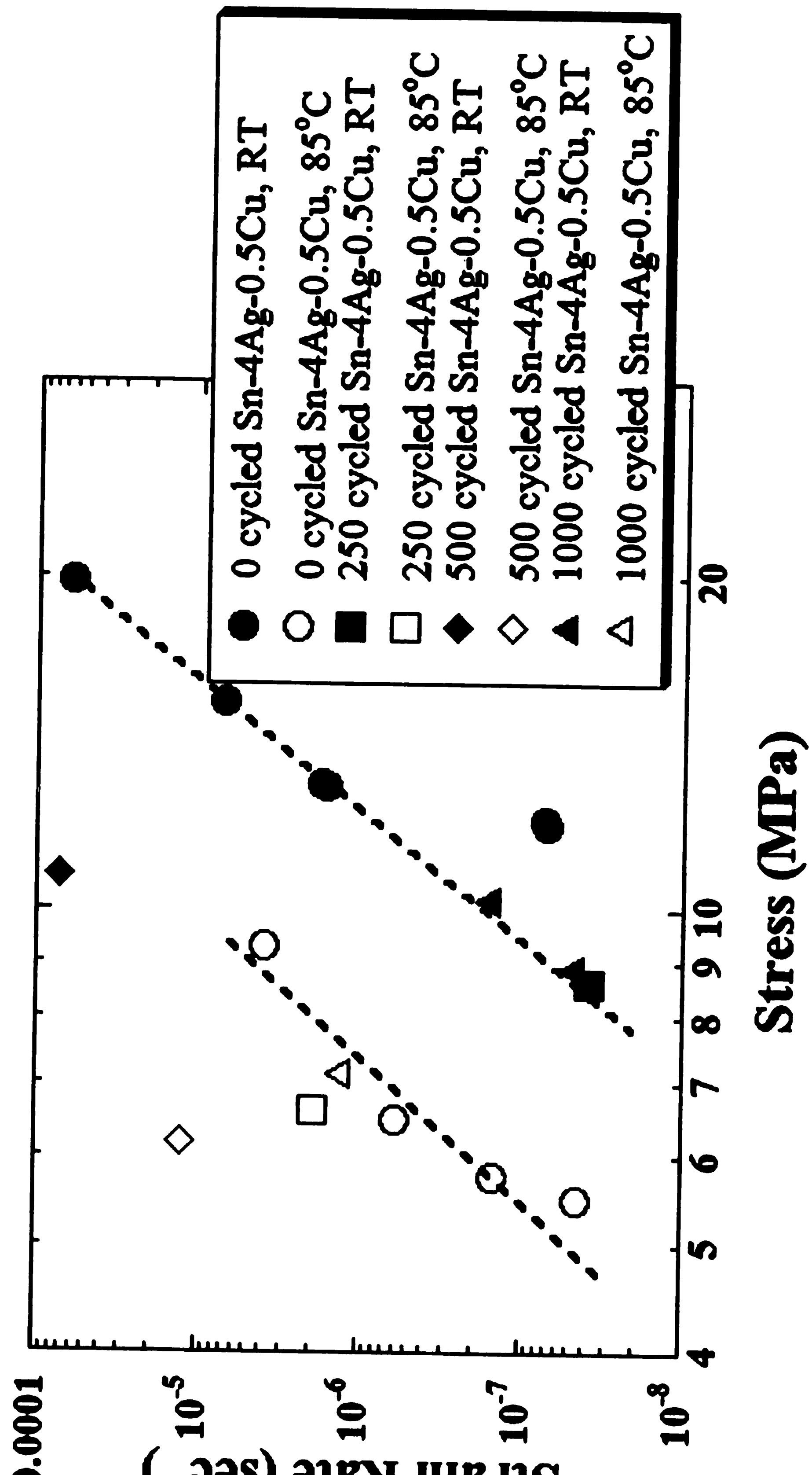

(b) Sn-4Ag-0.5Cu (cont'd)

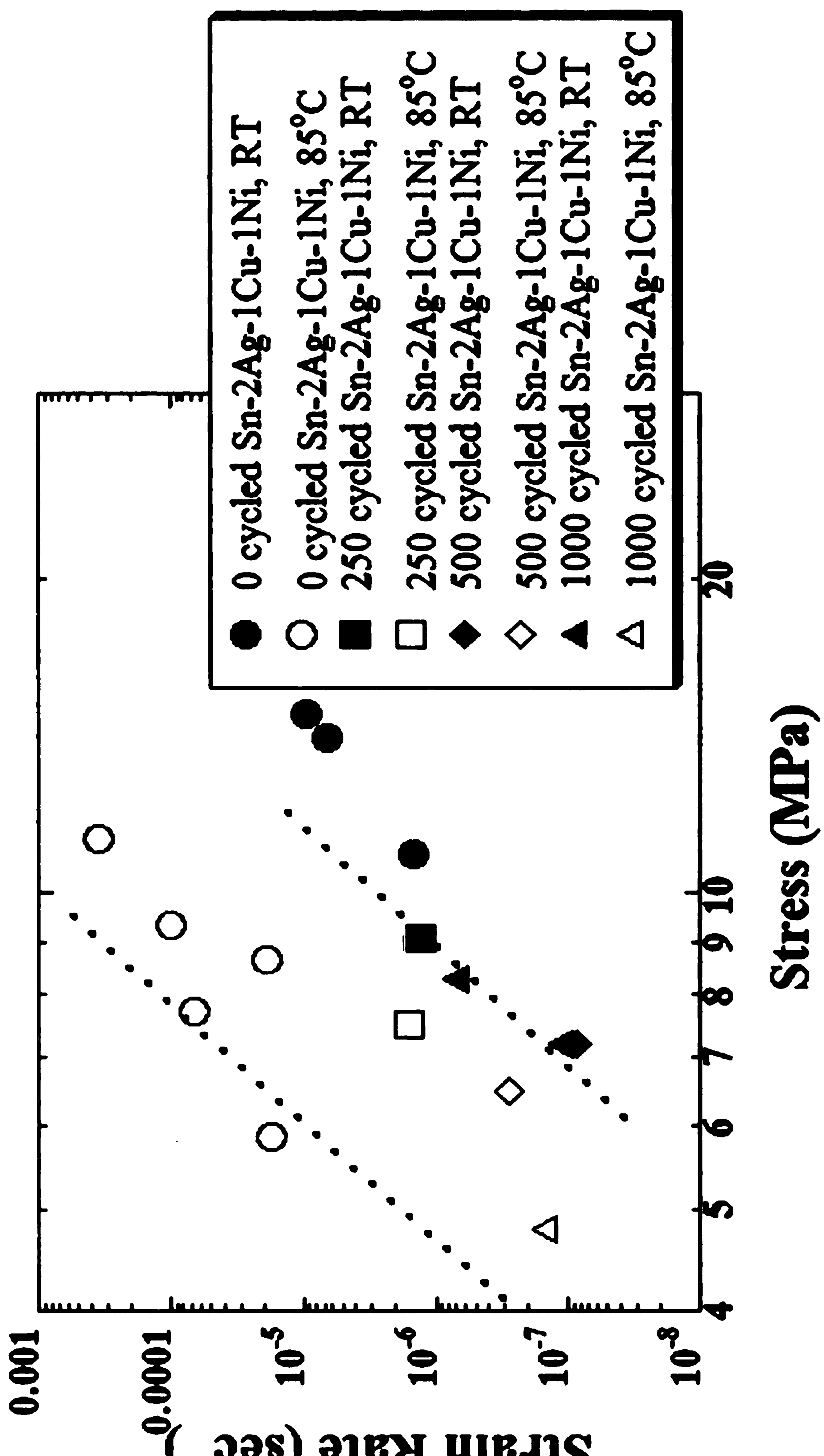

(c) Sn-2Ag-1Cu-1Ni

Figure 4.7. Comparison of steady-state creep rates of the four solder alloys subjected to 0, 250, 500, and 1000 TMF cycles as a function stress. [Note: In Figure 7 (b), the lower creep resistance of 500 TMF cycled joints (as compared to those with 250 TMF cycled ones) is attributed to the presence of large porosity in them]

consequence of TMF between 250, 500, and 1000 cycles. This trend agrees well with simple shear test results.

In contrast to eutectic Sn-3.5Ag, ternary Sn-4Ag-0.5Cu and quaternary Sn-2Ag-1Cu-1Ni showed only a slight decrease in creep resistance as a consequence of 1000 cycles of TMF. As can be observed from Figure 4.7(b) and (c), the residual creep resistance of these two alloys at room temperature and at 85°C after TMF is almost the same as that of specimens that were not subjected to TMF cycling.

Figure 4.8(a) and (b) show normalized strain-rate versus normalized stress for solder joints crept at room temperature and at 85°C, respectively. Data for aged eutectic Sn-3.5Ag solder joints adopted from Darveaux's studies are presented in these plots for comparison [80]. Closed symbols in Figure 4.8(a) and (b) correspond to solder joints that were not TMF'ed. As-fabricated solder joints used in the current study showed slightly better creep resistance than the aged solder joints used in studies of Darveaux and Banerji [80]. Although the creep behavior of solder joints after TMF did not apparently disobey the power law relation, it generally exhibited slightly less creep resistance than Darveaux's data. Similar behavior was also found for solder joints crept at 85°C.

4.3-3. Fracture of Solder Joints

The representative fracture surface of a crept solder joint is shown in Figure 4.9(a). Most specimens after fracture showed ductile smeared fracture surface due to failure by shear through the solder matrix. The highly ductile nature of the fracture can be noted from the spherical dimples present in Sn phase as shown in Figure 4.9(b). Thus, the

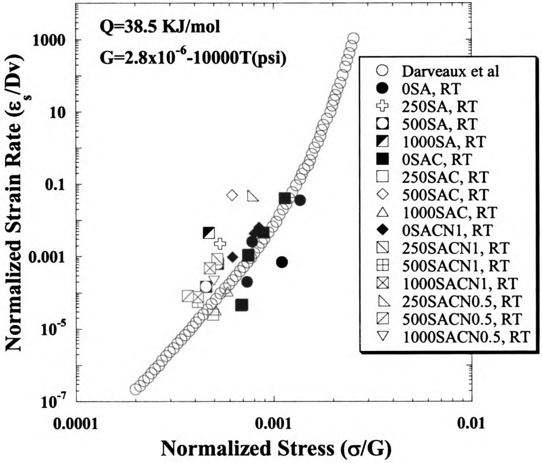

(a) Room Temperature (cont'd)

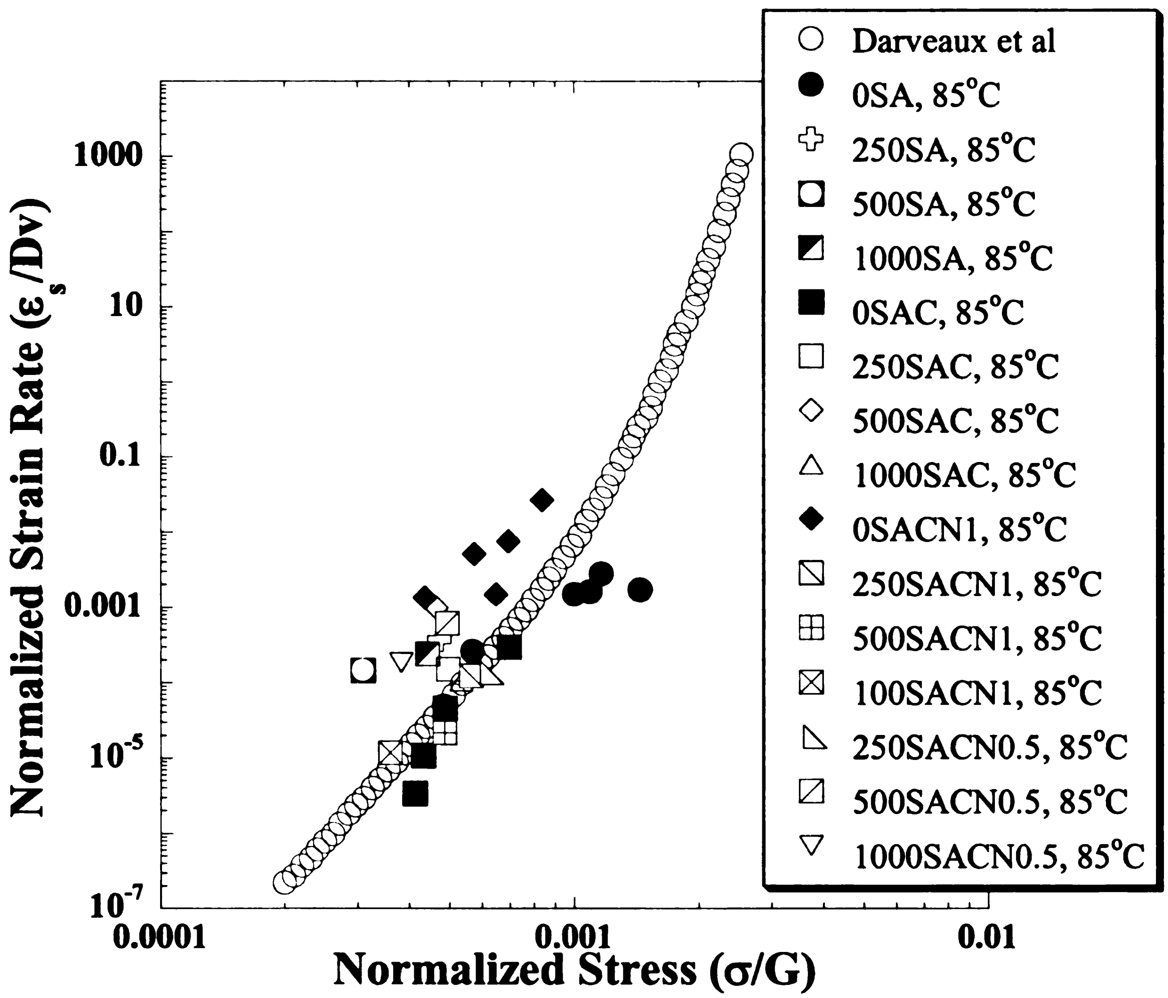

(b) 85°C

Figure 4.8. Normalized steady-state creep-strain rate versus normalized stress for TMF'ed and non-TMF'ed solder joints used in this study along with Darveaux's data for aged eutectic Sn-3.5Ag solder joints [79]. Abbreviations were used to identify each solder joint (i.e., SA is Sn-3.5Ag, SAC is Sn-4Ag-0.5Cu, SACN1 is Sn-2Ag-1Cu-1Ni, and SACN0.5 is Sn-2.5Ag-0.5Cu-0.5Ni). Number appearing before the abbreviation indicate the number of thermal cycles.

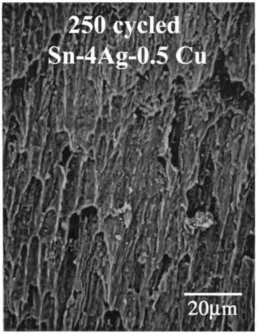

(a)

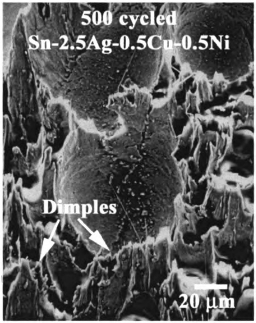

(b)

Figure 4.9. Representative fracture surface of the crept solder joints. (a) ductile fracture features smeared due to applied pure shear, (b) ductile dimple fracture.

creep fracture mode was found to be ductile for most solder joints indicating that the creep ductility of the solder joints was not significantly affected by the thermal cycles.

4.3-4. Possible Model of Observed Residual Behavior

The observed residual mechanical behavior could be attributed to an increase in crack density during early stages of TMF cycling. The residual strength of the solder joints after TMF appears to be controlled by increasing density of cracks that occurs during first few hundred TMF cycles. However, these cracks might be not connected together, and cause catastrophic failure. The ultimate TMF failure appears to occur when these crack interconnect. This behavior is very similar to that of thermal spalling in ceramics, where crack propagation is the controlling factor more than crack nucleation [81]. The preliminary proposed model is illustrated in Figure 4.10. Detail TMF damage accumulation modeling using this concept is currently in progress and will be presented in future publications.

4.4. CONCLUSION

TMF cycling four Sn-Ag based solder joints between –15°C and 150°C influences their residual mechanical properties in the following manner

1. Residual simple shear strength of Sn-Ag based solder joints decrease by 30-60% as a consequence of 250 TMF cycles. Between 250 cycles and 1000 cycles, no significant drop in strength was noted.

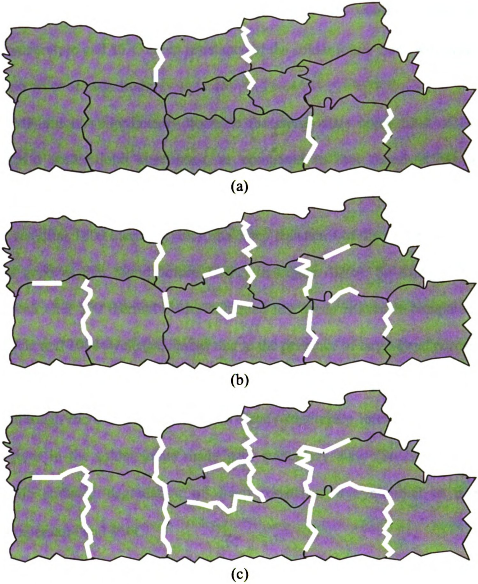

Figure 4.10. Schematic of possible crack behavior during TMF cycles. (a) Initially have minimum # of cracks at Sn grain boundaries, (b) # of cracks increase in the initial stage of TMF, and (c) TMF accident can connect these cracks to cause failure.

2. Among the solder alloy joints tested, only the eutectic Sn-3.5Ag solder joint exhibited a degraded creep resistance due to TMF. TMF degrades the room temperature and 85°C creep resistance of the solder joints made with this alloy by one order of magnitude
3. TMF did not significantly decrease the steady-state creep rates of Sn-4.0Ag-0.5Cu solder joint specimens, as compared to that found in the as-joined condition, at both room temperature and at 85oC.
4. Even after 1000 thermal cycles, the creep resistance of the solder joints remained as good as that found before TMF. In Figure 4.7(b), Sn-4.0Ag-0.5Cu solder joints after 500 thermal cycles exhibited less creep resistance compared to 250-cycle and 1000-cycle specimens due to the presence of large-sized porosity in the joints during fabrication.
5. Although there is some increase in steady-state creep rates observed after TMF cycles in the solder joints made with quaternary alloy (Sn-2Ag-1Cu-1Ni), the TMF induced degradation of creep resistance was minimal at both room temperature and 85oC.

CHAPTER 5

EFFECT OF DWELL TIMES ON THERMOMECHANICAL FATIGUE BEHAVIOR OF TIN-SILVER BASED SOLDER JOINTS

ABSTRACT

Thermomechanical fatigue (TMF) due to the mismatch in coefficient of thermal expansion (CTE) between solder and substrate gradually degrades the mechanical properties of solder joints during service. Solder joints fabricated with eutectic Sn-Ag, and Sn-Ag solder with Cu and/or Ni, were subjected to TMF between –15°C and +150°C with dwell times of 115 min. at high temperature extreme and 20 min. at low temperature extreme. Characterization of surface damage and residual mechanical strength of these solder joints were carried out after 0, 250, 500, and 1000 TMF cycles. Results obtained from this study were compared with those obtained with longer dwell time at lower temperature extreme. The solder joints that experienced longer dwell times at high temperature extreme exhibited less surface damage accumulation and less decrease in simple shear strength as compared to those experienced longer dwell times at low temperature extreme. Quaternary alloys containing small amounts of Cu and Ni exhibit better TMF performance than binary and ternary alloys under TMF cycling with longer dwell times at high temperature extreme.

5.1. INTRODUCTION

Eutectic Sn-Ag is an attractive candidate for replacing Pb-bearing electronic solders to meet the requirements for demanding high temperature service environments such as automotive under-the-hood applications. Since physical and thermal properties can be improved with additional elements to eutectic Sn-Ag, new Pb-free solders are likely to have multi-components [12-16]. Sn-Ag based solder alloys with improve TMF performance may be a ternary or quaternary alloy with additions of small amounts of alloying elements such as copper and/or nickel [44,82].

Advances in packaging technologies, driven by the desire for miniaturization and increased circuit speed result in severe operating conditions that raise reliability concerns of solder joints. Also, the mismatched thermal expansion characteristics of the materials joined by the solder, and the temperature excursions normally encountered during service, constitute a TMF condition for the constrained solder present in the joint. The reliability of solder interconnections under TMF becomes more critical as new electronic packaging technologies evolve [12,13].

The design of solder joints in electronic packages requires a good understanding of the mechanisms that control the deformation under service environment. However, the dominant mechanism, which contributes to TMF, has not yet been fully identified. Studies have reported that the deformation mechanisms in TMF are creep/stress relaxation, aging, reversed shear, and anisotropy of tin [18,78,83-91]. Recent studies have brought out the importance of reversed shear and anisotropy of tin on damage accumulation during TMF [89-91].

Evaluations of TMF damage accumulation and resultant residual mechanical properties of Sn-Ag based solder joints that have experienced longer dwell time at low temperature extreme during TMF cycling have been documented in our prior publications [44,82]. However, surface damage evaluation and residual mechanical behavior of Sn-Ag based solder joints that experience longer dwell times at high temperature extreme during TMF have not yet been documented. The long dwell time at low temperature extreme during TMF represents conditions such as, automotive under-the-hood applications, with service role of commuting to work, or shopping trips, etc. The solder joints operating under such a mode are used for shorter period of time in service with longer period of time in non-service mode. The current study is aimed at the evaluation of the TMF damage accumulation and residual mechanical behavior in lead-free Sn-Ag single shear-lap solder joints with realistic thickness under temperature excursions with longer dwell time at high temperature extreme. The situations for longer dwell time at high temperature extremes during TMF can represent long hauling trucks, taxis, or airplanes. This study is aimed at comparing the relative roles of longer dwell times at low or high temperature extremes during TMF on the damage accumulation and resultant mechanical properties of Sn-Ag based solder joints.

5.2. EXPERIMENTAL PROCEDURE

The current study dealt with solder joints made with (*i*) Eutectic Sn-3.5Ag, (*ii*) Sn-4Ag-0.5Cu, (*iii*) Sn-2.5Ag-0.5Cu-0.5Ni, and (*iv*) Sn-2Ag-1Cu-1Ni solder pastes to facilitate a comparison with the results obtained in earlier studies [44,82].

The detailed configurations of the dog-bone shaped single shear-lap solder joint and soldering procedure used have been reported elsewhere [79,89]. Cross sections of solder joints were metallurgically polished prior to subjecting them to TMF test.

A thermomechanical fatigue set-up with controllable ramp and dwell times was designed. This set-up consisted of an electric hot-plate as a heating source inside a common household freezer used as the cooling source. A copper plate placed on the hot plate was used as a stage for the solder joint specimens. Thermocouples were placed on the metal stage to measure and control the temperature. The heating element was turned on and off by an external timer. Power to the heating element was provided through a variable transformer so that the heating rate can be adjusted and controlled. The dwell times at the temperature extremes was controlled by an external timer, which turned the heater on or off.

Thermal cycling between $-15^{\circ}C$ and $+150^{\circ}C$ was imposed on the solder joints with this set-up. The ramp-rate for the heating segment of the cycle was $25^{\circ}C/min$ and the dwell time at the high temperature end was about 115 minutes. The ramp-rate for the cooling segment of the cycle was $7^{\circ}C/min$ and the dwell at the low temperature extreme of the cycle was about 20 minutes. This TMF cycling has the same ramp rates and temperature extremes used in our earlier studies to facilitate the comparison of the role of longer dwell times at low and high temperature extremes. The temperature profiles obtained with this set-up for prior and current studies are given in Figure 5.1. In the current study about eight TMF cycles could be imposed per day, and the solder joints were subjected to for a maximum of 1000 cycles. Surface damage accumulation at the

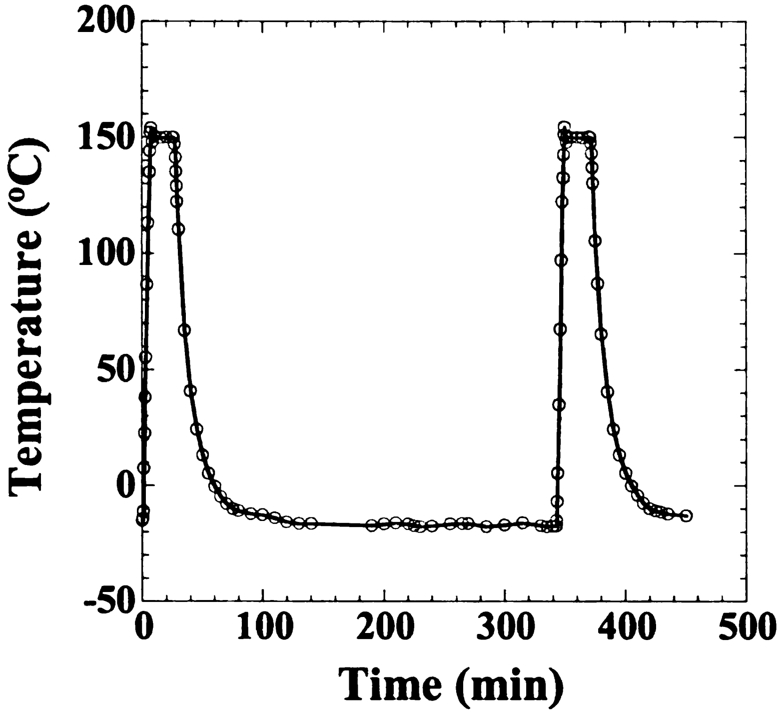

(a) long dwell time (330 min) at low temperature (-15°C) extreme

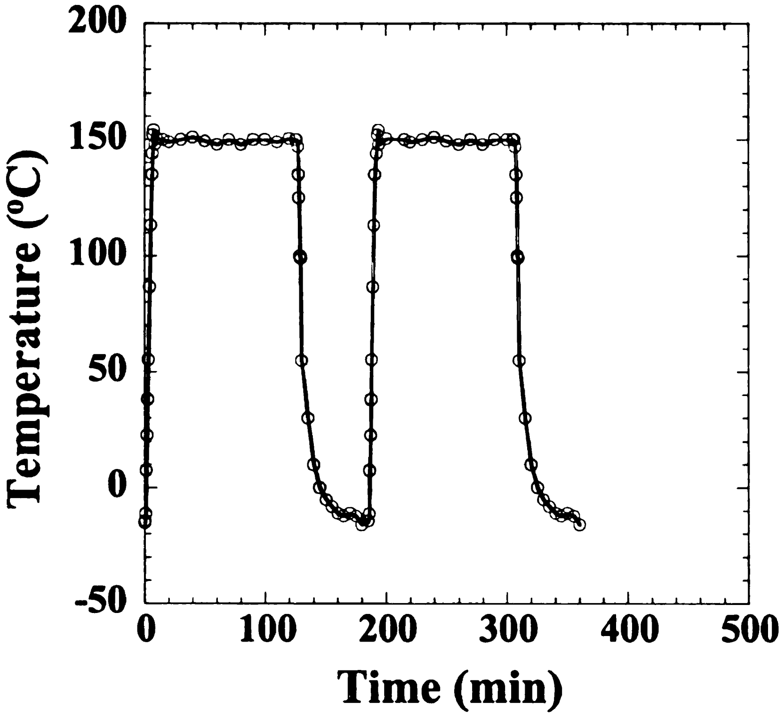

(b) long dwell time (115 min) at low temperature (150°C) extreme

Figure 5.1. Temperature-time profiles of (a) long dwell time at low temperature extreme (prior study) and (b) long dwell time at high temperature extreme (current study)

exac

250.

wer

beh

tem

5.3

5.3

acc

init

inte

bar

(c)

be

Th

re

da

in

Sn-exact same-targeted area was observed in all the four Sn-Ag based solder joints after 0, 250, 500, and 1000 cycles by Scanning Electronic Microscopy. Some of the solder joints were removed after 250 and 500 cycle intervals to assess the residual mechanical behavior with tensile testing machine at a crosshead speed of 0.5 mm/min at room temperature.

5.3. RESULTS AND DISCUSSION

5.3-1. Surface Damage Accumulation in Sn-Ag Based Solder Joints that Experienced Longer Dwell Time at High Temperature (+150°C) extreme During TMF

Binary eutectic Sn-3.5 Ag solder joints showed progress of surface damage accumulation with increasing number of TMF cycles as shown in Figure 5.2. The initially polished surface shown in Figure 5.2(a) experienced shear banding near the intermetallic interface due to TMF as shown in Figure. 5.2(b). The intensity of this shear banding became stronger with increasing number of TMF cycles (Figure. 5.2(b). thru (c)). The surface damage accumulation in eutectic Sn-3.5Ag solder joints was found to be the worst after 1000 TMF cycles in current study.

Microstructures of the ternary alloy, Sn-4Ag-0.5Cu, after 0, 250, 500, and 1000 TMF cycles are illustrated in Figure 5.3. Visible grain boundary sliding occurred at a region away from intermetallic interface during first few hundred TMF cycles and the damage accumulation intensified with increasing number of TMF cycles as can be seen in Figure. 5.3(a). thru (d). There was an apparent crack growth within the solder between Sn-Sn grains due to grain boundary sliding between 500 and 1000 TMF cycles.

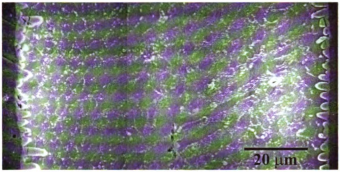

(a) 0 TMF cycle

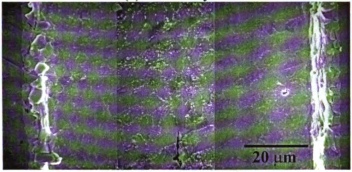

(b) 250 TMF cycles

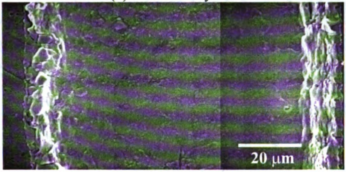

(c) 500 TMF cycles

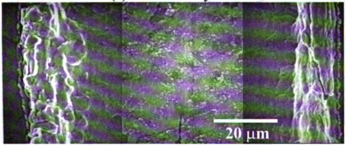

(d) 1000 TMF cycles

Figure 5.2. SEM images of surface damage accumulation of eutectic Sn-3.5Ag with long dwell time at high temperature showing increasing intensity of shear banding near intermetallic interface with increasing number of TMF cycles.

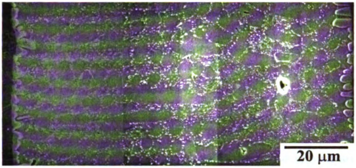

(a) 0 TMF cycle

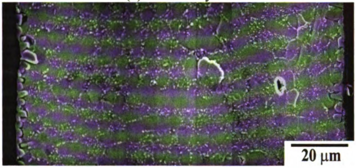

(b) 250 TMF cycles

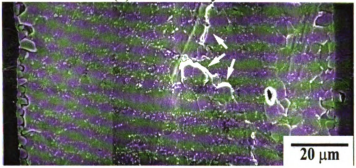

(c) 500 TMF cycles

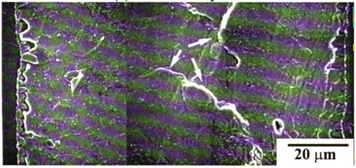

(d) 1000 TMF cycles

Figure 5.3. SEM images of surface damage accumulation of Sn-4Ag-0.5 Cu with long dwell time at high temperature showing clear grain boundary sliding in the solder area with increasing number of TMF cycles (arrows indicate cracks).

A comparison of Figure 5.2 and 5.3 suggests that the ternary alloy (Sn-4Ag-0.5Cu) exhibits less surface damage than the binary eutectic Sn-Ag due to TMF cycle imposed in the current study.

Both quaternary alloys used in this study showed almost no visible surface damage accumulation even after 1000 TMF cycles. Figure. 5.4 shows an example of the microstructures of Sn-2.5Ag-0.5Cu-0.5Ni solder joints after TMF. No significant damage was found between 0 and 1000 TMF cycles. Similar behavior can also be noted for Sn-2Ag-1Cu-1Ni as illustrated in Figure. 5.5.

The most predominate surface damages after 1000 TMF cycles in eutectic Sn-3.5Ag and Sn-4Ag-0.5Cu were grain boundary sliding as shown in Figure 5.6(a) and (b). The quaternary alloys showed no such damage since there was only minimal or no surface damage present in these solder joints even after 1000 TMF cycles.

5.3-2. Comparison of Damage Accumulation in Specimens with Long Dwell Times at Low and High Temperature Extremes

Micrographs comparing surface damage accumulation after 1000 TMF cycles in the four solder alloys studied with different dwell times at low or high temperature extremes are presented in Figure 5.7 through 5.10. The amount of visible surface damage in eutectic Sn3.5Ag joints after 1000 TMF cycles was similar for specimens experiencing long dwell time at low [44] and high (present study) temperature extremes as illustrated in Figure 5.7(a). and (b).

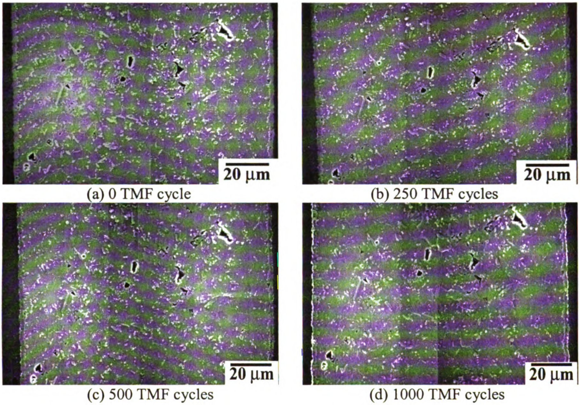

Figure 5.4. SEM images of thermomechanically fatigued Sn-2.5Ag-0.5 Cu-0.5 Ni with long dwell time at high temperature showing no significant surface damage accumulation even after 1000 TMF cycles.

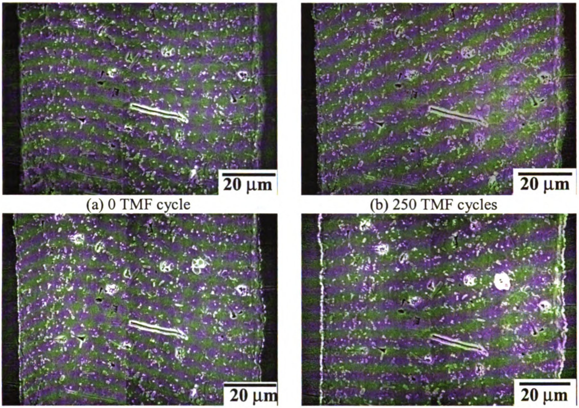

(a) 0 TMF cycle
(b) 250 TMF cycles
(c) 500 TMF cycles
(d) 1000 TMF cycles

Figure 5.5. SEM images of thermomechanically fatigued Sn-2Ag-1 Cu-1 Ni with long dwell time at high temperature showing no significant surface damage accumulation even after 1000 TMF cycles.

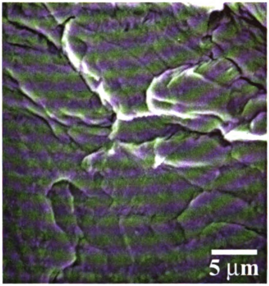

(a)

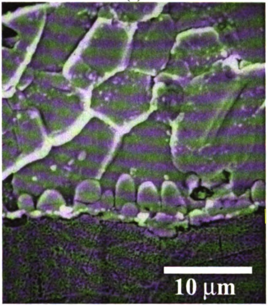

(b)

Figure 5.6. SEM micrographs showing grain boundary sliding after 1000 TMF cycles. (a) Sn-Sn grain boundary sliding of eutectic Sn-3.5Ag and (b) Sn-Sn grain boundary cracks form near intermetallic interface for Sn-4Ag-0.5Cu.

Although a prior study [44] with longer dwell time at low temperature extreme indicated that Sn-4Ag-0.5Cu solder joints exhibited more visual deformation as compared to eutectic Sn-3.5Ag solder joints, the present study with longer dwell time at high temperature extreme revealed that the Sn-4Ag-0.5Cu exhibits less damage as compared to the eutectic Sn-3.5Ag (Figure 5.8.). As from Figures 5.7 and 5.8, the surface damage due to TMF in the ternary alloy occurs within the solder matrix while that in the binary is mainly confined to regions near the solder/substrate interface. Such a behavior can probably be attributed to the presence of Cu-Sn intermetallic precipitates in the ternary alloy along the grain boundaries at regions near the solder/substrate region. These precipitates may retard grain boundary sliding that can occur during the dwell time at the high temperature extreme of TMF cycling.

Sn-2.5Ag-0.5Cu-0.5Ni solder joints showed the least visually noticeable surface deformation after 1000 TMF cycles with longer dwell time at low temperature extreme. As shown in Figure 5.9(b), no significant of damage occurs in this alloy with longer dwell time at high temperature extreme. Sn-2Ag-1Cu-1Ni solder joints exhibited no significant surface damage with long dwell time at high temperature extreme. However, some surface damage observed in this alloy for long dwell time at low temperature extreme, as can be seen in Figure 5.10(a) and (b).

In general, the quaternary alloys developed less surface damage accumulation during TMF tests with long dwell times at low and high temperature extremes. However, their behavior was much better in situation with longer dwell time at high temperature extreme.

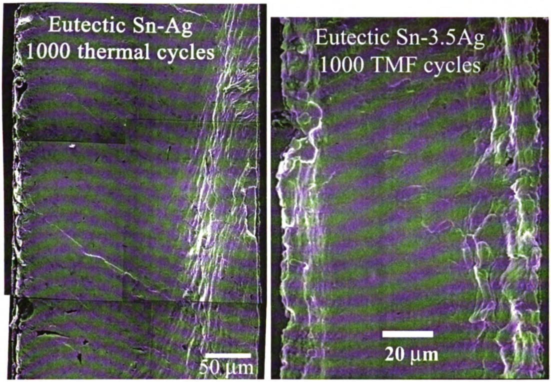

(a) (b)

Figure 5.7. Comparison of surface microstructures of 1000 TMF cycled eutectic Sn-3.5Ag solder joints. (a) long dwell time at low temperature extreme [adopted from ref. 44] and (b) long dwell time at high temperature extreme.

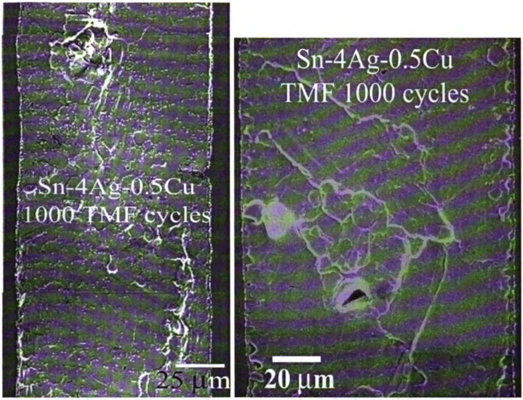

(a) (b)

Figure 5.8. Comparison of surface microstructures of 1000 TMF cycled Sn-4Ag-0.5Cu solder joints. (a) long dwell time at low temperature extreme [adopted from ref. 44] and (b) long dwell time at high temperature extreme.

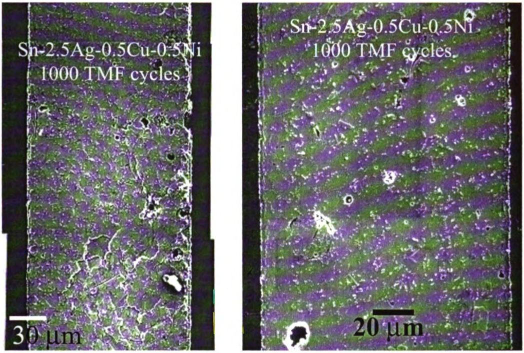

(a) (b)

Figure 5.9. Comparison of surface microstructures of 1000 TMF cycled eutectic Sn-2.5Ag-0.5Cu-0.5Ni solder joints. (a) long dwell time at low temperature extreme [adopted from ref. 44] and (b) long dwell time at high temperature extreme.

During the heating part of the TMF cycle, the solder becomes softer due to the raising temperature. In addition, as the temperature raises the peak shear stress that can develop in the solder joints also decreases. Stress relaxation studies carried out at 150°C and room temperature have shown that the stress drop is much higher at 150°C [86]. Based on these observations, it is reasonable to expect the stress that develops due to CTE mismatch during heating part of the TMF cycle to build up to a very low magnitude. In addition, residual stress that contributes to creep can be expected to be relaxed more easily at the high temperature extreme of the TMF cycle. As a consequence, only minimal damage accumulation results in such a case irrespective of the extent of dwell time at this temperature.

On the other hand, during the cooling part of the TMF cycle, the solder becomes less compliant with decreasing temperature. In addition, the solder joint can develop higher peak shear stresses at lower temperatures. Such a stress is not easily relaxed at the low temperature extreme of the TMF cycle. Under such conditions large stresses present at the lower temperature can cause more damage during longer dwell time at this temperature.

5.3-3. Comparison of the Effect of Dwell Times at Different Temperature Extremes on Residual Simple Shear Behavior of Solder Joints After TMF

The residual mechanical behavior of four Sn-Ag based solder joints that experienced longer dwell time at high temperature extremes can be compared with those from a prior study [82] with longer dwell time at low temperature extreme (Figures 11(a) and (b).). As can be observed from Figure 11(a), there is an initial drop in residual-simple shear

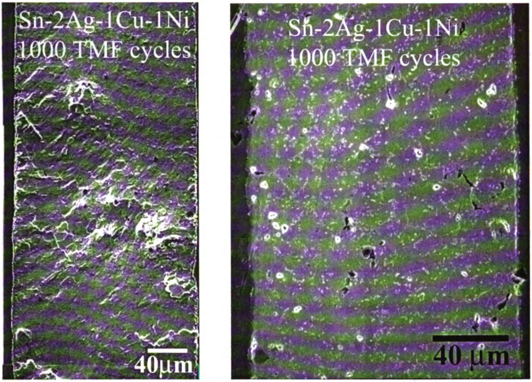

(a) (b)

Figure 5.10. Comparison of surface microstructures of 1000 TMF cycled eutectic Sn-2Ag-1Cu-1Ni solder joints. (a) long dwell time at low temperature extreme [adopted from ref. 44] and (b) long dwell time at high temperature extreme.

strength as a consequence of 250 TMF cycles in all four Sn-Ag based solder joints. However, no significant decrease of the residual-simple shear strength was generally noted between 250 and 1000 TMF cycles. The drop in the residual-simple shear strength was approximately 30~60 % after 250 TMF cycles for solder joints that experienced longer dwell time at low temperature extreme. However, from Figure 5.11(b), the decrease in simple residual shear strength is less for solder joints that experienced longer dwell time at high temperature extreme. Although the behavior exhibited is similar to that which occurred in Figure 5.11(a), the drop in the residual-simple shear strength is only about 20 % after initial few hundred TMF cycles. As noted from Figure 5.11(b), almost no significant decrease in residual simple shear strength can be observed in Sn-2Ag-1Cu-1Ni solder joints even after 1000 TMF cycles.

Residual mechanical behavior exhibited by the solder joints after TMF are consistent with the observations presented in the previous sections. Since the specimens that experience longer dwell time at the high temperature extreme of TMF exhibit less damage accumulation than those with longer dwell time at the lower temperature extreme, they retain more of their mechanical capabilities.

The quaternary alloys exhibit less damage accumulation and loss of mechanical strength due to TMF, especially in the current study. Alloys containing 1% Ni and 1%Cu do not show damage accumulation or decrease in strength even after 1000 TMF cycles with longer dwell times at high temperature extreme. These quaternary alloys have also been found to exhibit better isothermal creep properties [55]. The roles of Cu and Ni, especially when both are present as alloying elements, for the improved performance of

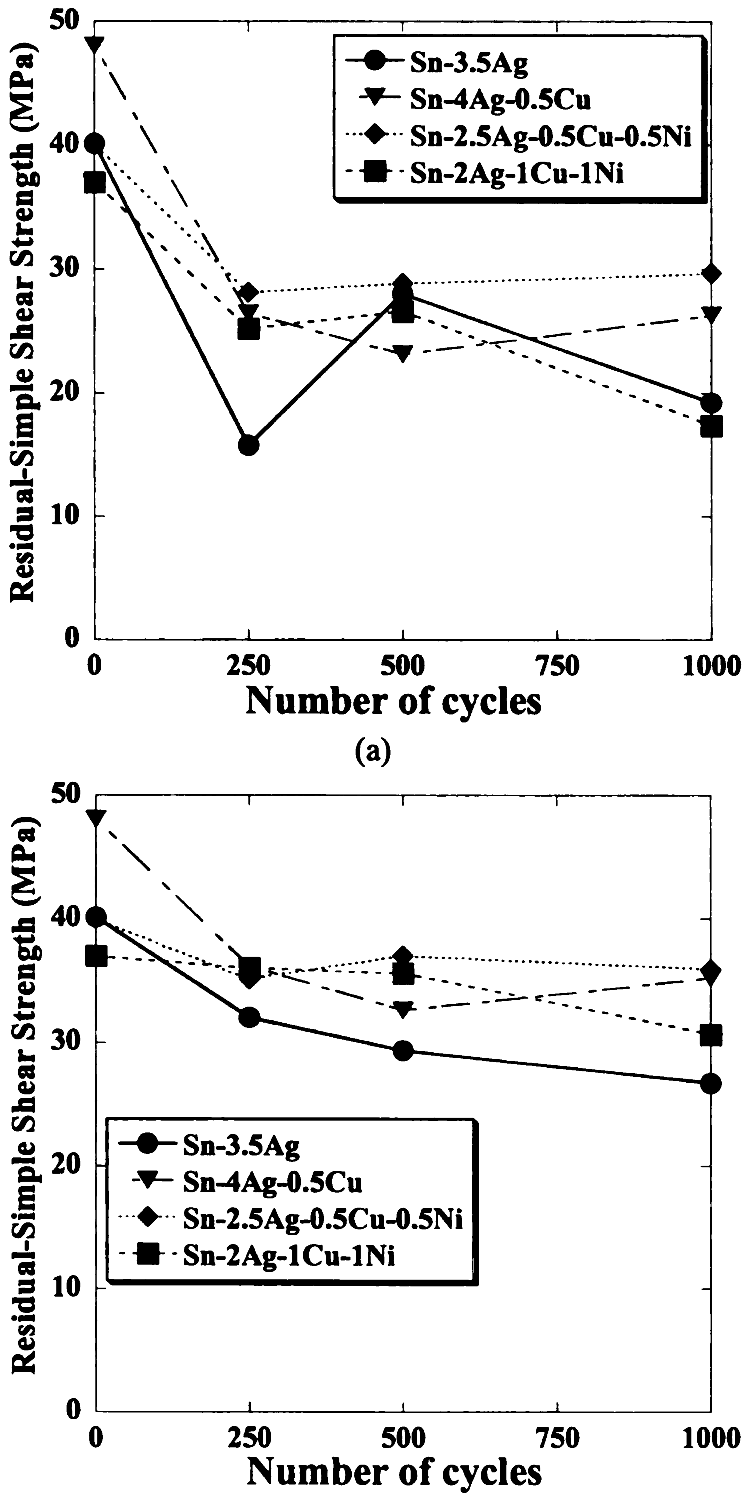

(a)

(b)

Figure 5.11. Effect of thermal cycles on the residual-simple shear strength of four Sn-Ag based solder joints showing minimal drop in simple shear strength in solder joints experienced long dwell time at high temperature extreme. (a) long dwell time at low temperature extreme [adopted from ref. 82] and (b) long dwell time at high temperature extreme.

Sn-Ag based solder is not fully understood at this time, and further investigations are in progress.

5.4. SUMMARY

The following summary can be made based on the present study,

1. TMF cycling using long dwell time at high temperature extreme produced deformation and damage very similar to that observed with longer dwell time at low temperature extreme in eutectic Sn-3.5Ag and Sn-4Ag-0.5Cu solder joints.
2. No significant surface damage could be noted in Sn-2.5Ag-0.5Cu-0.5Ni and Sn-2Ag-1Cu-1Ni solder joints that experienced long dwell time at high temperature extreme even after 1000 TMF cycles.
3. A comparison of damage accumulation and decrease in simple shear strength of Sn-Ag based solder joints that experienced longer dwell times at low or high temperature extremes after TMF indicates solder joints that experienced longer dwell time at high temperature extreme exhibited less surface damage accumulation and less decrease in simple shear strength.
4. In general, small Ni addition along with small Cu addition to Sn-Ag based solder to produce quaternary alloys results in better TMF performance.

CHAPTER 6

EFFECTS OF TMF HEATING RATES ON DAMAGE ACCUMULATION AND RESULTANT MECHANICAL BEHAVIOR OF TIN-SILVER BASED SOLDER JOINTS

ABSTRACT

Solder joint reliability depends on several service parameters such as temperature extremes encountered, dwell times at these temperatures, and the ramp-rates representing the rate at which the temperature changes are imposed. TMF of Sn-Ag based solder alloy joints of realistic dimensions were carried out with dwell of 115 minutes and 20 minutes at 150°C and −15°C respectively. Different heating rates were obtained by controlling the power input during heating part of TMF cycles. Surface damage and residual mechanical strength of these solder joints were characterized after 0, 250, 500, and 1000 TMF cycles to evaluate the role of TMF heating rate on the solder joint integrity.

6.1. INTRODUCTION

Thermomechanical fatigue (TMF) is a major cause of failure in electronic and power devices [92-95]. A typical thermal cycle that leads to failure of solder joint consists of two ramp times of comparatively short duration during which the device heats up to operational temperature (high temperature extreme) or cools down to ambient temperature (low temperature extreme) and two longer dwell times at each temperature extreme which separates these two ramps [27,34]. During service, the device may experience long dwell at the high temperature extreme or long dwell at low temperature extreme depending on applications. Also, cooling rate and heating rate can be changed with external environment, internal heating from power dissipation, or both. In addition to these service parameters, the temperature regime imposed and difference in temperature extremes may be important factors that can contribute to TMF behavior of electronic solder joints, as illustrated in Figure 6.1. However, only a few studies have been attempted to understand the role of such individual service parameters on the TMF behavior of solder joints [96-98].

There are certain requirements needed in order to investigate roles of each of these parameters separately. Such requirements include, (i) the same solder joint geometry, (ii) varying one parameter while maintaining the other parameters constant, (iii) use of same solder materials, and (iv) comparison after a fixed number of TMF cycles.

Effect of dwell times on TMF behavior of Sn-Ag based solder joints have been reported in an earlier publication [99]. In that study, the geometry of solder joints, imposed temperature range, heating rate, and cooling rate were held and fixed on Sn-Ag

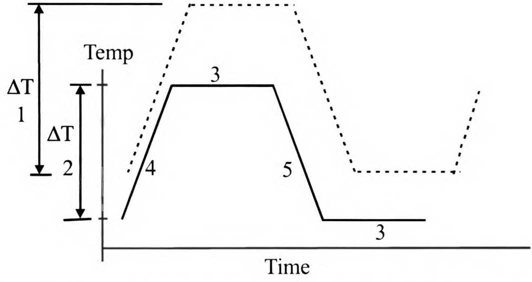

Figure 6.1. Schematic of various service parameters that can affect thermomechanical fatigue (TMF) damage of electronic solder joints.

based solder joints while the dwell times at each temperature extreme were the varied service parameters [99].

The aim of this study is to investigate the effects of ramp rates during heating segment of TMF cycles and to compare it with results from prior TMF study with a slow heating rate. Such a comparison includes the resultant residual mechanical behavior and surface damage accumulation.

6.2. EXPERIMENTAL PROCEDURE

The current study deals with solder joints made with eutectic Sn-3.5Ag, Sn-4Ag-0.5Cu, Sn-2.5Ag-0.5Cu-0.5Ni, and Sn-2Ag-1Cu-1Ni solder pastes to facilitate a comparison with the results obtained in earlier studies [99]. These solder joints, with ~100μm thickness and 1×1 mm^2 area, have been used in prior TMF studies [44,82,99]. The detailed configurations of the dog-bone shaped single shear-lap solder joint geometry and soldering procedure used have been reported elsewhere [87,88]. The edge of the solder joints were metallurgically polished prior to TMF testing.

A thermomechanical fatigue set-up with controllable ramp-up and dwell times was designed. This set-up consisted of a hot-plate as a heating source inside a common household freezer with inside temperature of -15°C. A copper plate placed on the hot plate was used as a stage for holding the solder joint specimens. Thermocouples were placed on the metal stage to measure and control the temperature. The heating element was turned on and off by an external timer. Power to the heating element was provided through a variable transformer so that the heating rate can be adjusted and controlled.

The dwell times at the temperature extreme was controlled by the external timer, which turned the heater on or off.

Thermal cycling between $-15^{\circ}C$ and $+150^{\circ}C$ ($\Delta=165^{\circ}C$) was imposed on the solder joints with this set-up. The dwell time at the high temperature extreme was about 115 minutes and the dwell at the low temperature extreme of the cycle was about 20 minutes. The ramp-rate for the cooling segment of the cycle was $\sim 0.07^{\circ}C/sec$. This TMF cycling has almost the same temperature extremes and cooling rate used in our earlier studies to facilitate the comparison of the role of heating rates. The temperature profiles obtained with this set-up for prior and current studies are given in Figure 6.2. In the current study, the ramp-rate for the heating segment of the cycle was $\sim 1.1^{\circ}C/sec$. This heating rate is twice as fast as heating rate used in earlier studies ($\sim 0.55^{\circ}C/sec$) as can be noted in Figure 6.2(b). The solder joints were subjected to a maximum of 1000 TMF cycles.

Surface damage accumulation at the exact same-targeted area was observed in all the four Sn-Ag based solder joints after 0, 250, 500, and 1000 cycles by Scanning Electronic Microscopy. Some of the solder joints were removed after 250 and 500 cycle intervals to assess the residual mechanical behavior in shear with a tensile testing machine at a crosshead speed of 0.5 mm/min at room temperature.

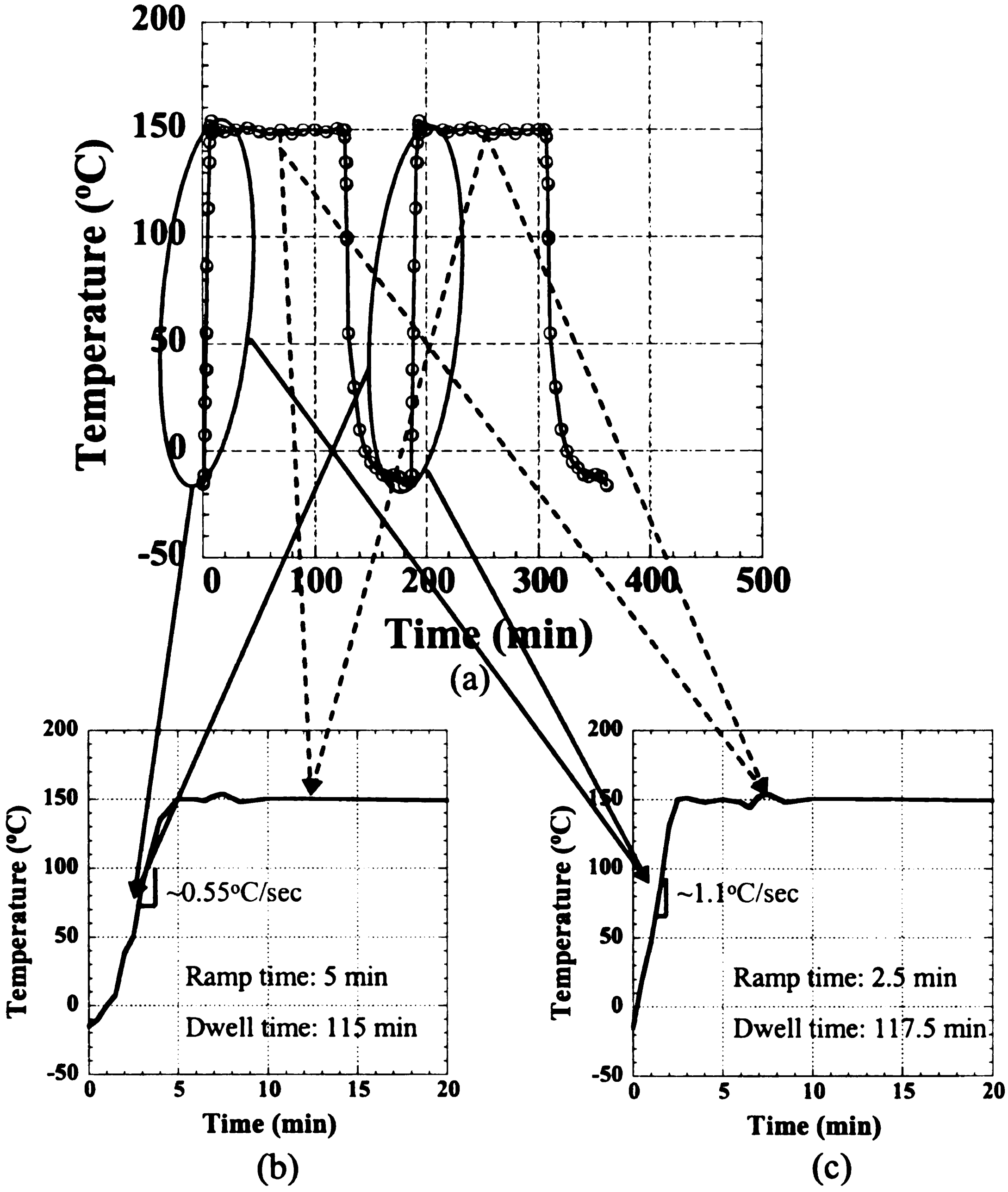

Figure 6.2. Temperature-time profiles of TMF. (a) overall temperature-time profile showing fixed dwell times at each temperature extremes and cooling rate, (b) slow heating rate with fixed dwell times and cooling rate, and (c) fast heating rate with fixed dwell times and cooling rate.

6.3.RESULTS AND DISCUSSION

6.3-1. Surface Damage Accumulation in Sn-Ag Based Solder Joints that Experienced Fast Heating Rate During TMF

Eutectic Sn-3.5 Ag solder joints showed progress of surface damage accumulation with increasing number of TMF cycles as shown in Figure 6.3. The initially polished surface, shown in Figure. 6.3(a)., exhibits shear banding near the intermetallic interface layer due to TMF as shown in Figure 6.3(b). The intensity of this shear banding became stronger with increasing number of TMF cycles (Figures 6.3(b). through (d)). This highly localized shear banding was also found in an earlier study with slow heating rate imposed during TMF. The SEM images of eutectic Sn-Ag solder joints after a maximum of 1000 TMF cycles with different heating rates imposed during TMF are presented in Figure 6.4. More highly localized damage was observed in solder joints that experienced TMF with faster heating rate than that of solder joints experienced TMF with slower heating rate as noted in Figures 6.4(a) and (b). Rhee et. al.[100] have reported effects of shear-strain rates at various temperatures using same geometry of eutectic Sn-3.5Ag solder joints. They have reported that concentrated deformation was found in localized region with higher imposed rates of shear-strain while lower rates of simple shear-strain resulted in diffused deformation characteristics under isothermal shear tests [100].

Microstructures of the ternary alloy, Sn-4Ag-0.5Cu, after 0, 250, 500, and 1000 TMF cycles are illustrated in Figure 6.5. Apparently grain boundary sliding occurred at a region away from the intermetallic interface during the first few hundred TMF cycles and the damage accumulation intensified with increasing number of TMF cycles which can be seen in Figures 6.5(a) through (d). There was an obvious crack growth within solder between Sn-Sn grains due to grain boundary sliding between 500 and 1000 TMF cycles.

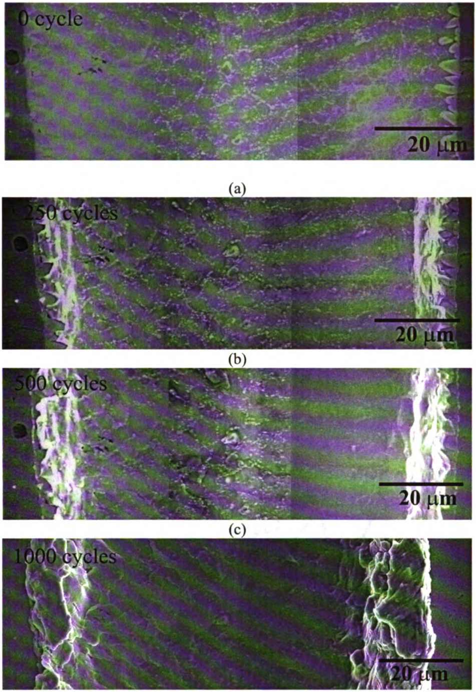

Figure 6.3. Surface damage accumulation on eutectic Sn-Ag solder joint undergoing TMF with faster heating rate. (a) 0 TMF cycle, (b) 250 TMF cycles, (c) 500 TMF cycles, and (d) 1000 TMF cycles.

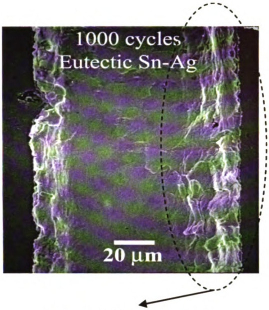

(a)

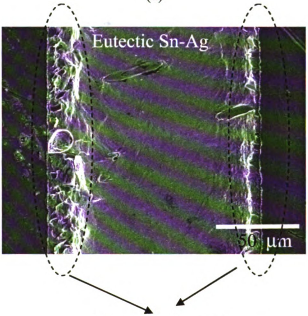

(b)

Figure 6.4. Surface damage accumulation in eutectic Sn-Ag solder joints after 1000 TMF cycles. (a) slower heating rate imposed during TMF, and (b) faster heating rate imposed during TMF.

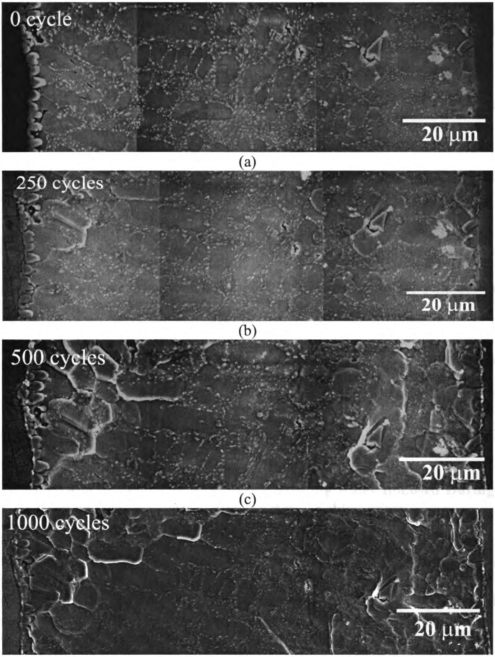

(a) (b) (c) (d)

Figure 6.5. Surface damage accumulation in Sn-4Ag-0.5Cu solder joint undergoing TMF under faster heating rate. (a) 0 TMF cycle, (b) 250 TMF cycles, (c) 500 TMF cycles, and (d) 1000 TMF cycles.

Micrographs comparing surface damage accumulation after 1000 TMF cycles in Sn-4Ag-0.5Cu studied with different heating rates imposed during TMF are presented in Figure 6.6. Similar to surface damage that found in eutectic Sn-3.5Ag solder joints, highly localized surface damage was found in Sn-4Ag-0.5Cu solder joints after TMF with faster heating rate.

Both quaternary alloys used in this study showed almost no visible surface damage accumulation even after 1000 TMF cycles. Figure 6.7 shows examples of the microstructures of Sn-2.5Ag-0.5Cu-0.5Ni solder joints after TMF. No significant surface damage was found to occur between 0 and 1000 TMF cycles. Similar behavior can also be noted for Sn-2Ag-1Cu-1Ni as illustrated in Figure 6.8.

Irrespective of slow or fast heating rate, the surface damage accumulation was found to be minimal in both quaternary solder joints studied, as compared to the binary and ternary alloy joints after 1000 TMF cycles, as can be seen in Figures 6.9 and 6.10.

6.3-2. Comparison of the Effect of Different Heating Rates Imposed During TMF on Residual Shear Strength of Sn-Ag Based Solder Joints

The residual mechanical behavior of the four Sn-Ag based solder joints that experienced faster heating rate can be compared with those from a prior study [10] with slower heating rate (Figure 6.11).

For eutectic Sn-3.5Ag solder joints, the residual shear strength was initially decreased about 20 % within first few hundred TMF cycles with additional gradual drop between 250 and 500 cycles. No significant drop in residual shear strength was noted between 500 and 1000 TMF cycles with the slow heating rate imposed during TMF, indicating that the residual shear strength for eutectic Sn-Ag solder joints stabilized after

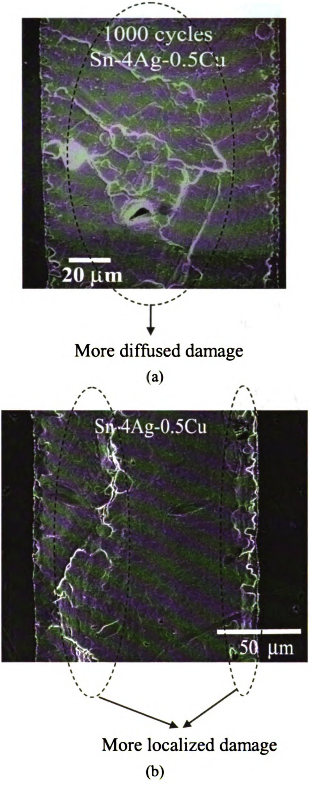

Figure 6.6. Surface damage accumulation in Sn-4Ag-0.5Cu solder joints after 1000 TMF cycles. (a) slower heating rate, and (b) faster heating rate.

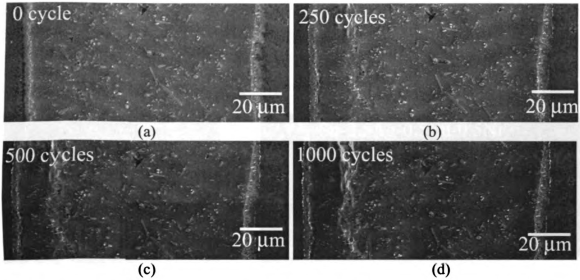

Figure 6.7. Surface damage accumulation in Sn-2.5Ag-0.5Cu-0.5Ni solder joint undergoing TMF with faster heating rate. (a) 0 TMF cycle, (b) 250 TMF cycles, (c) 500 TMF cycles, and (d) 1000 TMF cycles.

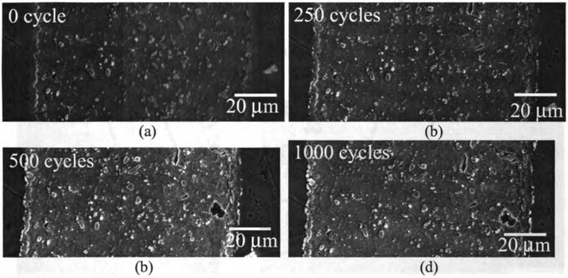

Figure 6.8. Surface damage accumulation in Sn-2Ag-1Cu-1Ni solder joint undergoing TMF with faster heating rate. (a) 0 TMF cycle, (b) 250 TMF cycles, (c) 500 TMF cycles, and (d) 1000 TMF cycles.

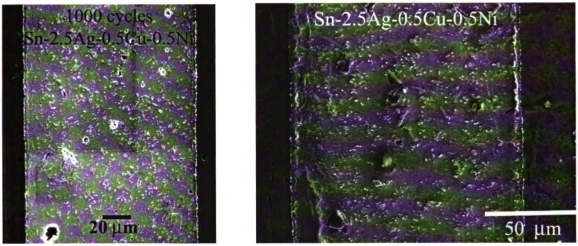

(a) (b)

Figure 6.9. Surface damage accumulation in Sn-2.5Ag-0.5Cu-0.5Ni solder joints after 1000 TMF cycles. (a) slower heating rate, and (b) faster heating rate.

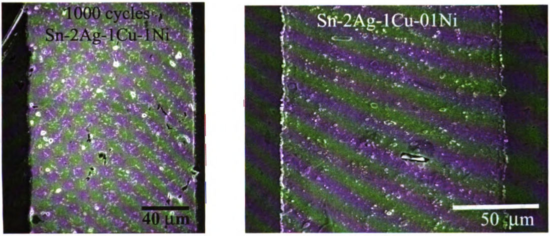

(a) (b)

Figure 6.10. Surface damage accumulation in Sn-2Ag-1Cu-1Ni solder joints after 1000 TMF cycles. (a) slower heating rate, and (b) faster heating rate.

500 TMF cycles. A total of 35 % decreases in residual shear strength were noted for eutectic Sn-3.5Ag solder joints after a maximum of 1000 TMF cycles (Figure 6.11(b)). However, with a faster heating rate the residual shear strengths of eutectic Sn-3.5Ag solder joints decreased dramatically with increase in number of TMF cycles, as can be seen in Figure 6.11(c) and (d). Drop in residual shear strength 1000 TMF cycles was about 42 %. Although this is only about 10 % worse after 1000 TMF cycles, the major difference arise from the fact that the residual shear strength continues to decrease even after TMF cycles with no stabilization. Continued intensified highly localized damage that results from TMF with fast heating rate could be a contributing fact for such continued deterioration.

As can be observed from Figures 6.11(a) and (b), Sn-4Ag-0.5Cu solder joints posses better initial shear strength than other Sn-Ag based solder joints studied. The decrease in shear strength was about 20 % after 250 TMF cycles with a slower heating rate. About 10 % additional decrease in shear strength was noted between 250 and 1000 TMF cycles under such condition (Figure 6.11(b)). After 1000 TMF cycles, the drop in shear strength was about 35 %. Under TMF with a faster heating rate, the residual shear strength of joints made with this alloy dropped linearly with increasing number of TMF cycles as can be seen in Figures 6.11(c) and (d). This decrease was about 60 % after a maximum of 1000 TMF cycles with a faster heating with no sign of stabilizing on further TMF cycling. Such observations indicate that Sn-4Ag-0.5 Cu solder joints are highly sensitive to change in imposed heating rates during TMF.

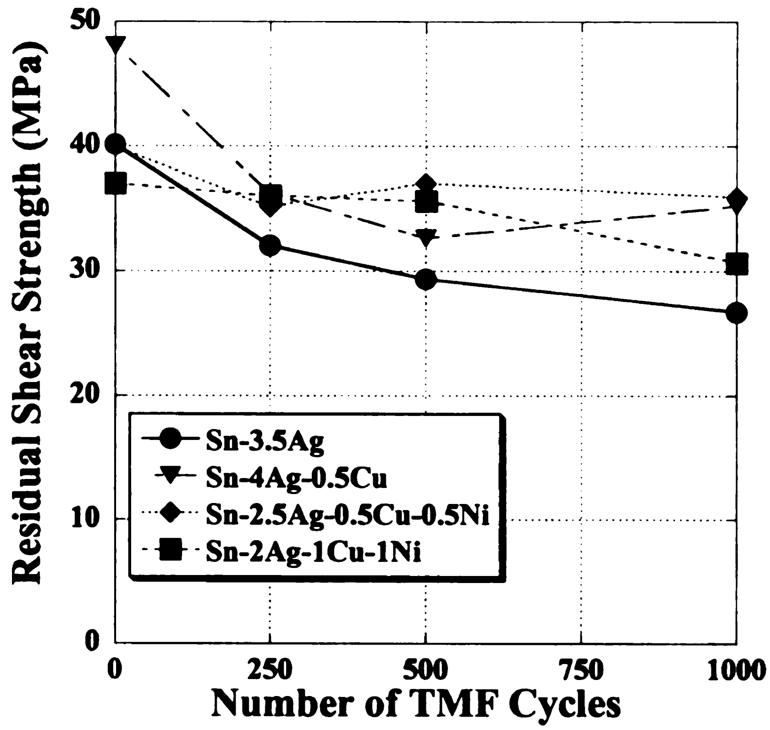

Residual Shear Strength (MPa)
50
40
30
20
10
0
0
250
500
750
1000
Number of TMF Cycles
Sn-3.5Ag
Sn-4Ag-0.5Cu
Sn-2.5Ag-0.5Cu-0.5Ni
Sn-2Ag-1Cu-1Ni

(a)

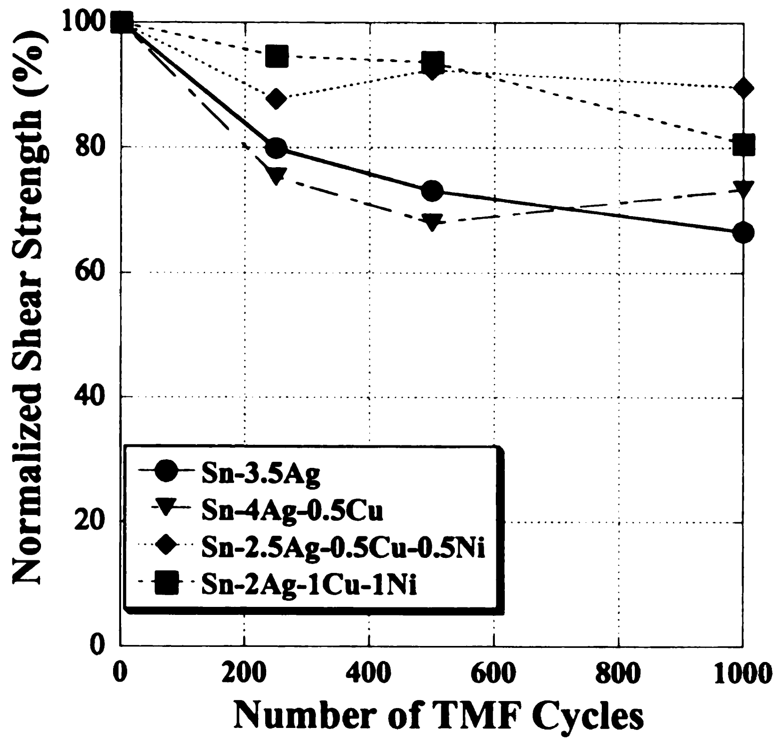

Normalized Shear Strength (%)
100
80
60
40
20
0
0
200
400
600
800
1000
Number of TMF Cycles
Sn-3.5Ag
Sn-4Ag-0.5Cu
Sn-2.5Ag-0.5Cu-0.5Ni
Sn-2Ag-1Cu-1Ni

(b)

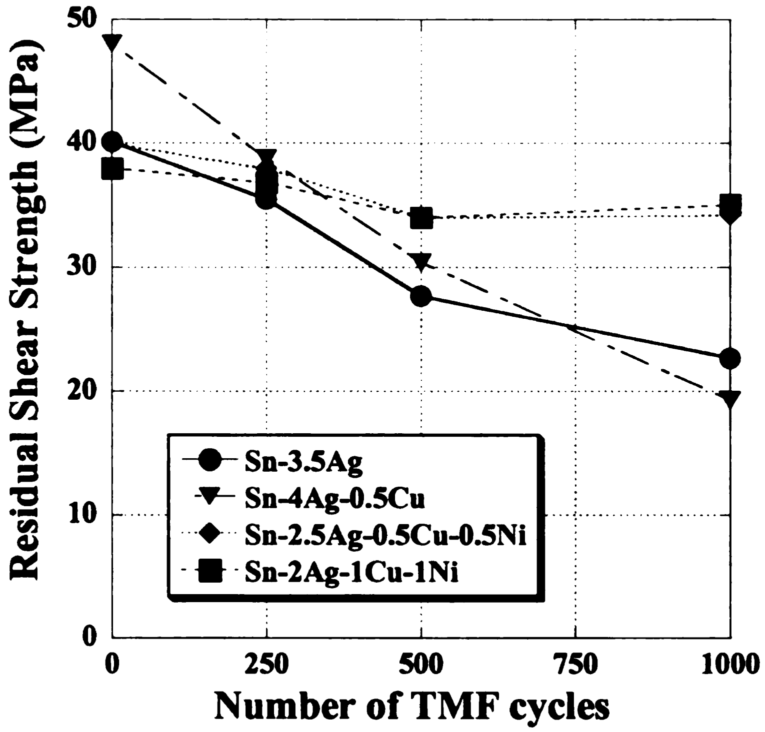

(c)

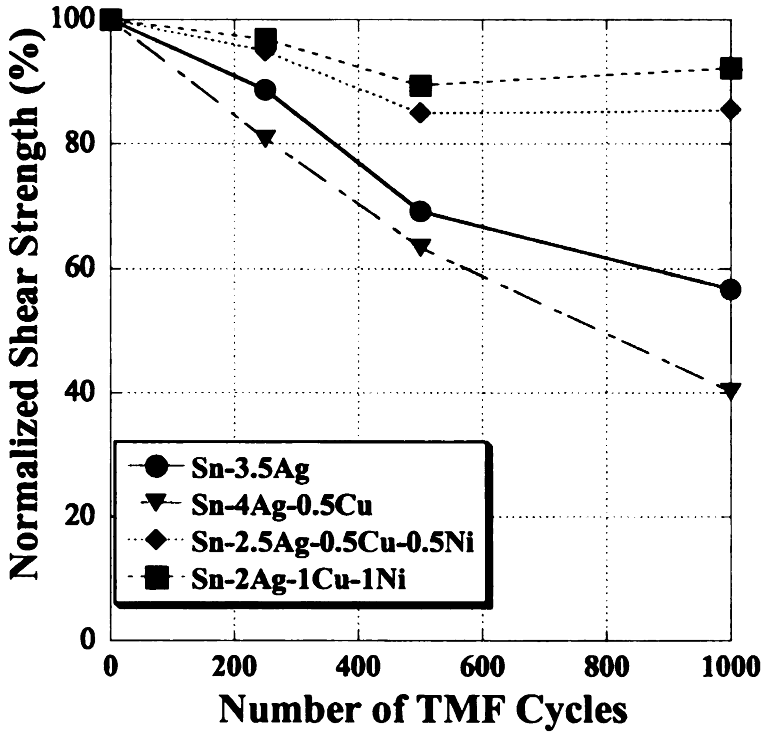

(d)

Figure 6.11. Residual mechanical behaviors of Sn-Ag based solder joints undergoing 1000 TMF cycles. (a) shear strength versus number of TMF cycles with slower heating rate, (b) normalized shear strength versus number of TMF cycles with slower heating rate, (c) shear strength versus number of TMF cycles with faster heating rate, and (d) normalized shear strength versus number of TMF cycles with faster heating rate.

Unlike binary and ternary solder joints, quaternary solder joints exhibited minimal drop in residual shear strength. The residual shear strength was decreased initially with few hundred TMF cycles. There was no significant drop in residual shear strength was noted between 250 and 1000 TMF cycles in quaternary solder joints, irrespective of different heating rates imposed. The decrease in residual shear strength was within 20 % even after 1000 TMF cycles with both slow and fast heating rates. It suggests that quaternary solder joints were not influenced significantly by change in heating rates during TMF.

6.3-3. Possible Reasons for Better TMF Behavior in Quaternary Solder Joints than That of Binary and Ternary Solder Joints

Quaternary alloys containing both Ni and Cu did not show significant surface damage accumulation or a decrease in strength even after 1000 TMF cycles, irrespective of imposed heating rates. These quaternary alloys have also been found to posses better high temperature creep properties than that of eutectic Sn-Ag [44]. The second phase IMC particles present in these quaternary solder joints are (Cu-Ni-Sn) IMC particles and these IMC particles did not coarsen even under long dwell time exposure at the high temperature extreme during TMF. Rhee et. al. [100] reported that in eutectic Sn-Ag solder joints, high temperature deformation is dominated by grain boundary sliding. Keying the grain boundary movement, to retard their relative movement can improve mechanical properties of Sn-Ag based solder joints, especially at high temperature.

Figures 6.12(a) and (b) are micrographs of eutectic Sn-Ag and Sn-2Ag-1Cu-1Ni solders after etching with 5 vol % HNO_3 and 95 vol % methanol for 1 second to reveal Sn grain boundaries in the solder area. Eutectic Sn-Ag exhibited Ag_3Sn IMC precipitates as can be seen in Figure 6.12(a). For Sn-2Ag-1Cu-1Ni solder joints, the (Cu-Ni-Sn) ternary IMC precipitates are present at the Sn-Sn grain boundaries, and smaller amounts of continuous narrow Ag_3Sn precipitates that are present within Sn grains can be noted in Figure 6.12(b). These (Cu-Ni-Sn) IMCs do not coarsen during TMF, probable due to the very slow diffusion of Ni in Sn [101]. The presence of these fine, stable, hard, sub-micron sized (Cu-Ni-Sn) IMC's at the grain boundaries can retard the relative grain boundary movements by keying the grain boundaries resulting in better TMF resistance, irrespective of heating rate imposed.

6.3-4. Possible Reasons for Worse TMF Behavior in Ternary Solder Joints Than That of binary And Quaternary Solder Joints

The second phase IMC precipitates present in Sn-4Ag-0.5Cu are Cu_6Sn_5 that formed during reflow. Initially, only a small number of Cu_6Sn_5 IMC particles formed during reflow as seen in Backscatter Electron (BE) image of an as-fabricated Sn-4Ag-0.5Cu solder joint (Figure 6.13). Cu_6Sn_5 IMC particles presented in the as-fabricated joint were generally very small, and they enhance initial mechanical strength of joint made with that solder. However, a large number of (Cu-Sn) IMC particles were found after 1000 TMF cycles. These (Cu-Sn) IMC particles were not easily detected by Scanning Electron (SE) images (Figure 6.14(a)), but BE images allowed to distinguish these (Cu-Sn) particles, as can be noted in Figure 6.14(b). Energy Dispersive Spectroscopy (EDS) analysis was carried out to determine the composition of these IMC particles, as can be seen in Figures 6.14(c) through (e). The size of (Cu-Sn) particles increased with increasing number of TMF cycles and resulted in significant coarsening during high temperature dwell in TMF. Accumulation of aging time at the

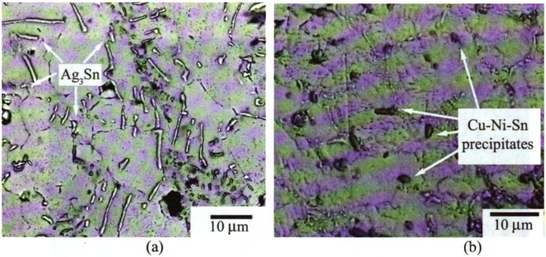

Figure 6.12. Etched microstructures of (a) eutectic Sn-Ag and (b) Sn-2Ag-1Cu-1Ni. (Cu-Ni-Sn) IMC precipitations that may key grain boundary movements can be seen in (b).

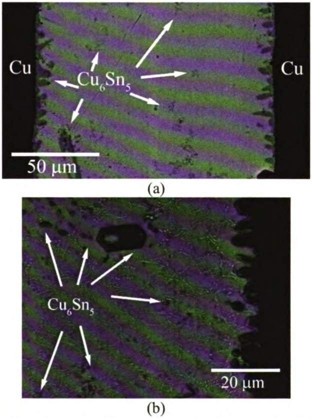

Figure 6.13. Backscatter Electron (BE) images of as-fabricated Sn-4Ag-0.5Cu showing small amounts of Cu_6Sn_5 IMC particles in as-fabricated condition. (a) low magnification, and (b) high magnification.

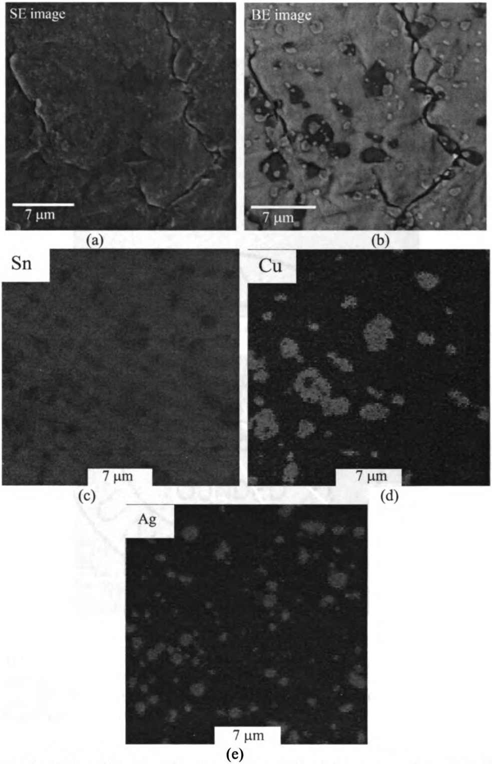

Figure 6.14. Series of images of Sn-4Ag-0.5Cu solder joint that experienced 1000 TMF cycles. (a) Scanning Electron (SE) image, (b) Backscatter Electron (BE) image, (c) Energy Dispersive Spectroscopy (EDS) mapping showing Sn in these particles, (d) EDS

mapping showing Cu in these particles, and (e) EDS mapping showing Ag in these particles.

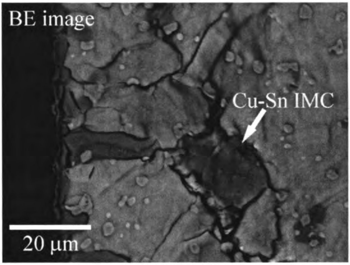

(a)

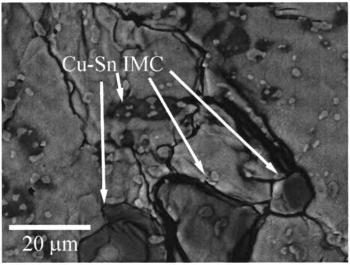

(b)

Figure 6.15. SEM images of Sn-4Ag-0.5Cu solder joints after 1000 TMF cycles. (a) Backscatter Electron (BE) image showing (Cu-Sn) IMC particles at cracked area near IMC layer, (b) Backscatter Electron (BE) image showing (Cu-Sn) IMC particles at cracked area with solder region.

temperature extreme during TMF cycle imposed was about 2000 hours after 1000 TMF cycles. This may cause significant coarsening of Cu-Sn IMC particles during TMF Cracks have been observed to form under such condition. Such a crack may propagate more easily with the growth of (Cu-Sn) IMC particles with increasing number of TMF cycles because of higher stress at Sn-Sn grain boundaries. These Cu-Sn particles were mostly found at highly damaged solder areas as can be seen in Figure 6.15. Cracks developed due to Cu-Sn IMC particles in Sn-4Ag-0.5Cu may result in significant deterioration in residual shear strength. Under a faster heating rate, Sn-4Ag-0.5Cu will experience a higher strain rate. High temperature strain rate sensitivity of Sn-Ag-Cu solder has been noted to be higher than those of other solders studied [102]

Creep studies carried by Grusd [54] indicated that Sn-4Ag-0.5Cu solder joints exhibited better creep-rupture resistance at room temperature than eutectic Sn-Ag solder joints. However, creep-rupture resistance of Sn-4Ag-0.5Cu solder at 100°C was the opposite of the room temperature creep behavior. Similarly, Guo et. al. [55] have reported that the eutectic Sn-Ag solder joints showed better creep resistance in terms of the maximum strain for onset of tertiary creep than Sn-4Ag-0.5Cu at high temperature (85°C) while Sn-4Ag-0.5Cu joints exhibited better room temperature creep resistance than Sn-Ag solder joints. Such findings are consistent with the observed poor performance of Sn-Ag-Cu solder under TMF with a fast heating rate.

Suhling et. al. [56] have reported effects of fourth alloying addition to 95.5Sn-3.8Ag-0.7Cu solder joints on TMF under two different temperature ranges (-40 to 125°C and -40 to 150°C). Sn-3.8Ag-0.7Cu solder joints exhibited worse TMF resistance than Sn-37Pb under TMF with a temperature range from -40°C to 150°C. However, the TMF resistance of SAC alloys were significantly improved with the addition of a forth element under TMF with a temperature range from -40°C to 150°C. Such findings indicate that a certain alloy addition can play significant roles in improving TMF resistance of Sn-Ag-Cu alloy.

6.4. SUMMARY

TMF with a fast heating rate produced significant visible damage in eutectic Sn-3.5Ag and Sn-4Ag-0.5Cu solder joints. Highly localized surface damage accumulation was found in eutectic Sn-3.5Ag and Sn-4Ag-0.5Cu solder joints under TMF with faster heating rate as compared to the same solder joints that under slower heating rate. About a 42 % of drop in residual shear strength was noted after 1000 TMF cycles with a fast heating rate in eutectic Sn-Ag solder joints. Residual shear strength of Sn-4Ag-0.5Cu continues to decrease even after TMF cycles, resulting in a decrease of about 60 % in the residual strength under faster heating rate. It exhibited only about 35 % drop due to TMF with slower heating rate.

Quaternary solder joints (Sn-2.5Ag-0.5Cu-0.5Ni and Sn-2Ag-1Cu-1Ni) showed minimal drop in simple shear strength even after a maximum of 1000 TMF cycles for both slow and fast heating rates. Sn-2.5Ag-0.5Cu-0.5Ni exhibits minimal surface undulations while Sn-2Ag-1Cu-1Ni exhibits almost no surface damage even after 1000 TMF cycles for both fast and slow heating rates. No significant interface IMC layer growth and particle coarsening were observed even after 1000 TMF cycles in these quaternary alloys.

Solder joints made with ternary Sn-4Ag-0.5Cu exhibited the worst TMF behavior among Sn-Ag based solder joints. Among all Sn-Ag based solder joints studied, ternary solder joints that contained small amounts of Cu were highly sensitive to change in heating rates during TMF.

CHAPTER 7

MICROSTRUCTURAL FEATURES CONTRIBUTING TO ENHANCED BEHAVIOR OF TIN-SILVER BASED SOLDER JOINTS

ABSTRACT

Role of microstructure of solder joints made with eutectic Sn-Ag solder and Sn-Ag solder with Cu and/or Ni additions on the creep and thermomechanical fatigue (TMF) properties was investigated. Quaternary alloys containing small amounts of Cu and Ni exhibited better creep resistance at higher temperatures, and also better TMF resistance with longer dwell times at high temperature extreme than eutectic Sn-Ag, and Sn-Ag-Cu ternary alloy solder joints. Microstructural studies of the quaternary solder alloys revealed the presence of ternary Cu-Ni-Sn intermetallic compound (IMC) second-phase at Sn grain boundaries. These precipitates can retard grain boundary sliding that will result during TMF with longer dwell times at high temperature extreme, and high temperature creep.

7.1. INTRODUCTION

Significant research efforts are being expended along various avenues to find suitable substitutes for the lead-bearing electronic solders e.g. [3,67,103,104]. Using eutectic Sn-Ag solder as a basis, several approaches have attempted to modify its properties to address in service needs. One such approach involves the development of ternary and quaternary alloys with additions of Cu, Ni, Bi, Sb, and rare-earth elements etc [11-16]. Thermomechanical Fatigue (TMF) failures that occur as a consequence of stresses that develop due to coefficient of thermal expansion (CTE) mismatches between component leads, the solder, and the substrate during temperature excursions experienced in service, are the a common cause of failure in electronic circuitry [104]. In order to understand the basic operating mechanisms and contributing factors to such failures in Pb-free solders, several focused studies have been conducted e.g. [44,55,82,85,86]. Such studies include the tests on the isothermal creep [55,85]/stress-relaxation [86] properties and TMF tests with different dwell times [44,82,99]. They have shown that quaternary solder alloys containing small amounts of Cu and Ni possess better high temperature creep resistance and better TMF resistance [55,99]. The presence of both Ni and Cu as alloying elements in Sn-Ag solder seems to be beneficial. The main objective of this study is to investigate the microstructural features that contribute to the enhanced performance of these quaternary alloys.

7.2. BACKGROUND

This background information is based on studies conducted with solder joints made with (*i*) eutectic Sn-Ag, (*ii*) Sn-4Ag-0.5Cu, (*iii*) Sn-2.5Ag-0.5Cu-0.5Ni, and (*iv*)

Sn-2Ag-1Cu-1Ni solder pastes. The detailed configurations of the dog-bone shaped single shear-lap solder joint and soldering procedure used in this study have been reported elsewhere [55,85,86].

Although the full details of test regime have been given [44,55,86], some of the important details are repeated here so as to provide a quick review. TMF cycling between –15°C and +150°C was imposed on the solder joints with controlled ramp rates and dwell times. A 25°C/min heating rate and 7°C/min cooling rate were imposed for two different dwell times to investigate the effect of dwell times. Firstly, TMF cycles with longer dwell times at the low temperature extreme were carried out, with a dwell for 300 min at the low temperature extreme and a dwell for 20 min at the high temperature extreme. Secondly, a longer dwell time at the high temperature extreme was imposed. i.e. 115 min at the high temperature extreme and 20 min at low temperature extreme. Mechanical tests to measure the residual shear strength of the solder joints after TMF were carried out using a simple shear test. A more comprehensive description of the experimental details of these shear tests is available elsewhere [44,82,99]. Details of the creep test procedure have been reported in several earlier publications [55,85]. These tests were carried out 22°C and 85°C with stress range from 5.5 to 24 MPa [55]

Quaternary alloy solder joints that were subjected to the TMF with a longer dwell time at the high temperature extreme exhibited better TMF resistance compared to eutectic Sn-Ag, as seen in Table 7.1 [99]. Even after 1000 TMF cycles, almost no surface damage was noted in joints made with the quaternary alloys. Surface damage due to TMF in joints made with eutectic Sn-Ag and the ternary alloy tends to increase significantly with an increasing number of TMF cycles. Joints made with Sn-2Ag-1Cu-

Table 7.1. Residual shear strength of Sn-Ag base solder joints underwent TMF with different dwell times at low and high temperature extremes after maximum 1000 TMF cycles [99].

Materials	% drop in residual shear strength with long dwell time at low temperature extreme	% drop in residual shear strength with long dwell time at high temperature extreme
Eutectic Sn-Ag	~52%	~ 40 %
Sn-4Ag-0.5Cu	~45%	~ 27 %
Sn-2.5Ag-0.5Cu-0.5Ni	~39%	~ 20 %
Sn-2Ag-1Cu-1Ni	~55%	~ 20 %

Table 7.2. Comparison of strain for the onset of tertiary creep between eutectic Sn-Ag solder joints and Sn-2Ag-1Cu-1Ni crept at 22°C and 85°C under stresses ranging from 5.5 to 24 MPa [55].

Materials	Crept at 22°C	Crept at 85°C
Eutectic Sn-Ag	~0.3	~0.3
Sn-2Ag-1Cu-1Ni	~0.3	~0.5

1Ni solder exhibited a drop in residual simple shear strength of about 20 % after 1000 TMF cycles, while eutectic Sn-Ag solder exhibited a drop of 40 % after 1000 TMF cycles with a long dwell time at the high temperature extreme [99]

All these four solder alloy joints exhibited surface damage accumulation due to the TMF cycles with longer dwell time at the lower temperature extreme. Among these alloys under such conditions, minimum surface damage was noted in joints made with quaternary alloys [44]. The residual mechanical strength of all these alloys under such condition decreased by about 40-55 % after 1000 TMF cycles [99]

All these four solder alloy joints exhibited surface damage accumulation due to the TMF cycles with longer dwell time at the lower temperature extreme. Among these alloys under such conditions, minimum surface damage was noted in joints made with quaternary alloys [44]. The residual mechanical strength of all these alloys under such condition decreased by about 40-55 % after 1000 TMF cycles [99].

In high temperature (85°C) creep tests, the quaternary alloy (Sn-2Ag-1Cu-1Ni) showed better creep resistance in terms of the lowest secondary creep rate and the highest strain for onset of tertiary creep. Strain for the onset of tertiary creep in the quaternary alloy was about 66 % higher than that for the eutectic Sn-Ag solder joints as indicated in Table 7.2 [55]. However, the creep resistance of this quaternary solder alloy is not significantly improved during room temperature creep [55].

7.3. EXPERIMENTAL PROCEDURE

To investigate the role of microstructural features contributing to the observed behaviour, specimens were made with these four Sn-Ag based solder pastes by reflow on copper substrates (2cm x 2cm x 1.5cm) with the same heating profile used to fabricate the single shear-lap solder joints. Although results cited from prior studies are based on tests carried out on actual solder joints, it was too difficult to etch the small solder area of the single shear-lap joints. As a consequence, the following alternative method was used to observe a larger etched solder area to reveal the Sn-Sn grain boundaries and the location of any precipitates. The solder buttons formed on the Cu substrates were sectioned and the cut surfaces of these specimens were metallurgically polished. The details of the specimen configuration and the experimental procedure for polishing can be found elsewhere [105]. These specimens were then etched with 5 vol % HNO_3 and 95 vol % methanol for 1 second and washed with water. The polished and etched face of cross section specimens then were examined using SEM. The solder joints used for creep and TMF studies had a joint thickness of about 100 μm. As a consequence, the specimens cross-sectioned and etched were observed in regions within 50 μm from the Cu/solder interface, as illustrated in Figure 7.1.

7.4. RESULTS AND DISCUSSION

The microstructures of polished and un-etched solder specimens made with these solder alloys on Cu substrates are shown in Figure 7.2. The microstructures of the eutectic Sn-Ag and ternary alloy (Sn-4Ag-0.5Cu) are similar, since Sn cells separated by wide bands of Ag_3Sn precipitates characterize these solders. However, the difference between these two solders is the presence of small amounts of Cu_6Sn_5. Since there is less Ag in these alloys, the Ag_3Sn bands are narrower and more uniform than in eutectic Sn-Ag and Sn-4Ag-0.5Cu. Especially, Sn-2Ag-1Cu-1Ni has much thinner Ag_3Sn bands

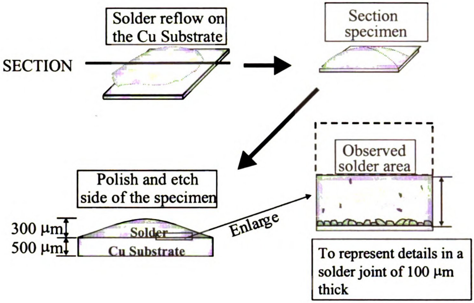

Figure 7.1. Schematic drawing of solder specimens used in the present study.

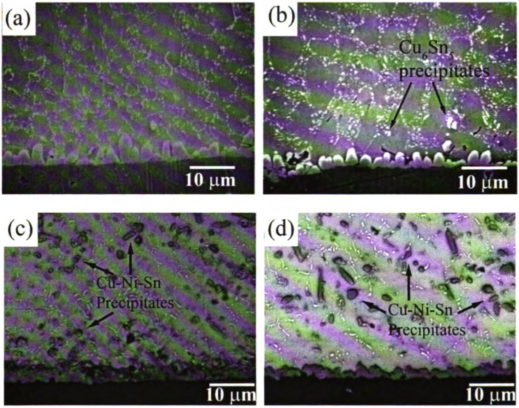

Figure 7.2. SEM images of as-fabricated specimens without etching. (a) Eutectic Sn-3.5Ag, (b) Sn-4Ag-0.5Cu, (c) Sn-2.5Ag-0.5Cu-0.5Ni, and (d) Sn-2Ag-1Cu-1Ni.

and more Cu-Ni-Sn intermetallic precipitates due to the presence of more Cu and Ni, and less Ag, since both have the same alloying elements. As seen in Figures 7.2(c) and 7.2(d), multiple Cu-Ni-Sn ternary IMC precipitates are present through out the solder area.

Backscatter electron (BE) images of etched eutectic Sn-Ag solder specimens show wide primary Ag_3Sn bands and Sn grain cells as shown in Figure 7.3. No second-phase precipitates, except Ag_3Sn, are present at the grain boundaries and this solder exhibits the worst high temperature creep resistance and TMF resistance.

In order to identify the composition of second phase IMC precipitate in ternary and quaternary solder alloys, Energy Dispersive Spectroscopy (EDS) analysis was carried out across these IMC precipitates as seen in Figure 7.4. Figure 7.4(a) shows second phase IMC precipitates, which consist of mainly Cu and Sn that is identified as Cu_6Sn_5 in Cu containing Sn-Ag based solder joints. The second phase IMC precipitates found in the quaternary alloy solder joints consisted of Cu-Ni-Sn ternary IMC as seen in Figure 7.4(b). This Cu-Ni-Sn ternary IMC was identified Chuang *et. al,* [106] as $(Cu, Ni)_6Sn_5$ in Ni containing Sn-Ag based solders.

BE images of ternary Sn-4Ag-0.5Cu are provided in Figure 7.5. As seen in Figure 7.5(b), Cu_6Sn_5 binary IMC precipitates are located at the Sn-Sn grain boundaries. The TMF resistances of these solder joints have been shown to be slightly better than those of eutectic Sn-Ag [99]. A possible explanation for this is that the binary Cu_6Sn_5 second-phase precipitates located at Sn-Sn grain boundaries may retard grain boundary sliding that can occur during the dwell times at the high temperature extreme of TMF cycling and high temperature creep [55,99]. The creep properties of this ternary alloy

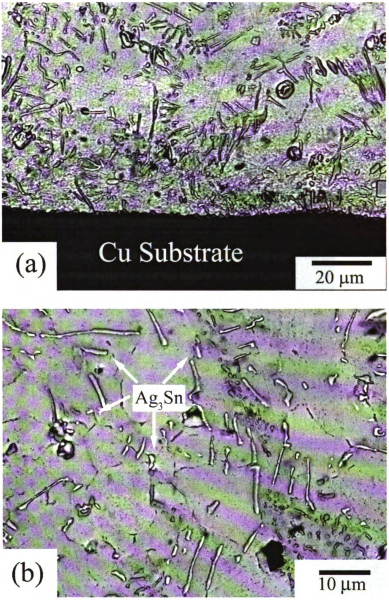

Figure 7.3. BE images of etched eutectic Sn-Ag. (a) Low magnification micrograph of solder specimen showing Cu substrate and IMC layer, (b) High magnification micrograph of solder specimen showing Sn-Sn grain boundaries and Ag_3Sn precipitates (typical eutectic microstructure of Sn-Ag solder).

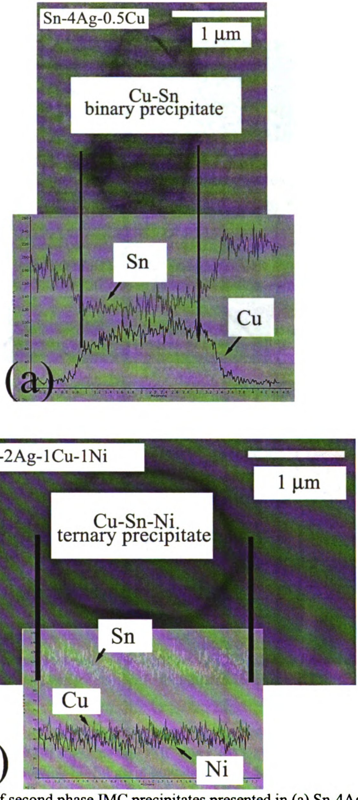

Figure 7.4. EDS of second phase IMC precipitates presented in (a) Sn-4Ag-0.5Cu, and (b) Sn-2Ag-1Cu-1Ni.

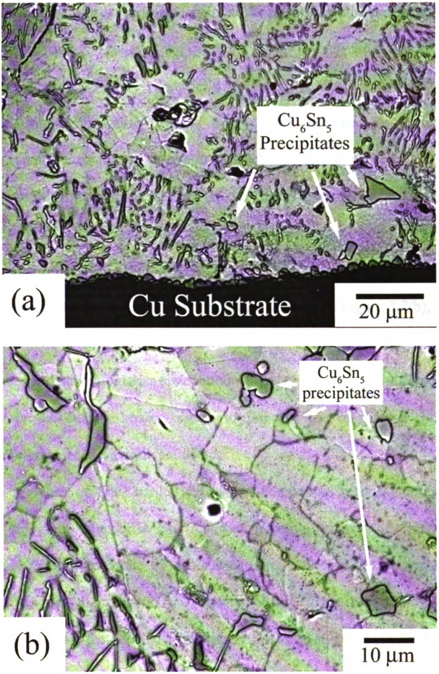

Figure 7.5. BE images of etched Sn-4Ag-0.5Cu. (a) Low magnification micrograph of solder specimen showing Cu substrate and IMC layer, (b) High magnification micrograph of solder specimen showing Sn-Sn grain boundaries, Ag_3Sn precipitates and Cu_6Sn_5 binary IMC precipitates located at Sn-Sn grain boundaries.

are comparable with, but slightly better than, those of eutectic Sn-Ag due to the presence of small amount of Cu_6Sn_5 binary IMC precipitates at Sn-Sn grain boundaries preventing grain boundary sliding. However, the quaternary alloys developed less surface damage accumulation during TMF tests. Especially, quaternary solder joints subjected to a long dwell at the high temperature extreme during TMF exhibited no surface damage accumulation and the smallest decrease in residual mechanical strength [99]. The Cu-Ni-Sn ternary IMC precipitates present at the Sn-Sn grain boundaries, and smaller amounts of continuous Ag_3Sn precipitates that are narrow present within Sn grains can be noted in Figures 7.6 and 7.7.

The small white precipitates seen in Figure 7.6(b) and Figure 7.7(b), are Ag_3Sn, and the dark precipitates are Cu-Ni-Sn ternary IMC. Some of the Ag_3Sn precipitates that are located at grain boundaries are continuous and very small. The presence of such precipitates in the eutectic matrix seems to improve the mechanical behaviour of materials, although not to a significant extent.

The presence of fine, stable, and system-compatible second-phase precipitates located at the grain boundaries can retard coarsening, enhance mechanical fatigue behavior, and reduce creep rate by decreasing grain-boundary sliding tendency [107]. Precipitates present at a grain boundary represent obstacles that resist sliding between the Sn-Sn grains that share the boundary. Temperature can also affect the fracture behavior of Sn-Ag based solder joints. Studies have shown that shear banding is the dominant mode of deformation in solder joints deformed at room temperature, while grain boundary sliding is the dominant mode of deformation at high temperature [107]. As a consequence, during high temperature creep and TMF with a longer dwell times at the

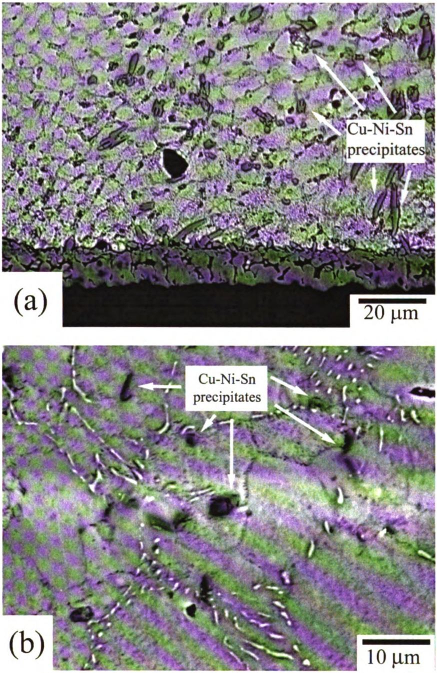

Figure 7.6. BE images of etched Sn-2.5Ag-0.5Cu-0.5Ni. (a) Low magnification micrograph of solder specimen showing Cu substrate and IMC layer, (b) High magnification micrograph of solder specimen showing Sn-Sn grain boundaries, Ag_3Sn precipitates, and Cu-Ni-Sn ternary IMC precipitates located at Sn-Sn grain boundaries.

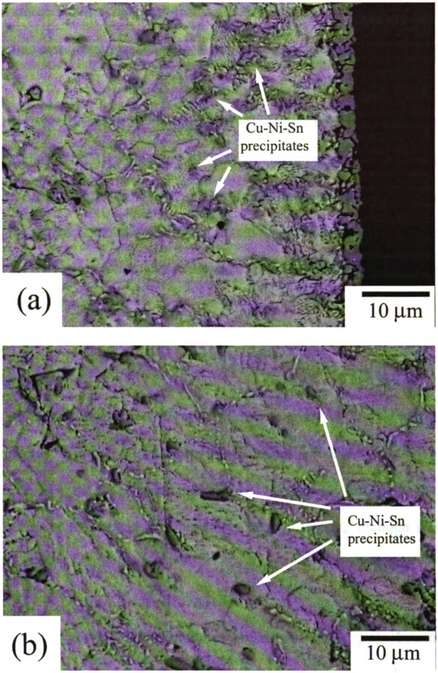

Figure 7.7. BE images of etched Sn-2Ag-1Cu-1Ni. (a) Solder specimen showing Cu substrate and IMC layer, (b) Solder specimen showing Sn-Sn grain boundaries, Ag_3Sn precipitates, and Cu-Ni-Sn ternary IMC precipitates located at Sn-Sn grain boundaries.

high temperature extreme, the dominant deformation mechanism is grain boundary sliding, and this can be minimized with the presence of discrete Cu-Ni-Sn ternary IMC precipitates.

Other studies documented in various alloy systems indicate that such precipitates may constrain plastic flow during creep or TMF at high temperature because the height of the climb barrier is larger, hindering dislocation climb and retarding grain boundary sliding motion. For example, in nickel based super alloys, discrete second-phase precipitates present at grain boundaries increase the strength and high temperature creep resistance of these alloys [108].

7.5. SUMMARY

1. Slightly better creep and TMF properties were noted in Sn-4Ag-0.5Cu compared to eutectic Sn-Ag, due to the presence of small amounts of Cu_6Sn_5 binary IMC precipitates at the Sn-Sn grain boundaries. Ag_3Sn may influence the mechanical behaviour of Sn-Ag based solder joints to some extent, although it may not be significant.

2. Discrete Cu-Ni-Sn IMC precipitates present at Sn-Sn grain boundaries were observed in Sn-2.5Ag-0.5Cu-0.5Ni and Sn-2Ag-1Cu-1Ni. These quaternary alloys exhibited a lower secondary creep rate and higher strain for onset of tertiary creep at high temperature (85°C), and better TMF performance under a longer dwell times at the high temperature extreme, indicating that the precipitates present at Sn-Sn grain boundaries can improve the performance of the solder

joints, especially at high temperature when the deformation is dominated by grain boundary sliding.

CHAPTER 8

SUMMARY

Deformation behavior and damage accumulation during thermomechanical fatigue (TMF) under different service conditions were characterized using the single shear-lap eutectic Sn-3.5Ag, Sn-4Ag-0.5Cu, Sn-2.5Ag-0.5Cu-0.5Ni, and Sn-2Ag-1Cu-1Ni solder joints. The important findings from those studies are summarized.

Microstructural studies of four Sn-Ag based solder joints that underwent 0, 250, 500 and 1000 TMF cycles between $-15^{\circ}C$ and $+150^{\circ}C$, with a 20 minute hold time at the low temperature extreme and with a 330 minute hold time at the high temperature extreme were performed. Damage during thermomechanical fatigue initiated on the surface and intensified with additional number of TMF cycles. The crack that would cause a catastrophic failure of solder joint occurred very near the IMC layer in the shear direction. Residual shear strength of Sn-Ag based solder joints decrease by 30-60% as a consequence of 250 TMF cycles. Between 250 cycles and 1000 cycles, no significant drop in strength was noted due to TMF with a long dwell time at the low temperature extreme. Small amounts of alloy additions (Cu or Cu and Ni) did not have any pronounced effect on Sn-Ag solder joints under TMF with a longer dwell times at the low temperature extreme. Significant amounts of surface damage were developed with increasing number of TMF cycles. Surface damage features due to TMF under a long dwell time at the low temperature were concentrated shear banding, Sn-Sn grain boundary sliding, and grain decohesion.

TMF with a long dwell time at the high temperature extreme, where dwell times at the high temperature extreme was 115 minutes and dwell times at the low temperature extreme was 20 minutes, resulted in significant surface damage in eutectic Sn-3.5Ag and Sn-4Ag-0.5Cu solder joints. TMF cycling using a long dwell time at the high temperature extreme produced deformation and damage very similar to that observed with longer dwell time at low temperature extreme in eutectic Sn-3.5Ag and Sn-4Ag-0.5Cu solder joints. Overall residual shear strengths of all four Sn-Ag based solder joints were better than that of solder joints that underwent a longer dwell time at the low temperature extreme. Less surface damage and loss of residual shear strength were found in quaternary solder joints that containing small amounts of Cu and Ni.

TMF with a faster heating rate produced more visible damage in eutectic Sn-3.5Ag and Sn-4Ag-0.5Cu solder joints (with a long dwell time at the high temperature extreme). The damage accumulation of these solder joints was more localized as compared to solder joints that were subjected to slower ramp rate during heating segment of TMF cycles About 40 % drop in residual strength was noted after 1000 TMF cycles with the faster heating rate in eutectic Sn-Ag solder joints. Residual shear strength of Sn-4Ag-0.5Cu decreases with additional TMF cycles, which results in a drop of about 60 % in the residual strength due to faster heating rate as compare to solder joints that experienced slower heating rate during TMF. Residual shear strength in Sn-4Ag-0.5Cu decreased significantly with additional TMF cycles with faster heating rate imposed. Sn-2.5Ag-0.5Cu-0.5Ni and Sn-2Ag-1Cu-1Ni showed minimal drop in simple shear strength even after a maximum of 1000 TMF cycles for both slow and fast heating rates imposed. Quaternary solder joints, Sn-2.5Ag-0.5Cu-0.5Ni exhibits minimal surface undulations while Sn-2Ag-1Cu-1Ni exhibits almost no damage even after 1000 TMF cycles for both fast and slow heating rates. No significant interface IMC layer growth and particle coarsening were observed even after 1000 TMF cycles in quaternary solder joints. Solder joints made with ternary Sn-4Ag-0.5Cu exhibited the worst TMF residual strength among Sn-Ag based solder joints under TMF with faster heating rate. Among Sn-Ag based solder joints studied, ternary solder joints containing small amounts of Cu were highly sensitive to change in heating rates during TMF with a long dwell time at the high temperature.

The microstructure of eutectic Sn-Ag and Sn-4Ag-0.5Cu were similar in as-fabricated conditions. However, significant coarsening of (Cu-Sn) IMC particles were found in Sn-4Ag-0.5Cu solder joints under TMF with a longer dwell time at the high temperature extreme under faster heating rate imposed due to long accumulation aging times. Sn-Sn grain boundary sliding was the major deformation features during high temperature shear test in eutectic Sn-3.5Ag solder joints. It suggests that preventing the Sn-Sn grain boundary sliding will result in minimum plastic strain during TMF under a long dwell time at the high temperature extreme. Discrete (Cu-Ni-Sn) IMC precipitates present at Sn-Sn grain boundaries were observed in Sn-2.5Ag-0.5Cu-0.5Ni and Sn-2Ag-1Cu-1Ni. Such precipitates were not observed in the other alloys, so it is hypothesized that these (Cu-Ni-Sn) precipitates are responsible for the improved TMF performance especially at high temperature.

Alloying additions that may be responsible to observed TMF behaviors were discussed. Under different TMF conditions, Sn-Ag based solder joints containing small amounts of Cu and, Cu and Ni exhibited superior TMF behaviors due to presence of (Cu-

Ni-Sn) IMC precipitates in the solder joints. These precipitated keyed the Sn-Sn grain boundaries and made sliding difficult. In ternary alloys, the shapes of precipitates were not as effective in keying grain boundaries. In order to verify the suggested hypotheses regarding microsturctural issues, further systematic experimental study on TMF deformation of the Sn-Ag based solder joints should be conducted.

APPENDEX

EVALUATION OF MATERIAL-RELATED PARAMETERS AFFECTING THE SERVICE LIFE OF TIN-BASED SOLDER JOINTS EXPERIENCING THERMOMECHANICAL FATIGUE

ABSTRACT

A simple parametric empirical approach to predict service life of Sn-based solder joints can be developed. This paper evaluates the material-related parameters in such an empirical equation, that affect the service life of Sn-based solder joints under realistic thermal excursions encountered in service, by incorporating findings from studies related to material and service issues. It also examines the roles of these parameters and their relative importance by analyzing results from studies on Sn-based solder joints of realistic dimensions under realistic thermomechanical fatigue (TMF) cycling, and isothermal shear testing.

1. Introduction

Estimation of service life of solder joints is essential to predict the reliability of electronic devices since the solder joints are the weakest link in electronic devices [12,13,110,111]. The major cause of failure in electronic devices in service is TMF that arises due to differences in coefficient of thermal expansion (CTE) between the entities present in the system [111-114].

There are no simple models available to quickly check the ***useful service life*** of a solder joint under different service conditions. Such service variables can be dwell times at temperature extremes, heating rate, cooling rate, temperature difference, frequency of temperature cycles, etc. Each of these affects the ***useful service life*** of Sn-based solder joints. Various material-related parameters have to be taken into account in such an estimation since they will have significant influences on the roles of these service variables. Prior studies have indicated the importance of such issues in controlling the ***useful service life*** of Sn-based solder joints [115]. Complexities involved in such an analysis are comparable to those encountered in estimation of tool life in machining processes. Tool life is affected by many variables and can be estimated using an empirical equation suggested by Taylor [116]. Similarly a simple parametric empirical approach can be used to evaluate the ***useful service life*** of Sn-based solder joints.

Useful service life prediction is different from predicting ***total lifetime*** of solder joints. Total lifetime of solder joint may correspond to failure of solder joint that can not carry any mechanical/electrical load. Methods suitable to evaluate the total lifetime prediction could be Coffin-Manson or Weibull distribution types of approaches. Weibull distribution, especially will be more appropriate to estimate the total lifetime of solder joints. In actual practice, one would like to remove the component out of service prior to accelerated catastrophic events begin to progress. As a consequence, evaluation of ***useful service life*** is more appropriate since solder joint is usually taken out of service before rapid progression of the damage. Such an approach is very similar to that used in tool life predictions, where one would like to change the tool before it begins to deteriorate rapidly [116]. Thus, the ***useful service life*** prediction might meet the industrial requirement rather than the total lifetime. Latter will have limited practical implications.

In this paper, actual evaluation of material-related parameters in an empirical parametric equation has been carried out from assessment of TMF performance of Sn-based solder joints. Results from realistic TMF tests with different ramp-rates and dwell times at temperature extremes, and supporting isothermal shear tests were used to evaluate these material-related parameters. Material-related parameters evaluated from extremely fast supplementary studies, such as isothermal shear testing and stress relaxation, are compared with those from realistic TMF tests providing a possibility to evaluate these material-related parameters in a rapid manner.

2. Experimental Details

Sn-Ag based solder pastes were sandwiched between two 0.5 mm thick half dog bone shaped Cu strips and subsequently reflowed to produce single shear-lap solder joints with ~ 100 μm thickness and 1mm^2 solder joint area. The detailed configurations of the dog-bone shaped single shear-lap solder joint and soldering procedure used have been reported elsewhere [78,87,88]. Different TMF test conditions used, such as different heating rates and dwell times at each temperature extreme, are listed in Tables IX.1 and 2. Further details can be found from earlier publications [99,117].

Isothermal shear tests using the same joint geometry were carried out with a fixed pre-strain of 0.1 imposed with different strain-rates (0.001/sec. and 0.0001/sec.) at 22°C and 150°C. Peak shear stress and resultant residual shear stress after stress relaxation were measured and used to evaluate some of the material-related parameters. Further details of isothermal shear tests have been reported in prior publications [100,118].

3. Results and Discussion

Apparent relationship between service life of solder joint and residual properties of solder joint should be inversely related to each other. Studies have shown that residual mechanical strength or electrical conductivity resulting from TMF tends to follow a logarithmic power-law type behavior, prior to stabilization followed by domination of

Table IX.1. Details of TMF conditions with two different dwell times at each temperature extreme to evaluate material-related parameter '*r*'. Note: ΔT is 165°C (-15°C to 150°C) for all TMF studies.

Conditions	Heating rate	Dwell time at high T	Cooling rate	Dwell time at low T
Long dwell time at low T	~0.55°C/sec	20 min.	~0.07°C/sec	330 min.
Long dwell time at high T	~0.55°C/sec	115 min.	~0.07°C/sec	20 min.

Table IX.2. Details of TMF conditions with two different heating rates to evaluate material-related parameter '*p*'. Note: ΔT is 165°C (-15°C to 150°C) for all TMF studies.

Conditions	Heating rate	Dwell time at high T	Cooling rate	Dwell time at low T
Slow heating rate	~0.55°C/sec	115 min.	~0.07°C/sec	20 min.
Fast heating rate	~1.1°C/sec	117.5 min.	~0.07°C/sec	20 min.

catastrophic events [82,99,117]. Since the catastrophic events progress rapidly, appropriate ***useful service life*** should be estimated within the regime of the stabilized behavior. As a first approximation each contributing service parameter can be assumed to influence the ***useful service life*** of solder joint in a power-law type relationship in this service regime. Following empirical equation can be employed to evaluate the ***useful service life of the solder joint***:

$$\textbf{\textit{Useful service life}} \propto [\Delta T]^{-m} [f]^{-n} [(dT/dt)_h]^{-p} [(dT/dt)_c]^{-q} [\Delta t_H/\Delta t_L]^{r} [\Delta M]^{s}$$

where, ΔT is imposed temperature difference, f is the frequency of thermal cycles, $(dT/dt)_h$ is heating rate, $(dT/dt)_c$ is cooling rate, $(\Delta t_H/\Delta t_L)$ is the ratio of dwell times at high and low temperature extremes, and (ΔM) is any other material parameter such as microstructure changes during TMF. m, n, p, q, r, and s are material-related parameters that can be determined from experimental results. The constant of proportionality can account for the influences of processing parameters and the joint geometry

In this paper, $(\Delta M)^s$ is assumed to remain constant since no significant surface microstructural changes were noted to result from TMF prior to catastrophic damage accumulation. $(\Delta M)^s$ will probably play significant roles in later stages of TMF when the relative influences of these material-related parameters on each other will become very dominant. Since, this paper deals with ***useful service life*** of the solder joint rather than total life, the role of $(\Delta M)^s$ is not included in the discussion. Solder joints are usually taken out of service before the damage progresses in such a catastrophic manner, just as tools that are taken out of service prior to rapid wear that occurs in the final stages of tool life. Appropriate material-related parameter affecting the role of frequency of thermal cycles, n, could not be evaluated at this time due to lack of available data.

As seen in Figure. IX.1, the lifetime or any other reliability related issues of a solder joint, could be depicted in three stages (internal damage build-up, surface manifestation of damage with no significant property changes, and progress of catastrophic failure). Such findings are very similar to those encountered in the life of a tool [116]. Tools exhibit rapid initial wear, followed by gradual wear and accelerated wear during service. Since machining by tools undergoing accelerated wear will be of poor quality, and the life time of the tools when machining under such conditions is highly unpredictable, they are taken out of service in the regime of gradual wear after undergoing certain extent of wear. So tool life prediction is based useful service life in the gradual wear regime.

Weibull distribution may be a better method to predict total lifetime of solder joints [119]. Although parametric empirical approach proposed in this study is simple, it will be more appropriate to predict ***useful service life*** of solder joint in a relatively quick manner. Thus, it provides an estimation of ***useful service life, rather than total lifetime,*** of Sn-based solder joints is the main focus of this paper.

In order to evaluate a given material-related parameter, certain conditions need to be met: (i) maintain process, and joint geometry parameters fixed, (ii) vary only the service parameter influenced by the chosen material-related parameter, and (iii) hold all other service parameters fixed.

Method to evaluate a given material-related parameter from actual TMF results consisted of the following steps:

(i) take ratio of percent decrease in residual properties for two different conditions,

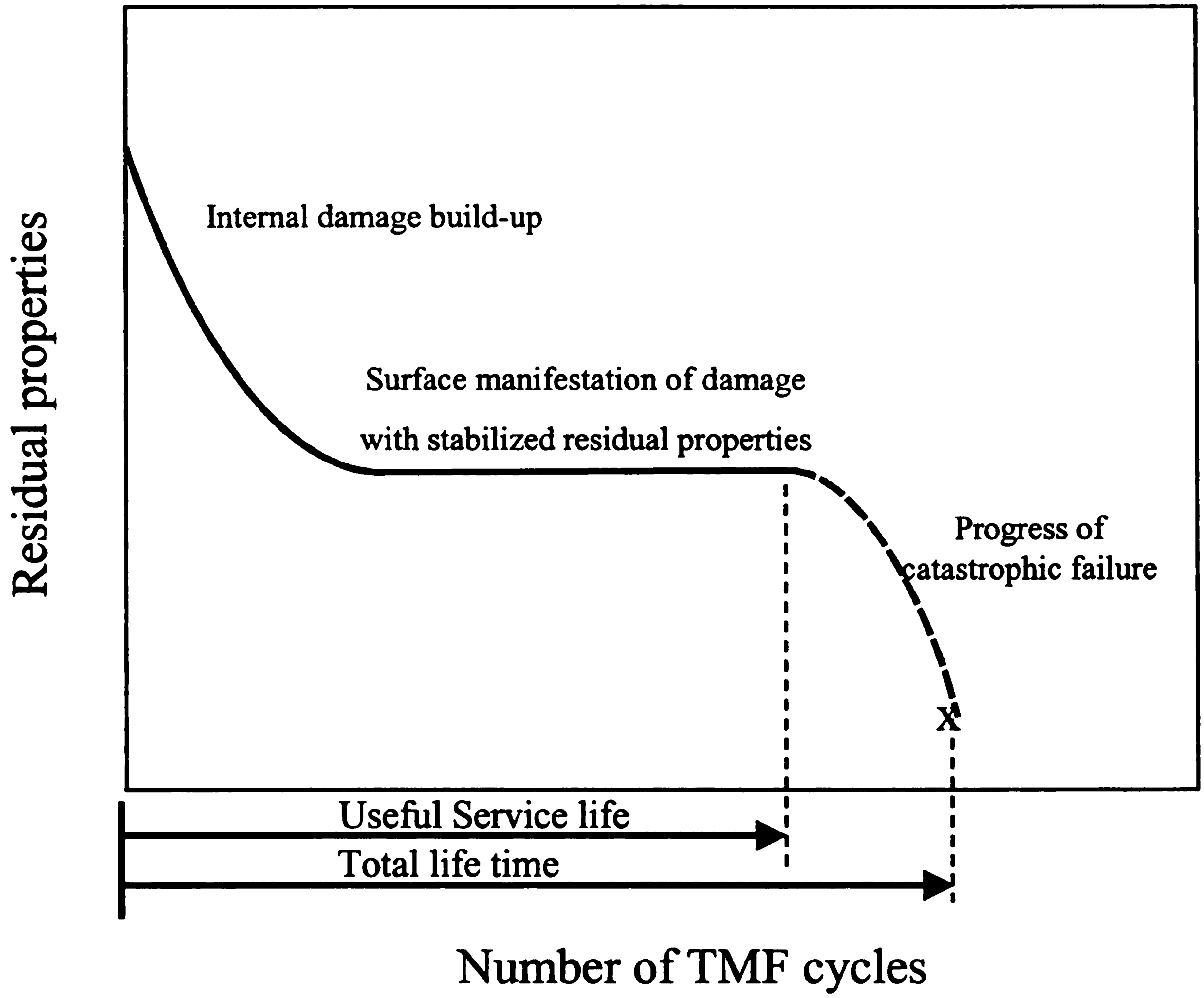

Figure IX.1. A schematic of residual properties of solder joints under TMF conditions classified into three stages. Solid line represents region of ***useful life*** of solder joint. The dot line represents the range in which catastrophic failure takes place and is not addressed in this study.

(ii) use this ratio to represent ratio of damage accumulation under these conditions, and evaluate the approximate material-related parameter using these two conditions.

Evaluation of 'r' in $[\Delta t_H/\Delta t_L]^r$ and 'p' in $[(dT/dt)_h]^{-p}$ from Actual TMF Results

Material-related parameters r in $[\Delta t_H/\Delta t_L]^r$ and p in $[(dT/dt)_h]^{-p}$ were evaluated by using results from actual TMF tests on solder joints made with four different Sn-Ag based solder alloys.

As mentioned in the earlier section (see Table IX.1), dwell times at each temperature extreme were the only varied service parameter in this case. Figure IX.2 provides the values of parameter *'r'* in $[\Delta t_H/\Delta t_L]^r$ evaluated four Sn-Ag based solder alloy joints. The exponent *'r'* ranged from 0.11 to 0.21 depending on the solder alloy. Solder joints made with quaternary alloys were more sensitive to dwell time changes than the binary and ternary solders. Prior studies [99,117] have indicated that quaternary solder alloy joints containing small amounts of Cu and Ni possess better TMF performance under long dwell times at high temperature extreme [82].

With two different heating rates during the TMF cycles (see Table VIIII.2), material-related parameter *'p'* in $[(dT/dt)_h]^{-p}$ can be evaluated. As can be seen in Figure VIII.3, value of parameter *'p'* is larger than *'r'* for all the four Sn-Ag based solder alloys studied. Such a finding indicates that varying heating rate could have more influence on the ***useful service life*** of Sn-Ag based solder joints than changes in dwell times at temperature extremes. This data also indicates that ***useful service life*** of quaternary alloys are less sensitive to heating rate than eutectic Sn-Ag.

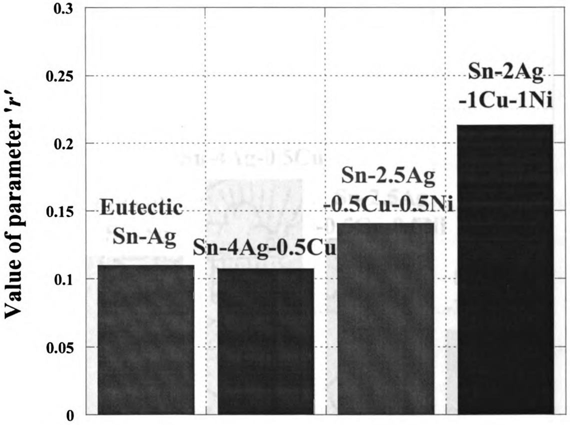

Figure IX.2. Material-related parameter *'r'* in $[\Delta t_H/\Delta t_L]^r$ for Sn-Ag based single shear-lap solder joints.

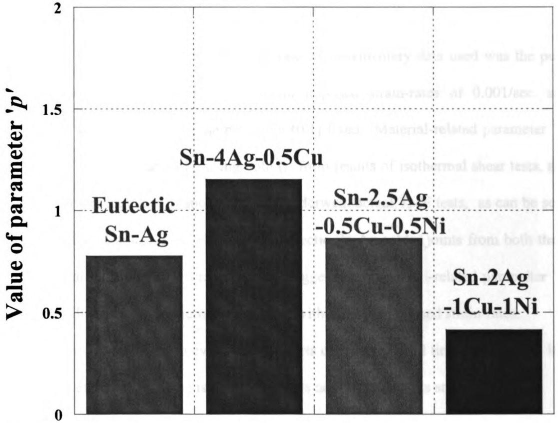

Figure IX.3. Material-related parameter *'p'* in $[(dT/dt)_h]^{-p}$ for Sn-Ag based single shear-lap solder joints.

Evaluation of Material-Related Parameters from Supporting Studies (from Isothermal Shear Tests)

In isothermal shear tests, peak shear stress can be assumed to represent damage accumulation for a given strain. Similarly, the resultant residual shear stress after stress relaxation can also be assumed to represent damage accumulation resulting from an imposed pre-strain.

In order to check the effect of heating rates, supplementary data used was the peak shear stresses at 150°C with two different imposed strain-rates of 0.001/sec. and 0.0001/sec., while maintaining the pre-strain (0.1) fixed. Material-related parameter *'p'* in $[(dT/dt)_h]^{-p}$ was evaluated by using both (i) from results of isothermal shear tests, and (ii), residual strength data of specimens that underwent actual TMF tests, as can be seen in Figure IX.4. Values of *'p'* obtained for eutectic Sn-Ag solder joints from both these approaches are fairly close. Such a finding suggests that material-related parameter *'p'* could be evaluated from isothermal shear tests with different imposed strain-rates.

However, a scheme to evaluate the effects of ratio of dwell times at high and low temperature extremes by using isothermal tests is not devised at this stage.

Similarly, effects of cooling rate can be evaluated from results of isothermal shear tests. Such an evaluation used the peak shear stresses, for two different strain-rates at lower temperature extreme. Again, the pre-strain (0.1) was fixed for this computation. As can be seen in Figure IX.5, varying cooling rates has almost the same effect as varying heating rates on ***useful service life*** of eutectic Sn-Ag solder joints..

One of the important findings from evaluation of parameters from isothermal shear tests was the ratio representing different strain-rate conditions for fixed pre-strain,

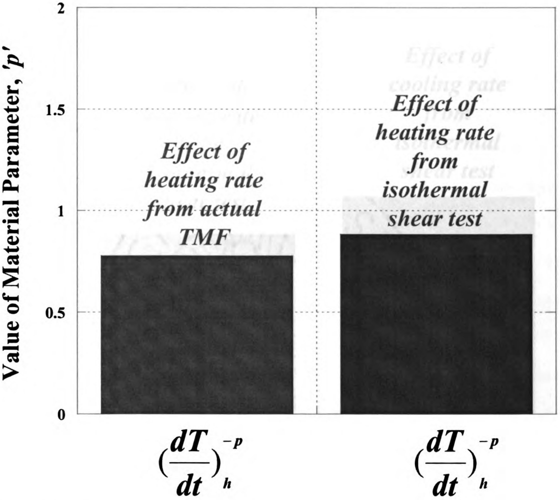

Figure IX.4. Comparison of material-related parameter *'p'* in $[(dT/dt)_h]^{-p}$ for eutectic Sn-Ag solder joints evaluated from both actual TMF test and isothermal shear test.

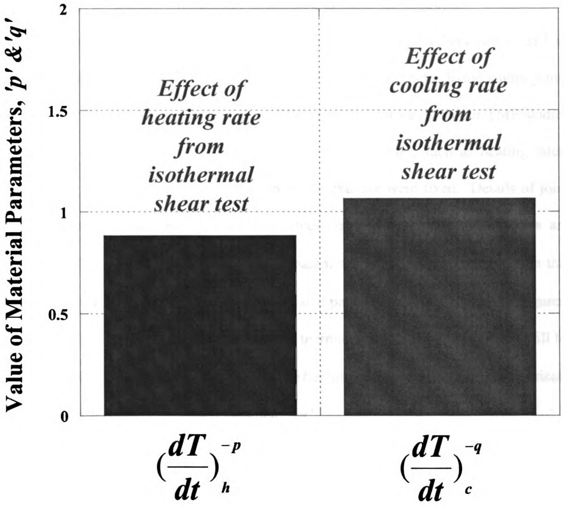

Figure IX.5. Material-related parameter *'p'* in $[(dT/dt)_h]^{-p}$ and *'q'* in $[(dT/dt)_c]^{-q}$ for eutectic Sn-Ag solder joints from isothermal shear test.

were about the same irrespective of whether it was calculated using peak shear stress or the stabilized stress after relaxation.

Evaluation of 'm' in $(\Delta T)^{-m}$ from Published Work of Other Investigators

Results from two TMF studies, published by other researchers, were used to evaluate the effect of temperature difference during TMF on Sn-Ag based solder joints for this part of analysis, since temperature difference was not varied in our TMF studies [45,46]. In each of these published studies, service variables, such as heating rates, cooling rates, and dwell times at each temperature extreme were fixed. Details of joint geometry, material used, temperature differences employed by these investigators are provided in Table IX.3. The material-related parameter *'m'* in $(\Delta T)^{-m}$ obtained from this analysis is much greater than other material-related parameters as can be seen in Figures. IX.6 and IX.7. It is expected to be large since thermal stress causing the damage will be directly proportionally to ΔT. As expected different solder materials used to fabricate solder joints affect material-related parameter *'m'*.

Most well-known approach to predict the total lifetime of solder joints under TMF is Coffin-Manson equation. However, this equation deals with strain range, especially plastic range within single cycle under isothermal condition, and it might overestimate the actual lifetime of solder joints [3,119]. This model does not account for the effects of time and temperature which are important factors for materials stressed at above one half of the melting point in degrees absolute [120]. In order to consider the effects of temperature and frequency, modified Coffin-Manson (Norris-Landsberg) equation has

Table IX.3. Details of joint geometry and different imposed temperature difference used to evaluate material-related parameter *'m'* from published literature [45,46].

Ref.	Joint geometry	ΔT_1	ΔT_2	Materials used
Kariya et al. [45]	Quad Flat Pack Lead (QFP)	160°C (-30°~130°C)	100°C (0°~100°C)	Sn-Ag, Sn-Ag-0.5Cu, Sn-Ag-1Cu
Poon et al.[46]	SMT	150°C (-25°~125°C)	110°C (-25°~85°C)	Sn-Ag

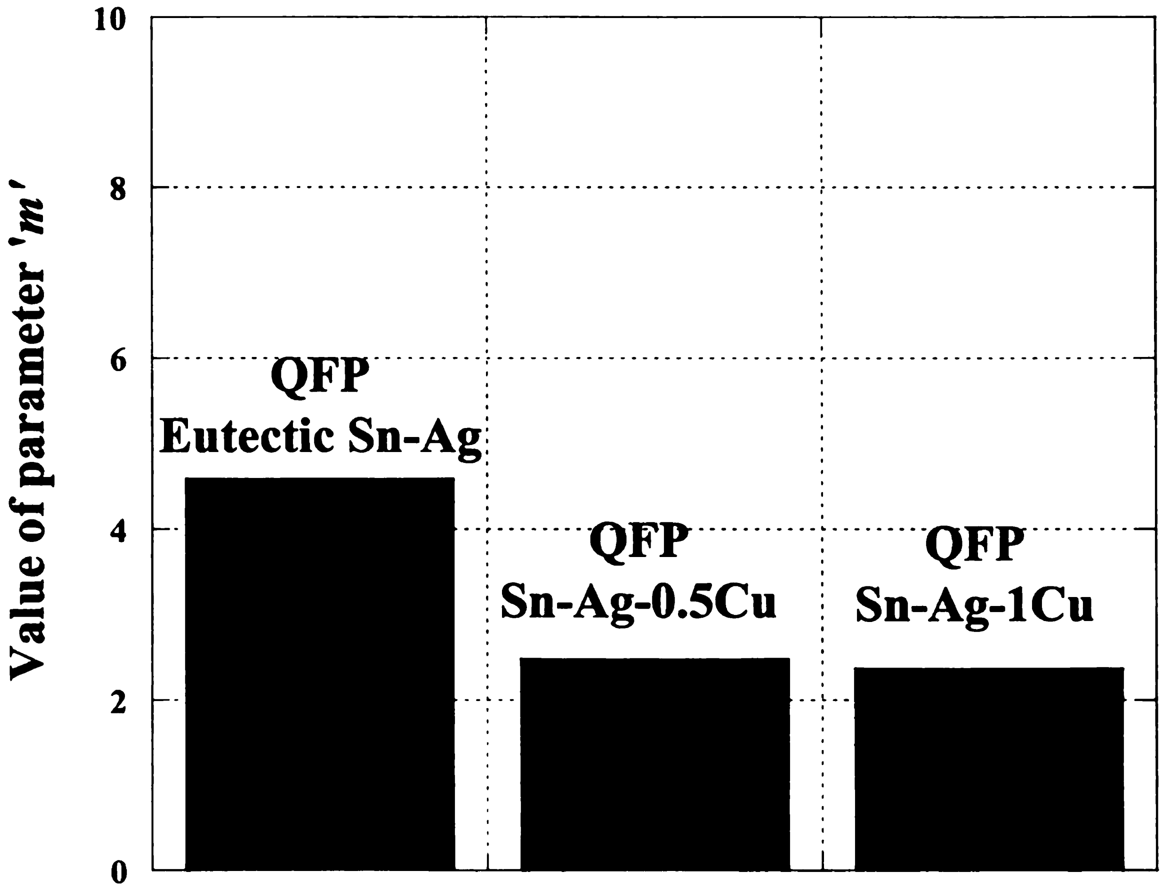

Figure IX.6. Effect of solder alloy on the material-related parameter *'m'* in $[\Delta T]^{-m}$.
Note: Joint geometry was the same for all these conditions.

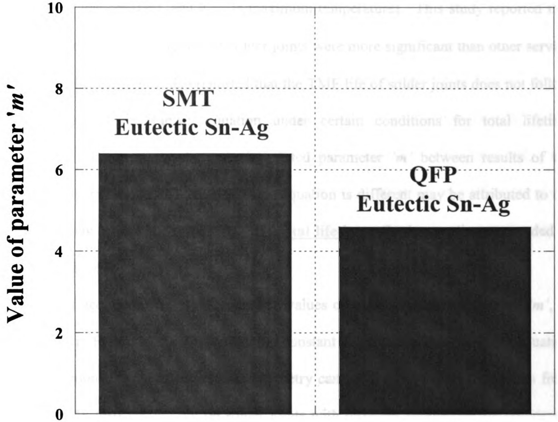

Figure IX.7. Effects of solder joint geometry on material-related parameter *'m'* in $[\Delta T]^{-m}$.

been used to predict **total lifetime** of solder joints [120]. Studies carried out by Shohji et al.[119] found that the material-related parameter '*m*' in $(\Delta T)^{-m}$ was about 1.9 after evaluating TMF lives of Sn-37Pb solder joints under various TMF conditions using modified Coffin-Manson equation ($N_f = C \cdot F^m \cdot (\Delta T)^{-m} \exp(Q/RT_{max})$, where N_f: thermal fatigue life, C is a constant, F is frequency, ΔT is temperature range, Q is activation energy, R is gas constant, and T_{max} is maximum temperature). This study reported that the influence of (ΔT) on lifetime of solder joints were more significant than other service variables. However, they also reported that the TMF life of solder joints does not follow the modified Coffin-Manson equation under certain conditions for total lifetime predictions. The reason, why material-related parameter '*m*' between results of the present study and modified Coffin-Manson equation is different may be attributed to the difference between ***useful service life*** and **total lifetime**. Further studies are needed to clarify this issue.

Joint geometry affects the estimated values of material-related parameter '*m*', as can be seen in Figure IX.7. Proportionality constant in the proposed parametric equation that can account for the effect of joint geometry can be evaluated provided results from identical TMF tests carried out on solder joints with different geometries are compared. At present such a data is not available. Unluckily, the two published works used to calculate the parameter 'm' could not be used for this purpose since the heating rates, cooling rates, dwell times and temperature differences imposed are different in these two studies.

The purpose of the present study is to develop a simple method to predict ***useful service life*** of solder joints under various service conditions. The simple parametric approach proposed in this paper might be one of the possible effective methods to quickly obtain the ***useful service*** life of solder joints, and might suit the needs of industrial designers.

4. Summary

Material-related parameters in a parametric empirical equation to check reliability/***useful service life*** of solder joint were carried out. By using this approach one can judge the effectiveness of the various material modification approaches, such as alloying and use of reinforcements, to withstand the effects of various service parameters to be encountered. Material-related parameters evaluated from extremely fast supplementary studies, such as isothermal shear testing and stress relaxation, are about the same as those obtained with time consuming TMF studies carried out with realistic service conditions.

LIST OF REFERENCES

1. S. Jin, *JOM*, **45**(7), 3(1993).

2. W.L. Winterbottom, *JOM*, **45**(7), 20(1993).

3. P.T. Vianco and D.R. Frear, *JOM*, **45**(7), 14(1993).

4. C. Melton, *JOM*, **45**(7), 33(1993).

5. M. McCormack and S. Jin, *JOM*, **45**(7), 36(1993).

6. http://ko.home.agilent.com/upload/cmc_upload/All/Oresjo_Ling_pbfreetest_082004.pdf

7. Environmental Protection Agency, National Air Quality and Emission Trend Report. 1989. EPA-450/4-91-003. Research Triangle Park. NC. 1991

8. W.J. Plumbridge,*Soldering and Surface Mount Technology*, **12** (1), 32 (2000)

9. D. Napp, Sampe Journal, **32** (2), 59 (1996)

10. C.L. Hernandez, P.T. Vianco, and J.A. Rejent, IPC/SMTA electronics Assembly Expo 1998, S-19-2-1(1998).

11. C.M.L Wu and M.L. Huang, Journal of Electronic Materials, **31** (5), 442 (2002)

12. D.R. Frear, J.W. Jang, J.K. Lin, and C.Zhang, JOM, **53** (6), 28 (2001)

13. S.K. Kang and T.G. Ference, Journal of Materials Research, **8** (5), 1033 (1993)

14. H. Takao and H. Hasegawa, Journal of Electronic Materials, **30** (9), 1060 (2001)

15. C.S. Oh, J.H., Shim, B.J. Lee, and D.N. Lee, Journal of Alloys And Compounds, **238** (1-2), 155 (1996)

16. Z.D. Xia, Z.G. Chen, Y.W. Shi, N. Mu, and N. Sun, Journal of Electronic Materials, **31** (6), 564 (2002)

17. R.N. Wild, Welding Research, 521-s (1972).

18. H.J. Frost and R.T. Howard, Transactions on Components, Hybrids, and Manufacturing Technology, **13** (4), 727 (1990).

19. W.F. Feng, C.Q. Wang, and M. Morinaga, Journal of Electronic Materials, **31** (3), 185 (2002).

20. L.J. Matienzo and R.R. Schaffer, Journal of Materials Science, **26** (3), 787 (1991).

21. S. Russell, A. Grigals, and E. Clemente, Journal of Electronic Materials, **28** (9), 1008 (1999).

22. http://www.necel.com/pkg/en/pk_02.html.

23. B.T.K. Barry and C.J. Thwaites, "Tin and Its Alloys and Compounds", John Wiley & Sons: New York, 1985; pp. 16

24. W. Steurer, R. Ferro and A. Saccone, Physical Metallurgy 4th edition, Vol. 1, editors, R. W. Cahn, and P. Haasen, Elsevier Science B.V., Amsterdam, The Netherlands, 25 & 284 (1996).

25. M.J. Sullivan and S.J. Kilpatick, "Degradation Phenomena", *Puttliz/Handbook of Lead (Pb) – Free Technology for Microelectronic Assembly, Chapter 22*, pp. 926-927, (2004).

26. Y. Kariya, C.R. Gagg, and W.J. Plumbridge, "Tin pest in solder alloys", Soldering and Surface Mount Technology, **13**, pp. 39-40 (2001).

27. W.J. Plumbridge, "Long term mechanical reliability with lead-free solders", Soldering and Surface Mount Technology, **16** (2), pp. 13-20 (2004).

28. N. E. Dowling, *"Mechanical Behavior of Materials"*, Ed by D. Humphrey, Prentice Hall, Upper Saddle River, New Jersey, pp. 339 (1993)

29. M.A. Meyers and K.K. Chawla, *Mechanical Metallurgy principles and applications*, Prentice-Hall Inc., Englewood Cliffs, NJ, 692(1984).

30. N. E. Dowling, *"Mechanical Behavior of Materials"*, Ed by D. Humphrey, Prentice Hall, Upper Saddle River, New Jersey, pp. 625 (1993).

31. H.D. Solomon, *J. Electr. Packaging*, **113** (June), 102(1991).

32. C. Kanchanomai C, Y. Miyashita, and Y. Mutoh, J. of Electron Mater, **31** (2), 142 (2002).

33. A. Dasgupta, *Handbook of Electronic Packaging,* Edited by Michael Pecht, 1991, p.495.

34. C.H. Raeder, R.W. Messler Jr. and L.F. Coffin. Jr., J. of Electron Mater, **28** (9), 1045 (1999).

35. D.A. Miller, R.H. Priest, and E.G. Ellison, High temperature Materials and Processing, **6** (3&4), 155 (1984).

36. T.Y. Pan, IEEE Transactions on Components, Hybrids and Manufacturing Technology, **14** (4), 824 (1991).

37. E.C. Kubik and T.P.L. Li, "Thermal shock and Temperature Cycling Effects on Solder Joints of Hermetic Chip Carries Mounted on Cu Thick Film", Matin Marietta Aerospace Internal Rep., Microelectronic Center, Orendo, Fl., 32855

38. W.J. Plumbridge and Y. Kariya, Fatigue Fract Engng Mater Struct, **27**, 723 (2004)

39. D.R. Frear, *The Mechanics of Solder Alloy Interconnects*, Ed by H.S. Morgan and S.N. Burchett, 1993, p. 60-61.

40. D.A. Miller, R.H. Priest, and E.G. Ellison, High temperature Materials and Processing, **6** (3&4), 157-158 (1984).

41. M.J. Sullivan and S.J. Kilpatick, "Degradation Phenomena", *Puttliz/Handbook of Lead (Pb) – Free Technology for Microelectronic Assembly, Chapter 22*, pp. 928, (2004).

42. J.D. Lubahn and R.P. Felgar, "Plasticity and Creep of Metals", John Wiley & Sons, New York, 1961, pp. 217-220

43. S. Choi, K.N. Subramanian, J.P. Lucas, and T.R. Bieler, Journal of Electronic. Materials. **29**, 1249 (2000).

44. S. Choi, J.G. Lee, K.N. Subramanian, J.P. Lucas, and T.R. Bieler, Journal of Electronic Materials, **31** (4), 292 (2002).

45. Y. Kariya, Y. Hirata, and M. Ostuka, J. Electron. Mater, **28** (11), 1263 (1999).

46. N. M. Poon, C.M. Lawarence Wu, Joseph K. L. Lai, and Y. C. Chan, *IEEE Transactions on Advanced Packaging*, 23 (4), p. 708 (2000)

47. http://www.kester.com/en-us/leadfree/requirements.aspx

48. J. Glazer, J. of Electron. Mater, **23** (8), 693 (1994)

49. P. Viswanadham, S. O. Dunford, and J. Kivilahti, "Reliability Aspects of Lead-Free Solders in Ekectronic Assemblies", *Puttliz/Handbook of Lead (Pb) – Free Technology for Microelectronic Assembly, Chapter 19*, pp. 788, (2004).

50. C. Mackay and W. von Voss, Mater. Sci. Technol. **1** (3), 240 (1985).

51. M.E. Loomans and M.E. Fine, *Metall. Mater. Trans. A, Phys. Metall. Mater.Sci.* **31A,** 1155 (2000).

52. S.H. Huh, K.S. Kim, and K. Suganuma, *Mater. Trans. (Japan)* **42,** 739 (2001).

53. K.S. Kim, S.H. Huh, and K. Suganuma, *Mater. Sci. Eng. A* **333,** 106 (2002).

54. A.Z. Miric and A. Grusd, Soldering, Soldering & Surface Mount Technology, **10** (1), 19 (1998)

55. F. Guo, S. Choi, K.N. Subramanian, T.R. Bieler, J.P. Lucas, A. Achari, and M. Paruchuri, *Materials Science and Engineering A*, **351** (1-2), 190 (2003)

56. J.C. Suhling, H.S. Gale, R. W. Johnson, M. N. Islam, T. Shete, P. Lall, M.J. Bozack, J. L. Evans, P. Seto, T. Gupta, J. R. Thompson, *Soldering and Surface Mount Technology*, **16** (2), 77 (2004)

57. J.S. Hwang, *Soldering and Surface Mount Technology*, **14** (8), 20 (2000)

58. C. Kanchanomai, Y. Miyashita, and Y. Mutoh, J. of Electron Mater, **31** (5), 456 (2002)

59. Y. Kariya, T. Hosoi, T. Kimura, S. Terashima, and M. Tanaka, Materials Transactions, **45** (3), 689 (2004)

60. M.A. Meyers and K.K. Chawla, *Mechanical Metallurgy principles and applications*, Prentice-Hall Inc., Englewood Cliffs, NJ, 402 (1984).

61. R. M. Brick, A.W. Pense, and R. B. Gordon, *"Structure and Properties of Engineering Materials"*, 4^{th} edition, Ed by M. B. Bever, McGraw-Hill, New York, NY, pp. 93 (1983).

62. H. Mavoori and S. Jin, J. of Electron Mater, **27** (11), 1216 (1998).

63. M.J. Sullivan and S.J. Kilpatick, "Degradation Phenomena", *Puttliz/Handbook of Lead (Pb) – Free Technology for Microelectronic Assembly, Chapter 22*, pp. 922, (2004)

64. K.N. Subramanian, T.R. Bieler and J.P. Lucas, J. Electron. Mater. **28** (11), 1176 (1999)

65. S. Choi, K.N. Subramanian, J.P. Lucas, and T.R. Bieler, J. Electron. Mater. **29**, 1249 (2000).

66. K. N. Subramanian, A. Lee, S. Choi, and P. Sonje, J. Electron. Mater. 30 (4), 372 (2001)

67. A.W. Gibson, S. Choi, T.R. Bieler, and K.N. Subramanian, *IEEE International Symposium on Electronics and Environment*, p. 246 (1997).

68.

69.

70.

71.

72.

73.

74.

75.

76.

77.

78.

79.

80.

81

82

83

68. Y. Kariya and M. Otsuka, J. Electron. Mater., **27** (7), 866 (1998)

69. M. McCormack and S. Jin, *1994 IEEE/CPMT 16th International Electronics Manufacturing Technology Symposium*, 1. The Institute and Electrical Electrons Engineers Piscataway, NJ, p.7 (1994a)

70. M. McCormack and S. Jin, J. Electron. Mater., **23** (7), 595 (1994b)

71. A. Dasgupta, P. Sharma, and K. Upadhyayui, International Journal of Damage Mechanics, 10, 101 (2001)

72. Y.H. Pao, S. Badgley, R. Govila, and E. Jih, *Fatigue of Electronic Materials*, Edited by S.A. Schroeder et. al., Publication of American Society for Testing and Materials, 60-81 (1994).

73. H.L.J. Pang, K.H. Tan, X.Q. Shi, and Z.P. Wang, Materials Science and Engineering, **A307**, 42 (2001).

74. W.W. Lee, L.T. Nguyen, and G.S. Selvaduray, Microelectronic Reliability, **40**, 231 (2000).

75. S. Ahat and M. Sheng, and L. Luo, *J. Mater. Res*, **16** (10), p. 2914 (2001).

76. S. Choi, T.R. Bieler, J.P. Lucas, and K.N. Subramanian, J. Electron. Mater. **28** (11), 1209 (1999).

77. A. W. Gibson, S. Choi, K. N. Subramanian, and T. R. Bieler, *Reliability of Solders and Solder joints*, R. K. Mahidhara *et. al.*, eds., TMS Warrendale, PA, p.97 (1997).

78. J.P. Lucas, F. Guo, J. Mcdougall, T. R. Bieler, K. N. Subramanian, and J. K. Park, J. Electron Mater, **22**, 1268 (1999).

79. F. Guo, J. Lee, J. P. Lucas, K. N. Subramanian, and T. R. Bieler, J. Electron. Mater. **30** (9), 1222 (2001).

80. R. Darveaux and K. Banerji, 1992 42nd Electronic Components and Technology Conference (ECTC), IEEE, Piscataway, NJ, p. 538 (1992).

81. D.P.H. Hasselman, J. Am. Ceram. Soc., **52** (11), 600 (1969).

82. J.G. Lee, F. Guo, S. Choi, K.N. Subramanian, T.R. Bieler, and J.P. Lucas, J of Electronic Materials, **31** (9), 946 (2002).

83. H. Yang, P. Deane, P. Magill, and K. L. Murty, IEEE Electronic Component and Technology Conference (ECTC), 1136 (1996).

84. H. L. Reynolds, S. H. Kang and J. W. Morris, Jr., J of Electronic Materials, **28** (1), 69 (1999).

85. S. Choi, J. Lee, F. Guo, T. R. Bieler, K. N. Subramanian and J. P. Lucas, JOM, **53** (6), 22 (2001).

86. S. G. Jadhav, K. N. Subramanian, T. R. Bieler and J. P. Lucas, J of Electronic Materials, **30** (9), 1197 (2001).

87. F. Guo, J. Lee, S. Choi, J.P. Lucas, T.R. Bieler, and K.N. Subramanian, J of Electronic Materials, **30** (9), 1073 (2001)

88. F. Guo, S. Choi, J. P. Lucas and K. N. Subramanian, Soldering and Surface Mount Technology, **13** (1), 7 (2001).

89. J. Howell, A. Telang, J.G. Lee, and K.N. Subramanian, J of Materials Science: Electronic Materials, **13**, 315 (2002).

90. K.C. Chen, A.U. Telang, J.G. Lee, and K.N. Subramanian, J of Electronic Materials **31** (11), 1118 (2002).

91. J.G. Lee, A.U. Telang, K.N. Subramanian, and T.R. Bieler, J of Electronic Materials **31** (11), 1152 (2002)

92. W.J. Plumbridge, *Soldering & Surface Mount Technology*, **11** (3), 8 (1999).

93. M. Farooq, C. Goldsmith C, R. Jackson, and G. Martin, J. of Electron Mater, **32** (12), 1421 (2004).

94. J. Lau, W. Dauksher, J. Smetana, R. Horsley, D. Shangguan, T. Castello, I. Menis, D. Love, and B. Sullivan, *Soldering & Surface Mount Technology*, **16** (1), 12 (2004).

95. G. Di Giacomo and S. Oggioni, Microelectronics Reliability, **42** (9-11), 1541 (2002)

96. C.J. Zhai, Sidharth, and R. Blish, IEEE Transactions on Device and Materials Reliability, **3** (4), 207 (2003).

97. T. Goswami and H. Hanninen, Materials & Design, **22** (3), 199 (2001).

98. B.Z. Hong and L.G. Burrell, IEEE Transactions on Components Packaging and Manufacturing Technology Part A, **20** (3), 280 (1997).

99. J.G. Lee and K.N. Subramanian, J. of Electron Mater, **32** (6), 523 (2003).

100. H. Rhee, K.N. Subramanian, A. Lee, and J.G. Lee, *Soldering &Surface Mount Technology*, **15** (3), pp. 21 (2003).

101. J.G. Lee and K.N. Suramanian, *Soldering and Surface Mount technology* (*in press*)

102. H. Rhee, private communication (2004).

103. P.T. Vianco (Proceeding of Surface Mount International Conference, San Jose, CA, Surface Mount International, Edina, MN 55424, USA), **2**, (1993), p. 725

104. J.S. Hwang and Z.F. Guo (Proceedings of Surface Mount International Conference, San Jose, CA), Pub. Surface Mount International, Edina, MN 55424, USA, **1.2**, (1993) p 732.

105. Guo F., Choi S., Lucas J.P., and Subramanian K.N., J of Electron Mater, **29** (10), 1241 (2002).

106. C. M. Chuang, P.C. Shin, and K.L. Lin, J of Electron Mater, **33** (1), 1 (2004).

107. F.J. Humphreys and P.N. Kalu, *Acta Metall*, **35**, 2815 (1987).

108. W.F. Smith in Structure and Properties of Engineering Alloys, 2nd edition, ED by R. Gibala, M. Tirrell, and C. Wert, McGraw-Hill, New York, NY, (1993) p.498-509.

109. W.B. Hampshire, *Soldering and Surface Mount Technology*, **5** (14), 49 (1993).

110. F. Hua and J. Glazer, "Lead-free solders for Electronic Assembly", in R.K. Mahidhara et. al. (Eds), *Design & Reliability of Solder and Solder Interconnects,* The Minerals, Metals, & Materials Society (TMS), Warrendale, PA, 65 (1997).

111. Z. Xia, Y. Shi, and Z. Chen, Journal of Materials Engineering And Performance, **11** (1) 107 (2002).

112. C. Basaran and R. Chandaroy, Journal of Electronic Packaging, **124** (1), 60 (2002).

113. L.J. Zhang, L. Wang, X.M. Xie, and W. Kempe, IEEE Transactions on Electronics Packaging Manufacturing, **25** (4), 284 (2002).

114. P.T. Vianco, J.A. Rejent, and A.C. Kilgo, J. of Electron Mater, **32** (3), 142 (2003).

115. K.N. Subramanian, Journal of Electronic Materials (*in press*).

116. Pollack and W. Herman "Tool Life", Englewood Cliffs, New Jersey: Prentice Hall, 1988.

117. J.G. Lee and K.N. Subramanian, "Effects of TMF Ramp Rates on Damage Accumulation and Resultant Mechanical Behavior of Sn-Ag Based Solder Joints", will be submitted to *Journal of Electronic Materials.*

118.H. Rhee and K.N. Subramanian, *Journal of Electronic Materials*, **32** (11), 1310(2003).

119.X. J. Zhao, G.Q. Zhang, J.F.J.M. Caers, and L.J. Ernst, Journal of Electronic Packaging, **125** (4), 582 (2003).

120.M.J. Sullivan and S.J. Kilpatrick, "Degration Phenomena", *Puttliz/Handbook of Lead (Pb) – Free Technology for Microelectronic Assembly, Chapter 22*, 967 (2004).

121.I. Shohji, H. Mori, and Y. Orii, Microelectronics Reliability, **44**, 269 (2004).